Ph.D. degree in Molecular Medicine

(Curriculum in Molecular Oncology)

European School of Molecular Medicine (SEMM)

University of Milan and University of Naples “Federico II”

Settore disciplinare: BIO/10

The role of protein arginine methylation in RBP-RNA interaction modulation and its implications in cancer stress response investigated by MS-proteomics

Maniaci Marianna

European Institute of Oncology (IEO), Milan

Matricola n. R12433

Supervisor: Dr. Tiziana Bonaldi
European Institute of Oncology (IEO), Milan, Italy

PhD Coordinator: Prof. Saverio Minucci

Anno accademico 2021-2022

Table of Contents

List of abbreviations

µ	mean
ACN	acetonitrile
ADMA	asymmetric di-methyl-arginine
AP	affinity-purification
BSA	bovine serum albumin
CDDP	cisplatin
CID	collision-induced dissociation
CLIP	cross-linking and immunoprecipitation
CSD	cold shock domain
Da	dalton
DDA	data-dependent acquisition
DIA	data independent acquisition
DMSO	dimethyl sulfoxide
DNAse I	deoxyribonuclease I
dsRBD	double-stranded RNA binding domain
DTT	dithiothreitol
ECD	electron capture dissociation
ECL	enhanced chemo-luminescence
ESI	electrospray ionization
ETD	electron transfer dissociation
EV	empty vector
FA	formic acid
FACS	fluorescence activated cell sorting
FBS	fetal bovine serum
FC	fold change
FDR	false discovery rate
FT	flow-through
FWD	forward
geLC-MS/MS	in-gel digestion couple to tandem mass spectrometry
GO	gene ontology
H	heavy
H4R3me2a	histone H4 arginine 3 asymmetric di-methylation
H4R3me2s	histone H4 arginine 3 asymmetric di-methylation
HCD	higher-energy collision dissociation
HILIC	hydrophilic interaction liquid chromatography
hmSILAC	heavy methyl SILAC
hnRNP	heterogeneous ribonucleoprotein
HpH	high-pH
HPLC	high pressure liquid chromatography
HSP70	heat shock protein 70
HSP90	heat shock protein 90
IDR	intrinsically disordered region
IgG	immunoglobulin G
IP	immuno-precipitation

iTRAQ	isobaric tags for relative and absolute quantitation
KD	knock down
KH	K Homology
L	light
LC region	low complexity region
LC	liquid chromatography
LC-MS/MS	liquid-chromatography tandem mass spectrometry
LFQ	label-free quantitation
LLPS	liquid-liquid phase separation
m/z	mass/charge ratio
me1	mono-methylation
me2	di-methylation
Met	methionine
MLOs	membrane less organelles
MMA	mono-methyl-arginine
MoRFs	molecular recognition features
MS/MS	tandem mass spectrometry
MS	mass-spectrometry
nLC	nano liquid chromatography
NT	not treated
OOPS	orthogonal organic phase separation
PIWI	p-element induced wimpy testis
PRMT	protein arginine methyltransferase
PTex	phenol toluol extraction
PTM	post translational modification
PUA	archaeosine transglycoslyase
PUM	pumillo-like repeat
R	arginine
RBD	RNA binding domain
RBP	RNA-binding protein
REV	reverse replicate
RIC	RNA interactome capture
RIP	RNA immunoprecipitation
RNaseA	ribonuclease A
RNA-seq	RNA sequencing
RP	reversed-phase
RRM	RNA recognition motif
SAM	S-adenosil-methionine
SASP	senescence-associated secretory phenotype
SAX	strong anion exchange
SCX	strong cation exchange
SDMA	symmetric di-methylated arginine
SDS	sodium dodecyl sulfate
SDS-PAGE	SDS - polyacrylamide gel electrophoresis
SGs	stress granules
shRNA	short hairpin RNA

SILAC	stable isotope labelling with amino acids in cell culture
SLiMs	short linear motifs
TFA	trifluoroacetic acid
TiO2	titanium dioxide
TMT	tandem mass tag
WB	western blot
WT	wild-type
XIC	extracted ion chromatogram
XRNAX	protein-crosslinked RNA extraction
YTH	YT521-B homology
ZnF	zinc finger
σ	standard deviation

Figure Index

1. ABSTRACT

Various post-translational modifications (PTMs) have been described to regulate RNA-binding protein (RBP) activity, subcellular localization, and interactions with other proteins or RNAs. Proteome-wide experiments recently carried out in our group have shown that RBPs are the most abundant arginine (R)-methylated proteins. However, the mechanisms by which changes in protein R-methylation may modulate RBP-RNA interactions is not well-understood. Protein Arginine Methyltransferases (PRMTs) are the enzymes responsible for the deposition of methylation on the guanidino group of arginines. Recent evidence indicated that protein R-hypomethylation could influence RBP phase-separation and consequent formation of Membrane-Less Organelles (MLOs), non-membranous structures mainly composed of untranslated mRNA and RBPs.

During my Ph.D., we setup, optimized and applied a quantitative proteomic approach that allows profiling global changes of RBP-RNA interactions upon modulation of protein R-methylation, both directly by using PRMT inhibitors and indirectly through cisplatin (CDDP)-induced PRMT1 re-localization on chromatin. In particular, we coupled the Orthogonal Organic Phase Separation (OOPS) strategy with quantitative proteomics and high-resolution mass spectrometry (MS) analysis and profiled RNA-protein interaction dynamics in dependence on R-methylation remodeling. Biochemical and immunofluorescence analysis confirmed that a set of RBPs displays a differential interaction with RNAs upon PRMT1 inhibition and that, at least in specific cases, this altered behavior is linked to their propensity to aggregate into MLOs.

We then applied the same experimental strategy to a more clinically-relevant model in order to assess to what extent the CDDP-induced protein-R-methylation rewiring could affect RBP-RNA interaction dynamics in the ovarian cancer cell line resistant to CDDP SK-OV3. Analysis of RBPs dynamics at the interface of an MS experiment upon CDDP revealed a

strong modulation of RBP-RNA interactions and suggested novel interesting protein targets possibly involved in the adaptive response of SK-OV-3 upon this drug. Currently, we are dissecting in depth the R-methylation state of the most promising RBPs and, in parallel, carrying out the RNA-seq analysis of the interface fraction in order to characterize the RNAs that interact differentially with the RBPs in the same conditions.

2. INTRODUCTION

2.1 Protein Post-Translational Modifications

Protein Post-Translational Modifications (PTMs) are covalent modifications that occur on side chains of proteins after transcription and translation. PTMs contribute to the phenomenon of “proteoform explosion” that has progressively replaced the long-lasting paradigm “one gene - one protein”: although the genetic information is almost identical in every human cell, DNA mutations, alternative splicing of RNA transcripts, and the addition of PTMs lead altogether to the formation of numberless protein isoforms (named “proteoforms”) from the same protein-coding gene (Forgrave et al., 2022) which exponentially increases the information complexity related to the final products of gene expression (**Fig.1**).

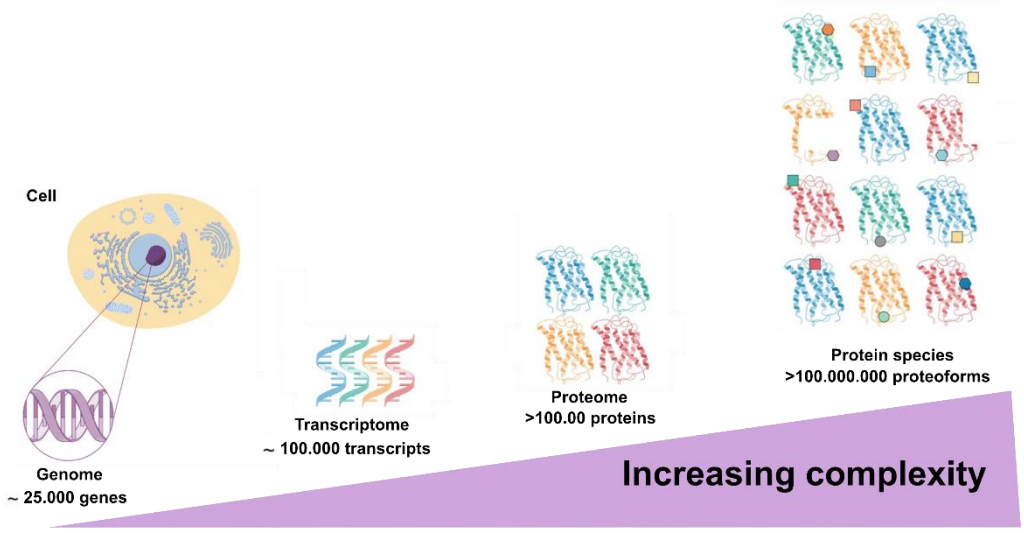

Figure 1: Increasing complexity of genetic information

Considering all possible genetic mutations, alternative splicing of RNA transcripts, and the combinatorial addition of single or multiple PTMs to the proteins, an exponential increase of proteoforms can be generated, starting from a much lower number of coding genes. Adapted from https://doi.org/10.1007/s10337-019-03796-9

Traditionally, individual protein modifications have been studied at amino acid residue resolution; however, it has become clear that several PTMs can simultaneously occur and reciprocally regulate each other. The best-characterized examples of multi-modified proteins are histones, where the presence of different PTM types constitutes the so-called "histone code" (Jenuwein & Allis, 2001). While PTMs decorating histone N-terminal tails are considered one of the major epigenetic mechanisms to fine-tune multiple processes occurring on DNA (such as transcription regulation), PTMs deposited on non-histone proteins can modulate protein stability, interaction capability, subcellular localization, and catalytic activity. Protein phosphorylation, acetylation, methylation, ubiquitination, and proteolytic cleavage are the most common PTMs. However, more than 200 PTM types, occurring on proteins in different conditions and functional states, have been identified (Jensen, 2006). Despite the great importance of PTMs, the lack of appropriate analytical tools has long prevented their thorough and systematic analysis. In the last 15 years, Mass Spectrometry (MS) has become the method of choice for qualitative and quantitative analysis of PTMs and has represented a powerful tool to investigate aspects that could not be addressed by any other molecular approach.

2.1.1 Protein arginine (R)-methylation

Arginine (R)-methylation is a post-translational modification (PTM) occurring on a variety of nuclear and cytoplasmic proteins, and it consists of the addition of one or more methyl (CH3) groups to the guanidino groups of R residues, within polypeptide chains.

R-methylation is involved in several biological processes, such as DNA damage repair (Giuliani et al., 2021; Hwang et al., 2020), transcriptional activation/repression (Guccione & Richard, 2019), splicing (Fong et al., 2019), translation (Bachand & Silver, 2004), miRNA biogenesis (Spadotto et al., 2020), immunological response (Srour et al., 2022), and cell cycle regulation (Raposo & Piller, 2018). Typically, PTMs are deposed by enzymes known

as “writers”, removed by “erasers”, and are recognized by “readers”(Biswas & Rao, 2018). The writers of R-methylation are enzymes named Protein Arginine Methyltransferases (PRMTs). PRMTs are grouped into three different classes, in accordance with their ability to add one methyl group (PRMT type III) or two methyl groups, in a symmetric (PRMTs type II) or asymmetric fashion (PRMTs type I), with respect to the guanidino group. Hence, the resulting R-methylation types can be classified as R-mono-methyl (MMA), symmetric R-di-methyl (SDMA), or asymmetric R-di-methyl (ADMA), respectively (**Fig.2**).

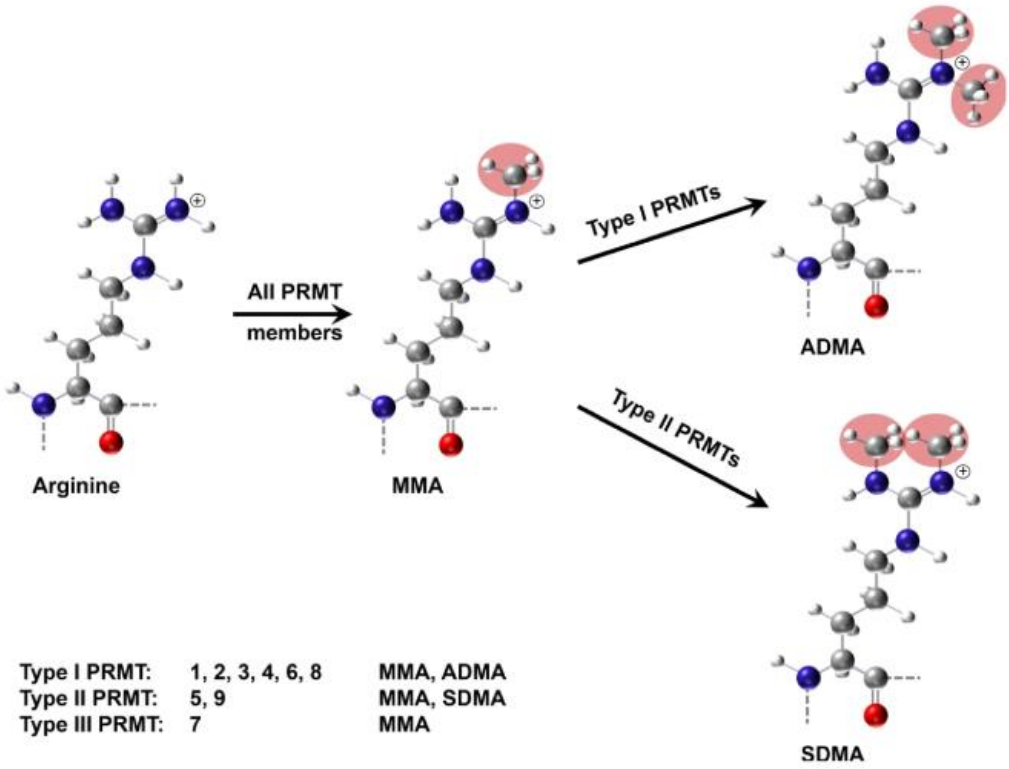

Figure 2: Arginine (R)-methylation

Molecular structure of unmodified, mono-methylated (MMA), asymmetrically di-methylated (ADMA), and symmetrically di-methylated arginine (SDMA). Taken from: https://doi.org/10.1016/j.ymeth.2019.09.014

Arginine flanked by glycine forms -the so-called RGG/RG regions- are generally preferred sites for methylation by PRMTs (Thandapani et al., 2013). However, more recently, some PRMT-specific preferential motifs have been discovered, such as arginine flanked by glycine on both

sides (“GRG”) for PRMT5 (Musiani et al., 2019a) or arginine flanked by proline (“PR”) for PRMT4 (Shishkova et al., 2017). PRMTs catalyze the transfer of methyl groups from the biological methyl-donor (Roje, 2006) S-Adenosyl-methionine (SAM, or AdoMet) to the positively-charged guanidino group of the R residues. The addition of a methyl group alters the steric footprint and hydrophobicity of the side chain of the R but does not change the cationic charge of the residue. Since the guanidino group contains five potential hydrogen-bond donors, the steric effect from adding a methyl group to the guanidino group is frequently responsible for the modulation of protein-protein, protein-RNA, and protein-DNA interaction (Blanc & Richard, 2017).

In contrast to lysine methylation, the existence of arginine demethylases (“erasers”) is still controversial. Although the 2-oxoglutarate-dependent JMJD6 de-methylase enzyme was reported to catalyze R-de-methylation of histones *in vitro* (Walport et al., 2016), the evidence supporting this observation is still disputed. Alternatively, the peptidyl-arginine deiminase 4 (PAD4) was described as a putative regulator of histone R-demethylation by converting the R-methyl site to citrulline (P. R. Thompson & Fast, 2006).

The best characterized “readers” of R-methylated proteins are the Tudor domain-containing proteins such as SMN, SPF30, and TDRD1/2/3/6/9/11. The Tudor domain aromatic residues interact with the methyl-R cationic carbon by forming an aromatic cage such that cation-π contacts, where the methyl groups of arginines provide increased hydrophobicity to enhance contacts within the cage (Blanc & Richard, 2017).

2.1.2 Protein Arginine Methyltransferases

While all PRMTs contain a highly conserved methyltransferase domain, they present different N-terminal regions that vary in length/sequence and may be responsible for substrate recognition and regulation of enzyme activity (**Fig.3**).

PRMT1 is the predominant type I PRMT and its activity is responsible for more than 85% of arginine methylation in mammalian cells (Tang et al., 2000). Human PRMT1 is encoded

by the PRMT1 gene, composed of 12 exons and 11 introns. Due to alternative splicing at the 5'-end, it exists in seven different isoforms (PRMT1v1-v7) (Thiebaut et al., 2021). On histones, PRMT1 methylates R3 of histone4 (H4), generating the H4R3me2a mark, which is functionally linked to transcriptional activation. Beyond histones, PRMT1 methylates numerous non-histone targets, both in the cytosol and in the nucleus of the cell.

PRMT2 belongs to the type I PRMT group and exhibits high sequence homology with PRMT1. PRMT2 contains the canonical methyltransferase domain and a unique Src homology 3 (SH3) domain at the N-terminal region (Cura & Cavarelli, 2021). Its best-characterized substrate is the R8 of histone 3 (H3), on which it can add two methyl groups generating the H4R8me2a mark. It was reported that PRMT2 overexpression and consequent increase of H4R8me2a in glioblastoma correlated with poor prognosis (Dong et al., 2018).

PRMT3 is a type I PRMT with a unique zinc finger (ZnF) domain at the N-terminal region. It shares some targets with PRMT1, including the H4R3me2a mark. Indeed, it was described that PRMT3 activates the expression of miR-3648 by enhancing H4R3me2a levels at the promoter region of the gene (Min et al., 2019). On the other hand, it was also demonstrated that PRMT3 can methylate unique targets, such as the ribosomal protein RPS2 (SWIERCZ et al., 2005), thus regulating ribosome homeostasis.

PRMT4, a type I PRMT, is also known as CARM1 (co-activator associated with arginine methyltransferase 1), due to its described role as a transcriptional co-activator of PRMT1. CARM1 is recruited to transcriptional promoters, where it modifies histone H3 at R17 and R26 (H3R17me2a, H3R26me2a) (Suresh et al., 2021), two marks associated with transcriptional activation. Like other PRMTs, CARM1 is frequently overexpressed in cancer. CARM1-mediated BAF155 methylation promotes cancer cell migration and metastasis (Hwang et al., 2021).

PRMT5 is the major type II PRMT in mammalian cells and it contains a unique TIM-barrel domain at the N-terminal region. Through the TIM-barrel domain, PRMT5 forms a hetero-

octamer complex with MEP50 ($PRMT5_4$:$MEP50_4$) (Antonysamy et al., 2012). The formation of this complex is frequently necessary to exert PRMT5 activity both in the nucleus and in the cytoplasm. In the nucleus, PRMT5 symmetrically di-methylates R3 of H4 (H4R3me2s) and R3 of histone 2A (H2AR3me2s). Both marks are associated to transcriptional repression (Guccione & Richard, 2019). In the cytoplasm, its best-characterized role is related to the regulation of the splicing machinery, in particular in snRNP (Small Nuclear Ribonucleoproteins) biogenesis.

PRMT6 is a nuclear type I PRMT with a sequence structure close to PRMT1 but with distinct substrate specificity (Frankel et al., 2002). Its main targets are R2 on histone H3 (H3R2me2a) and R29 on histone H2A (H2AR29me2a), both described as transcriptional repressive marks (Guccione & Richard, 2019). Moreover, PRTM6 regulates cell cycles by activating Cyclin D1 expression (Schneider et al., 2021). Indeed, the transcription factor LF1 interacts with PRMT6 and contributes to the recruitment of PRMT6 to the CCND1 gene (Cyclin D1). In addition, PRMT6 displays auto-methylation activity. In particular, PRMT6 R35 auto-methylation is important for PRMT6 stability and its ability to inhibit HIV-1 replication(Singhroy et al., 2013).

PRMT7 is the only annotated enzyme in the type III family. For a long time, it was considered a type II PRMT since it was described to enhance PRMT5 activity on histone H4; however, nowadays its activity has been demonstrated as only strictly linked to mono-methylation. Its peculiar sequence is composed of two tandem methyltransferase domains (Jain & Clarke, 2019). Moreover, differently from other PRMTs, PRMT7 shows a strong preference for RXR motifs surrounded by basic amino acids. Pharmacological inhibition of PRMT7 results in modulation of MMA at R469 of heat shock protein 70 (HSP70) (Szewczyk et al., 2020), and so it has been described as a crucial regulator of the cellular stress response. Recently, it was also described a reciprocal regulation between PRMT7-dependent R-methylation of eIF2α (Haghandish et al., 2019) and eIF2α serine 51

phosphorylation upon stress, suggesting a role in stress granules formation (see paragraph 2.8 of this Introduction).

PRMT8 is a type I PRMT and it owns several unique structural features in the N-terminal region. First, the presence of a myristoylation at the N-terminus mediates its anchorage to the plasma membrane. Second, PRMT8 contains a dual methyltransferase and phospholipase activity. Third, its N-terminal region harbors two proline-rich sequences which allow its binding to SH3 domain-containing proteins (R. Dong et al., 2021). Finally, its expression appears to be exclusive to the brain. Similar to PRMT6, also for PRMT8 auto-methylation was reported as an auto-inhibitory mechanism. The specificity of its substrates is linked to its exclusive expression in the brain. For instance, the Ewing sarcoma protein (EWS) was reported to be a PRMT8 substrate.

PRMT9, belongs to the type II PRMTs. Like PRMT7, PRMT9 contains duplicated methyltransferase domains. In addition, it harbors three tetratricopeptide repeats (TPRs) (Hadjikyriacou et al., 2015) in the N-terminal region. PRMT9 symmetrically di-methylates the spliceosome-associated protein SF3B2 (also known as SAP145) (Y. Yang et al., 2015), a component of the U2 snRNP. Furthermore, it was recently described that PRMT9 is a mitochondria-associated protein and that it may be involved in the regulation of anti-RNA virus infection (Bai et al., 2022)

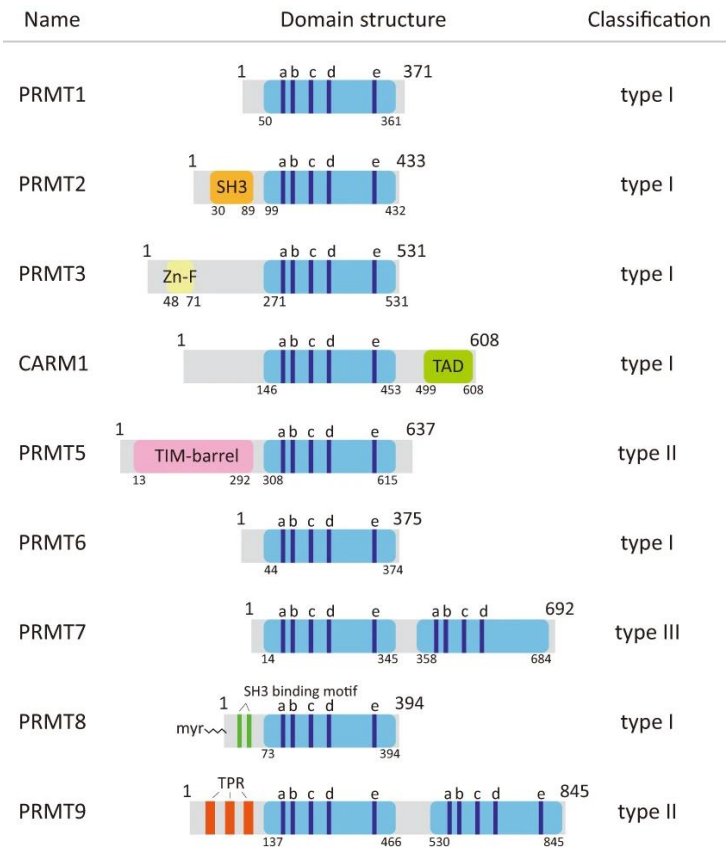

Figure 3: Protein R Methyltransferases

Graphical representation of the different Protein Arginine Methyltransferases (PRMTs) domains and PRMT classification. Adapted from https://doi.org/10.1038/s12276-021-00613-y

2.1.3 PRMTs in cancer

Abnormal expression and/or activity of PRMTs have been reported to be associated with various diseases and in particular with cancer. PRMTs are, frequently over-expressed in cancer (Chuang et al., 2017; Jing et al., 2018; Ryu et al., 2017) and correlate with poor prognosis (Lattouf et al., 2019; Song et al., 2020). For these reasons, PRMTs have emerged as promising targets for cancer therapy and several PRMT inhibitors are nowadays entering various clinical trials (Hwang et al., 2021b). As a result of the advances in PRMT inhibitors design, several pharmaceutical companies have initiated a phase I clinical trials targeting PRMT5 (GSK3326595, JNJ-64619178, PF06939999) and PRMT1 (GSK3368715) in solid and hematological disease (Jarrold & Davies, 2019). Moreover,

promising evidence showed that PRMT type I and type II inhibitors can synergize and increase mutual anti-tumor activity (Fedoriw et al., 2019).

Therefore, the clinical relevance of PRMT activity prompts scientists to study R-methylation and its modulation. Historically, *in vitro* methylation assay was used to evaluate the abilities of purified PRMTs to catalyze methylation of their substrates (Bikkavilli et al., 2014). However, recent advances in mass spectrometry instrumentation and in proteomic approach to enrich this PTM have opened new scenarios in the global and systematic analysis of R-methylation (Bedford & Clarke, 2009).

2.2 Mass spectrometry (MS) and MS-based proteomics

Mass spectrometry (MS) is an analytical tool that accurately measures the mass-to-charge ratio (m/z) of molecules. Thanks to technological improvements in the resolution, sensitivity, and performance of mass spectrometers, MS-based proteomics has become the method of choice for the analysis of complex protein samples (Aebersold & Mann, 2003). In a bottom-up strategy, the proteins are enzymatically digested into small peptides (<30 amino acids) which are then analyzed by MS. Since peptides are more easily fractionated, ionized, and fragmented than intact proteins, the bottom-up strategy is more universally adopted for the global protein analyses by MS. When bottom-up is performed on a mixture of proteins, it is also called “shotgun proteomics” (Y. Zhang et al., 2013). The classical workflow for the identification and characterization of proteins from a complex mixture through shotgun proteomics is illustrated in **Fig.4.** First, the proteins are extracted from the biological sample and enzymatically digested by proteases into peptides. The most common protease used in proteomics analyses is trypsin, which cleaves at the C-terminus of lysine and arginine residues. Trypsin is commonly used in shotgun proteomics because it generates peptides that are about 10-12 amino acids long, which are easily detectable by MS. Digested peptides are purified and concentrated through tips containing a C18 reversed-phase resin and then, PTM-specific immuno-affinity steps can be applied. Subsequently, to decrease

the sample complexity, the peptides are separated by reversed-phase nano-liquid chromatography (RP-nLC) directly ("online") connected to the mass spectrometer. In RP-nLC the peptides are separated according to their hydrophobicity and the mobile phase favors the transferring of ionized peptides into the mass spectrometer, which measures the mass-to-charge (m/z) ratios. In the mass spectrometer, precursor peptides are isolated and scanned (full scan MS or MS1) to identify the m/z that provides information on the elemental composition of the peptide. The precursors are then fragmented into the constituent fragment ions through MS/MS events (tandem MS or MS2). Peptide identification is achieved by comparing the experimental MS2 spectra derived from peptide fragmentation with theoretical MS2 spectra generated by *in silico* digestion of a protein database. Protein identification is then inferred by assigning peptide sequences to proteins. The False Discovery Rate (FDR) is usually estimated by using a target-decoy database strategy (Elias & Gygi, 2010). In the target-decoy search strategy, the MS2 spectra are searched against a target database of protein sequences expanded with the reversed sequences of the same database. Once the FDR is established, it is used to remove false positive peptide identifications. Different algorithms are available and employed for peptide and protein identification from MS raw data, such as Andromeda within the MaxQuant suite (Cox & Mann, 2008), MASCOT (Perkins et al., 1999), and SEQUEST (Yates et al., 1995) The target-decoy searching is applicable to data generated by any search engine.

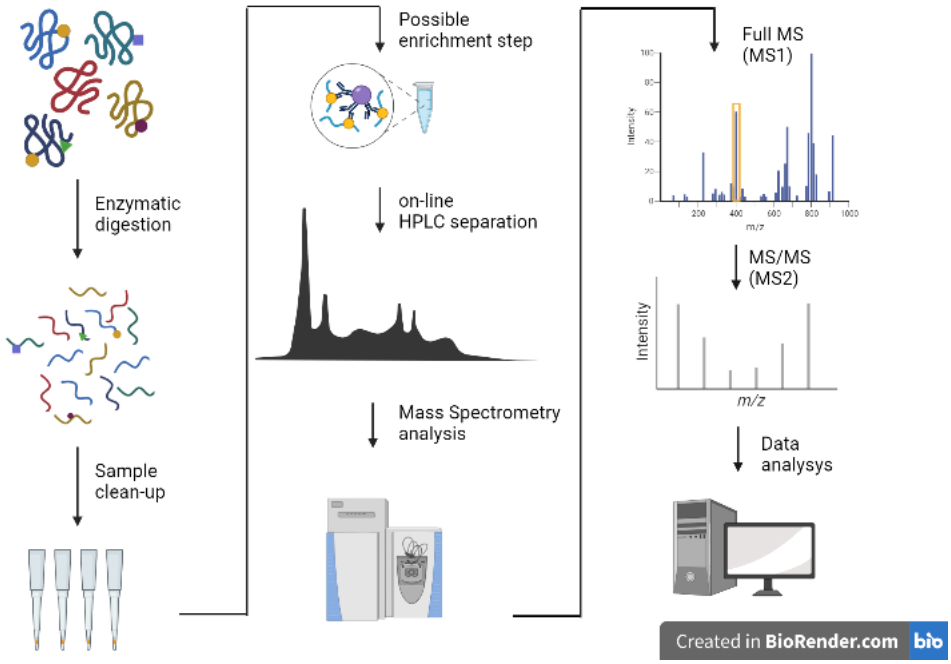

Figure 4: Workflow for MS-based shotgun proteomic approach

Proteins extracted from biological samples are enzymatically digested into peptides. Tryptic peptides are purified and concentrated through C18 RP stage tips. Here, immuno-affinity enrichment for specific PTM can be performed. Subsequently, High-Performance Liquid Chromatography (HPLC) separates digested peptides. Peptides are then ionized and analyzed by tandem mass spectrometry, generating MS (MS1) and MS/MS (MS2) spectra, respectively. MS2 spectra are searched against protein databases to obtain protein identification. This figure has been created in BioRender.com

Different types of mass spectrometers exist, but all consist of three essential parts that can be summarized as follow:

1. The ion source: mass spectrometers can measure m/z values of ionized molecules in the gas phase. However, since peptides are non-volatile and polar molecules, they must be ionized for the subsequent analysis. The most commonly employed strategies to produce ionized peptides are the so-called “soft-ionization” techniques, which allow the ionization of proteins and peptides without causing extensive degradation. Among them, two techniques are commonly used: matrix-assisted laser desorption ionization (MALDI) (Kaufmann, 1995)and electrospray ionization (ESI) (Konermann et al., 2013).

In a MALDI source, peptides are co-crystallized with a solid-phase matrix on a metal plate. When a laser irradiates the resulting solid mixture, this absorbs the laser energy and transfers it to the peptides. In parallel, the fast-heating causes desorption of both matrix and newly formed $[M+H]^+$ protonated peptides into the gas phase. In contrast, the ESI source produces ions from peptides dissolved in a solution. Peptides acquire a charge and become ions in solution because they contain functional groups whose ionization is controlled by the pH of the solvent. The ESI process consists of the formation of an electrically charged spray as a consequence of the application of a high voltage (2–6 kV) between the electrospray tip (capillary) and the inlet of the mass spectrometer. The electrically charged spray drives the desolvation of peptide-solvent droplets. The high temperature provided by a heated capillary and the sheath gas flow at the mass spectrometer inlet support this process (**Fig.5**).

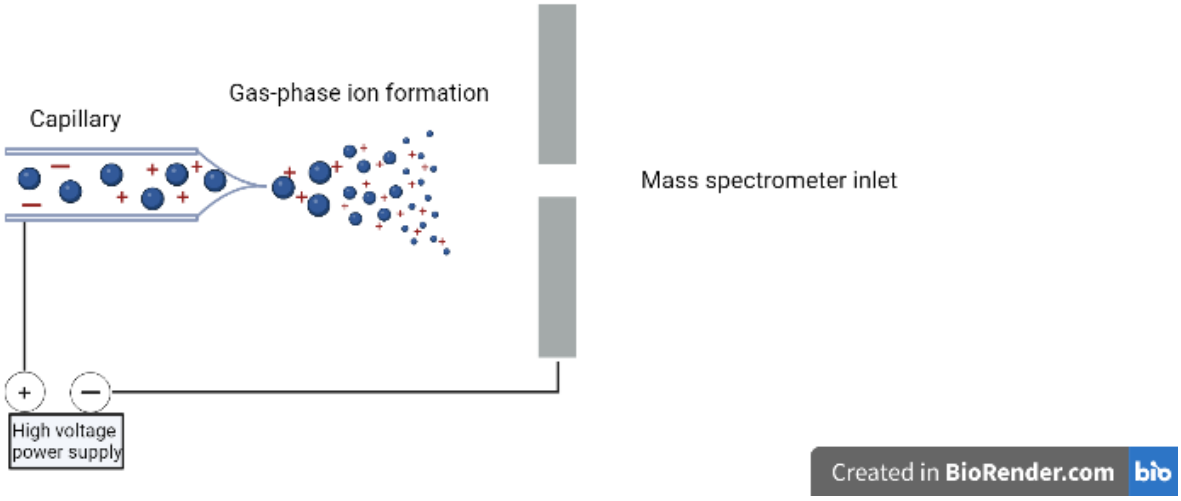

Figure 5: Scheme of the electrospray ionization (ESI) process

Peptides eluted from the chromatographic column are ionized by a high voltage applied between the capillary and the mass spectrometer inlet. Charged liquid forms a cone shape (known as the Taylor cone) and the analyte-solvent droplets burst away into a spray composed of droplets even smaller. This figure has been created in BioRender.com

ESI sources are typically combined with reverse-phase high-pressure liquid chromatography (RP-HPLC), which allows the separation of very complex peptide mixtures prior to MS analysis.

2. The mass analyzer: the mass analyzer is the core of the mass spectrometer and its key function is the storage and separation of ions based on their m/z. Common mass analyzers for the analysis of complex peptide mixtures are the Orbitrap, the quadrupole (Q), and the time-of-flight (TOF). Although these mass analyzers differ in their operation mode, they all select m/z species from a mixture of peptide ions and subsequently fragment them producing the MS2 spectrum. The criteria by which m/z species are selected for subsequent fragmentation are defined as acquisition mode. In a typical shotgun proteomics workflow, peptides are analyzed in a “data-dependent acquisition” (DDA) mode, in which the mass analyzer selects the most intense ions (typically “top 10” or “top 15” most intense precursors) in a certain time window and subject them to fragmentation. To overcome the bias towards the most abundant species associated with the DDA mode, a “data-independent acquisition” (DIA) mode (Krasny & Huang, 2021) (also known as “sequential window acquisition of all theoretical mass spectra” (SWATH-MS)) can be adopted. In the DIA strategy, all detected precursor ions within a survey scan are fragmented, thus post-acquisition in silico data processing steps to deconvolute the resulting complex fragment ion spectra are required. Targeted proteomics approaches can also be designed. In this case, LC-MS/MS analysis is performed on peptides that can uniquely represent the target proteins and are selectively analyzed by Selected/Multiple Reaction Monitoring (SRM/MRM).

Another difference can be constituted by the employed peptide fragmentation techniques. The most common are the Collision-Induced Dissociation (CID) and Higher energy Collision Dissociation (HCD) methods (Olsen et al., 2007), in which protonated peptides are subjected to multiple collisions with rare gas atoms, resulting in the breakage of the peptide backbone at -CO-NH- bonds and in the formation of the

characteristic b- and y-ions (at N- and C-terminus, respectively). Electron Capture Dissociation (ECD) and Electron Transfer Dissociation (ETD) (Zubarev et al., 2000)induce fragmentation of the peptide backbone based on gas phase reactions using either thermal electrons or the formation of radical ions, respectively, and are particularly suitable for sequencing longer peptides or whole proteins.

3. The detector: the detector is located at the end of the mass spectrometer and records the number of ions at each m/z value. Commonly, the detectors are electron multipliers that emit a cascade of electrons when each ion hits the detector (Finehout & Lee, 2004), which results in a measurable current. This process is performed in vacuum conditions to remove gas molecules and contaminants, which can collide with sample ions.

The experiments reported in this thesis were performed on a Q Exactive HF Quadrupole-Orbitrap mass spectrometer (Michalski et al., 2011), constituted of a nano-ESI ion source, quadrupole mass filter coupled to an orbitrap mass analyzer operating in DDA mode, and fragmenting peptide through HCD. Finally, ions reaching the detector are processed by an "enhanced Fourier Transformation" algorithm to yield high-resolution mass spectra.

2.3 Quantitative MS-based proteomics

Mass spectrometry is not inherently a quantitative technique, due to multiple reasons. First, the ion intensity is not directly proportional to the amount, because it also depends on the physicochemical properties of the corresponding peptide. Second, the analysis of different LC-MS/MS runs is not perfectly comparable because each run can be influenced by external variations, like temperature and chromatographic separation reproducibility. Third, in the DDA mode, the choice of the precursor ion to be fragmented depends mostly on its abundance, thus if the peptide of interest is low abundant, it may not be identified and, as a consequence, quantified leading to a bias against low abundant proteins quantification

2.3.1 Quantification strategies

To overcome these limitations, different strategies have been employed. The most used relative quantification strategies belong to two main groups: label-free quantification (LFQ) strategies and strategies based on isotope labeling (**Fig.6**).

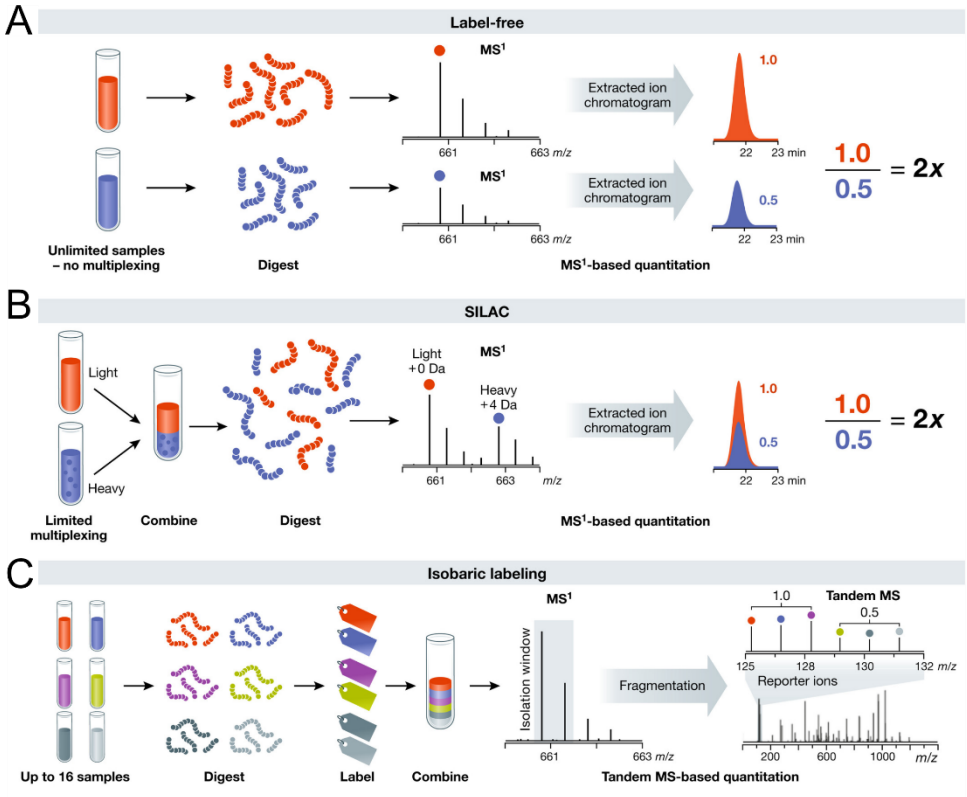

Figure 6: Quantitative MS-based proteomic approaches

Schematic representation of the most used MS-based approaches for quantitative proteomic analysis: **A**) label-free approach (XIC-based); **B**) Metabolic labeling approach (SILAC); **C**) Chemical labeling approach (TMT).
Adapted from: https://doi.org/10.15252/msb.20188792

Label-free strategies do not require a specific sample preparation because no labeling strategy is applied and the quantification is made post-acquisition. Among the label-free strategies we can further distinguish:

1) intensity-based strategies, where the quantification relies on the comparison of one or more peptide intensities of the same protein in different samples

2) spectral counting quantification strategies, based on the number of MS/MS spectra identified/annotated for the same protein in different samples.

In the first case, the ion chromatograms for every peptide are extracted from an LC-MS/MS run, and their mass spectrometric peak areas are integrated over the chromatographic time scale (Extracted ion chromatogram, XIC or area under the curve, AUC). XICs of the same peptide in different samples are extracted and compared for peptide quantification. Thus, these approaches require extremely reproducible chromatography among multiple runs and *ad hoc* software capable to perform retention time realignment and peptide intensity normalization over the global intensity. Instead, spectral counting strategies are based on the rationale that the abundance of a protein correlates linearly with the number of MS/MS spectra produced from its peptides. Thus, relative quantitation is achieved by comparing the number of such MS/MS spectra between a set of experiments. For this reason, a high number of acquired spectra is required, to avoid that the physicochemical properties of the peptides could influence the linear correlation between protein abundance and the number of spectra.

Label-free strategies have the big advantage that they can be extended to a theoretically infinite number of conditions and can be applied to every type of sample (such as cell lines, primary cells, tissues, etc.). However, LFQ requires much higher technical and experimental reproducibility to carry out robust statistical analysis and to distinguish reproducible biological variations from stochastic and technical signal fluctuations.

Isotope-based quantitation methods are all based on the same rationale. By creating a mass shift that distinguishes peptides deriving from different conditions within a single MS analysis, it is possible to reduce the variability due to multiple sample preparation and different MS runs. Depending on how proteins or peptides are labeled, isotope-based approaches can be grouped into two main strategies:

1) metabolic-labeling strategies

2) chemical-labeling strategies.

In the metabolic labeling strategy, the isotope is added to the media of growing cells as a metabolic precursor, so that it will be incorporated into the proteome during protein biosynthesis. The different conditions can be mixed, thanks to the fact the isotopes can be distinguished by MS. Moreover, sample mixing can be performed at the beginning of the proteomic workflow, thus minimizing processing errors and reducing operator work and machine time. The most successful metabolic labeling strategy is named Stable Isotope Labelling by Amino acids in Cell culture (SILAC) and was introduced by M. Mann and collaborators in 2002 (Ong et al., 2002) (See paragraph 2.3.2).

In chemical-labeling strategies, the tag is added covalently to the reactive side chains of amino acids either before or after the proteolytic cleavage through a chemical reaction. The most common methods for chemical labeling are isobaric tags for relative and absolute quantitation (iTRAQ) (Wiese et al., 2007)and tandem mass tags (TMT) (A. Thompson et al., 2003). In iTRAQ, side chains of lysine residues are labeled with an isobaric tag that allows the quantification at the MS2 level. The advantage of iTRAQ is the possibility of multiplexing, by using up to 8 different isobaric tags. However, the efficiency of the labeling is variable and depends on sample complexity. The TMT is based on the same principle, namely the use of isobaric tags attached at the N- terminus of a peptide or to a lysine residue, allowing the quantification at the MS2 level. Recently, kits for multiplexing with up to 16 different tags are commercially available. However, one limitation of these approaches is that the labeling is often performed at a later step of sample preparation, and this can result in less accurate protein quantification.

2.3.2 Stable Isotope Labeling by Amino acids in Cell culture (SILAC)

The Stable Isotope Labeling by Amino acids in Cell culture (SILAC), introduced by Mann and co-workers in 2002, is the most adopted metabolic labeling strategy. In a classical SILAC experiment, cell lines are grown in parallel in media supplemented either with standard essential amino acids (light, L) or with a non-radioactive isotopically labeled form of those amino acids (heavy, H). The cells are grown in these media for a sufficient number of cell doublings to ensure the full incorporation of the isotopes in the newly synthesized proteins. After complete labeling, cells grown in the two conditions will have two identical proteomes that differ only in isotope composition. In a standard SILAC experiment, the cells are usually labeled with H and L arginine and lysine, which in combination with trypsin digestion, ensure that all peptides of a protein (except the C-terminal one) carry one labeled amino acid. Upon MS analysis, every peptide will be represented as a peak pair, separated by a specific Δ mass that is dependent on both the type and the number of isotopically-encoded amino acids incorporated within the sequence **(Fig. 7)**.

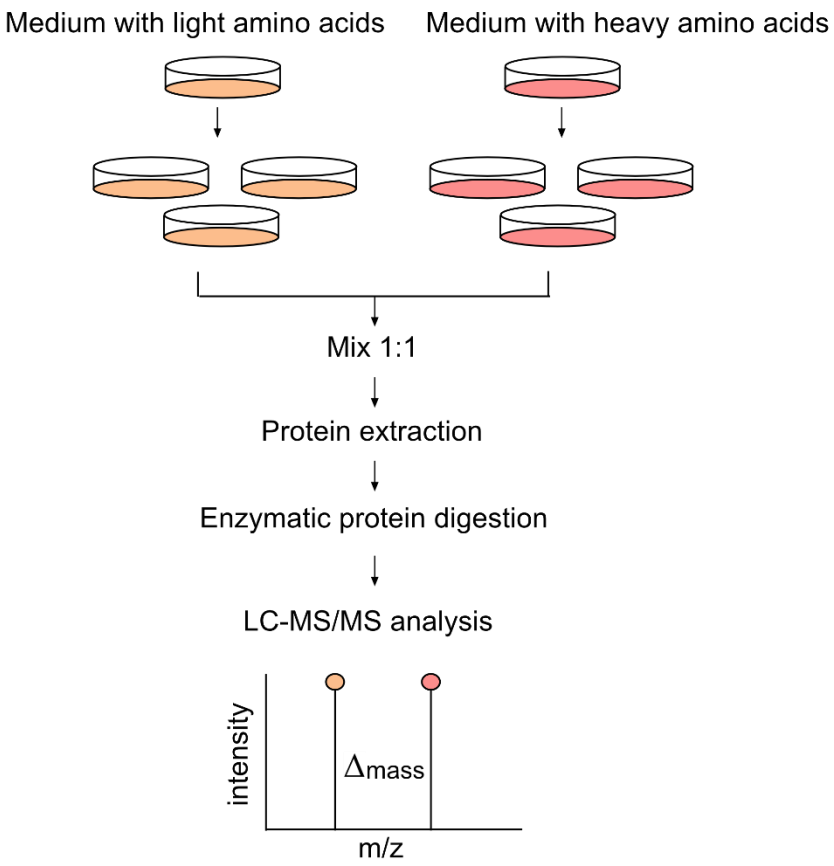

Figure 7: Scheme of a standard SILAC experiment

Two populations of the same cell line, one grown in a medium that contains 'light' (normal) amino acids and the other in a medium that contains 'heavy' amino acids, are kept in culture until full isotope incorporation (typically achieved through 8-10 replications cycles). Then two populations are harvested, mixed in 1:1 proportion, the proteins are then extracted, and enzymatically digested by protease into peptides, which are then subjected to MS analysis. The light and heavy forms of the same peptide can be distinguished by LC-MS/MS because of a specific delta mass; the relative intensity of the two peaks is considered proportional to the relative abundance of the corresponding protein of origin.

In the last years, the SILAC approach has been implemented and applied to a variety of proteomics workflows. Variations of the standard SILAC have also been described. For instance, it is possible to analyze three different functional states in a single run by adding a third channel composed of a different isotope mixture (triple SILAC) (Wang et al., 2018). Alternatively, it is possible to profile protein translation dynamics by the pulse SILAC (pSILAC) strategy (Schwanhäusser et al., 2009). Optionally, a particular variant of the SILAC approach named heavy methyl SILAC (hmSILAC) (Ong et al., 2004) can also be adapted for the high-confidence identification of methylated residues (more details in paragraph 2.4.2).

The main limitations of the SILAC strategy are the long time required for cell culturing to ensure full isotopic-amino acid incorporation and the limited multiplexing capability so that comparing more than three different conditions can only be achieved through complicated experimental setups.

2.4 MS-based proteomics to study protein PTMs

The PTM identification by MS relies on the detection of a mass difference (Δ mass) introduced by the modification compared to the mass of the unmodified peptide. PTM analyses are frequently conducted using procedures similar to those ones for protein identification, albeit these studies are more difficult because of some key features of PTMs. First, since modified peptides are sub-stoichiometric compared to unmodified ones, enrichment steps are essential for PTM analyses. Hence, for many PTMs, the absence of an efficient enrichment strategy is still a limiting factor. Second, it can be challenging to keep the peptide in its modified state during sample preparation because the covalent binding between the PTM and the amino acid side-chain of the peptide can be labile (as for phosphorylation). Third, some PTMs are quite dynamic, thus it is necessary to inhibit the erasers of the PTM of interest during sample manipulation, when possible.

2.4.1 Factors enhancing MS-based PTM analyses

To enrich modified peptides over unmodified peptides, a variety of strategies have been devised. These techniques include strong cation/anion exchange (SCX/SAX) chromatography, immobilized metal affinity chromatography (IMAC), titanium dioxide (TiO2) metal-based chromatography, hydrophilic interaction liquid chromatography (HILIC), and immuno-affinity enrichment of the modified peptide (Olsen & Mann, 2013). SCX and SAX are separation techniques that take advantage of the different charges acquired by peptides in the solution to reduce the sample complexity (Edelmann, 2011). For this reason,

they can be used as complementary strategies to reversed-phase chromatography. IMAC, TiO2, and HILIC are strategies widely used in phospho-proteomics studies and are based on the principle that Fe3+ or TiO2+ chelates the phosphate group of phospho-peptides (Ficarro et al., 2002; McNulty & Annan, 2008). Immuno-affinity enrichment (antibody-based) for modified peptides is strictly dependent on the antibody availability and efficiency and, with few exceptions, the required starting material is sensibly larger than the one typically needed for general proteomic analysis.

Furthermore, a general rule in MS-based global PTM studies is to produce adequate peptide fragmentation (MS/MS) for high-confidence sequence identification and modified site localization. Recently, new instruments have been developed that simultaneously offered high resolution and high mass measurement accuracy at the MS and MS/MS levels. This was made possible in part by the use of diverse fragmentation methods, such as ETD (see paragraph 2.2), which enhance the analysis of multi-modified peptides. In addition, to overcome the problems related to ambiguous PTM assignments, a number of algorithms, such as the PTM score, have been developed to statistically assess the location of a PTM on a peptide (Shteynberg et al., 2019).

2.4.2 Challenges in the MS-based analysis of protein R-methylation

Although MS-based proteomic is considered the best strategy available for global analysis of protein R-methylation, the application of MS-based workflows to this PTM appeared very challenging for a number of reasons.

a. As discussed above, also for this modification, the modified peptides are sub-stoichiometric compared to the unmodified ones and need to be enriched prior to MS. In the last years, a set of rather efficient pan-methyl antibodies against R-mono-methylated, R-asymmetrically- and R-symmetrically-di-methylated peptides were developed and put on the market. However, the antibodies recognizing the three types

of R-methylation did not display comparable immuno-precipitation efficacy, with a bias for the MMA towards the other modification degrees, which led to the initial hypothesis of MMA being much more abundant than the other R-methylations. Moreover, although rather selective, these antibodies display limited affinity, so very large amounts of starting material (at least 10mg of peptides) are required per experiment, which still represents a major limitation to their applicability.

b. Several amino acid substitutions are isobaric to R-methylation. Two (or more) ions are isobaric if they have the same nominal mass, but different exact masses. In this case, a peptide bearing an R mono-methylated differs from the same peptide bearing the unmodified R by a mass difference of +14.016 Da. Unfortunately, a peptide bearing glycine and methylated R would be indistinguishable from the same peptide with a glycine-to-alanine substitution, because they have the same nominal mass (Ong et al., 2004) and many other amino acid substitutions presenting the same nominal mass of methylation exist.

c. Also, chemical artifacts introduced during sample preparation can lead to the miss-assignment of an R-methylation. For instance, the use of methanol can cause mono-methylation of glutamic and aspartic residues, which can be undistinguishable from- and may be interpreted as the R-methylation assignment to a neighboring K/R in database searches, especially when a limited set of variable PTMs is provided to the search engine (Ong et al., 2004; Nielsen et al., 2006).

For all these reasons, the identification of R-methylated sites by MS can produce a high number of false positives (high FDRs). When studying PTMs, the standard method to control false positive peptide identifications is the application of the target-decoy approach (see paragraph 2.2), which allows estimating FDR. However, a study from the group of Mark Wilkins demonstrates that the application of <1% FDR for a large-scale methyl-proteomic analysis is not sufficient (Hart-Smith et al., 2016). Thus, nowadays the best strategy for high-confidence identification of *in vivo* enzymatically-

driven protein R-methylation is based on orthogonal validation, through the application of the hmSILAC labeling strategy at the level of sample preparation (Ong et al., 2004). In this variant of the standard SILAC, the cells are grown in a medium supplemented with either normal ("light") or "heavy" methionine. Heavy methionine ([$^{13}CD_3$]-methionine, or Met4) contains a methyl group with one carbon-13 and three deuterium atoms. Upon uptake by the cells, [$^{13}CD_3$]-methionine is metabolically converted into [$^{13}CD_3$]-adenosil-methionine (AdoMet or SAM), the only biological donor of methyl groups. The [$^{13}CD_3$]-methionine is therefore incorporated into the backbone of newly synthesized proteins and, in addition, the heavy methyl-groups are transferred by PRMTs from isotopically-encoded SAM to their substrates, resulting in the heavy labeling of all R-methyl sites on a protein (**Fig. 8A**). The workflow of a hmSILAC experiment is essentially identical to a standard SILAC experiment, except for the fact that the cells are grown in medium supplemented with heavy methionine instead of arginine and lysine. Upon channel mixing, protein extraction, and proteolytic digestion into peptides, LC-MS/MS analysis permits to identify of peptides as a pair that differs for +4 Da for each methyl group (in the case of R-methylation +4Da for mono-methylation, and +8 Da for di-methylation). Importantly, the use of hmSILAC strategy strongly increases the confidence in the MS-based identification of methyl-peptides, because the presence of the heavy and light pairs leads to distinguishing *in vivo* enzymatically-driven methylation from potential false positives, such as amino acids substitution (**Fig. 8B**).

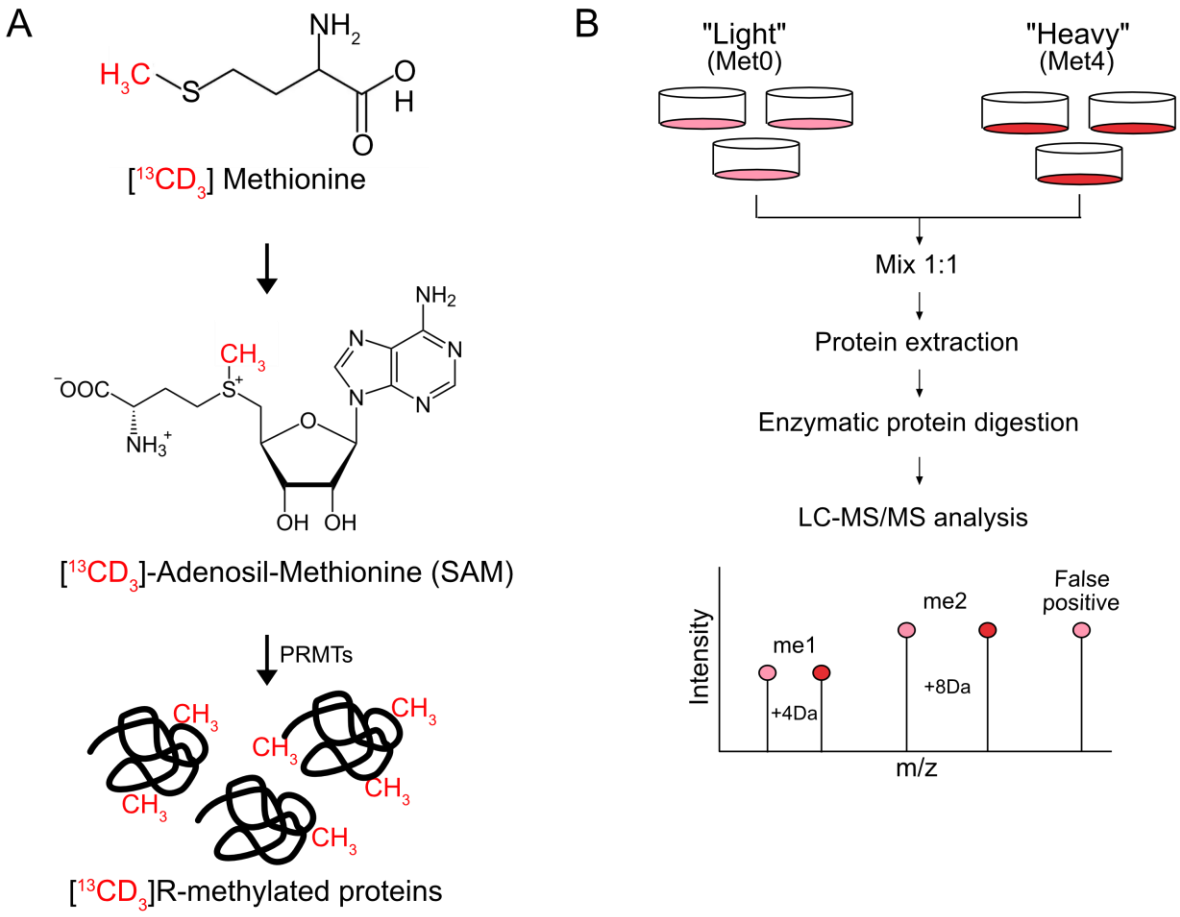

Figure 8: heavy methyl SILAC strategy

[$^{13}CD_3$]-methionine (heavy) is metabolically converted into heavy S-adenosyl-methionine (SAM) in the cell. Through enzymatic reactions, heavy methyl groups from SAM are transferred onto new R-methylated proteins by PRMTs. **B)** Upon mixing of the light (Met0) and heavy (Met4) labeled cells in equal amounts (1:1), protein extraction and proteolytic protein digestion into peptide are performed. The obtained peptides are analyzed by high-resolution MS, which can discern genuine methylated residues on the basis of the presence of peptide pairs bearing specific delta masses (4 Da = mono-methylation, 8 Da = di-methylation) from the false positive peak, which will appear as a singlet.

For this reason, hmSILAC has emerged as the “gold standard” to minimize FDR in a global analysis of protein methylation by MS (Musiani et al., 2019). In 2019, our group developed and published “hmSEEKER”, one of the first bioinformatic tools specifically designed for the identification of methyl-peptide pairs from hmSILAC MS raw data (Massignani et al., 2019). hmSEEKER searches for the isotopic peptide pairs (doublets) among all detected MS1 peaks, enabling the identification of methyl-doublets even if only one of the two peaks in the isotopic

peptide pair is fragmented in MS/MS. An example of a successful application was achieved in a recent publication from our group that I also co-authored: by combining hmSILAC labeling, protein immunoprecipitation, MS-based shotgun proteomic, and data analysis through hmSEEKER, we obtained the high confidence annotation of the large drosha complex (LDC) methyl-proteome. This dataset was subsequently used to orthogonally validate the R-methyl sites dynamically regulated in dependence on PRMT1 activity, which -in turn- allowed us to demonstrate a functional role of PRMT1 in modulating LDC activity and consequently miRNA biogenesis (Spadotto et al., 2020).

2.5 State-of-the-art on global R-methyl-proteomics studies and the contribution of our group in the field

In the last 20 years, a few groups exploited MS-based approaches to perform global analyses of protein R-methylation, undertaking different strategies for biochemical enrichment and fractionation methods of R-methylated peptides to increase their identification by MS. In 2004, Mann's group introduced for the first time the above-described hmSILAC strategy used in combination with antibody-based enrichment and identified 59 high-confidence *in vivo* methylated sites. The limited number of R-methylations detected was mainly due to two factors: 1) the use of antibodies recognizing methylated protein instead of methyl-peptides; 2) unfractionated whole-cell extracts used were used as input, thus missing the advantage of chromatographic fractionation to reduce sample complexity prior to affinity enrichment. In 2013, the hmSILAC was used by our group in combination with SDS-page and isoelectric focusing protein separation and antibody-based enrichment of R-methylated proteins, leading to the identification of 397 high-confidence *in vivo* R-methyl-sites (Bremang et al., 2013).

Since 2014, the commercialization of antibodies specifically raised against R-mono-, symmetrically, and asymmetrically di-methylated peptides created the condition for the development of more efficient protocols to enrich R-methylated peptides instead of proteins

prior to MS. In parallel, another crucial step to improve the R-methyl-proteomics workflow was the introduction of a step of peptide separation prior to the peptide affinity-purification: in particular, off-line high-pH (HpH) reversed phased (RP) peptide chromatographic fractionation was shown to be the most efficient principle for separation within this workflow. A few months ago, we published a methodological paper, that I co-authored, that describes the currently most efficient MS-based proteomic workflow for high-confidence R-methyl-peptides identification from cellular samples (Maniaci et al., 2022). This workflow couples hmSILAC metabolic labeling of cells with dual protease (trypsin and LysargiNase) in-solution protein digestion of whole cell extract followed by off-line High pH Reversed Phase (HpH-RP) chromatography fractionation and immuno-affinity enrichment of fractionated R-methyl-peptides using anti-pan-R-methyl antibodies. Upon high-resolution MS analysis, the raw data were processed with the MaxQuant software package, and the output data was analyzed by hmSEEKER to obtain the most comprehensive list of high-confidence truly methylated R sites (**Fig. 9**).

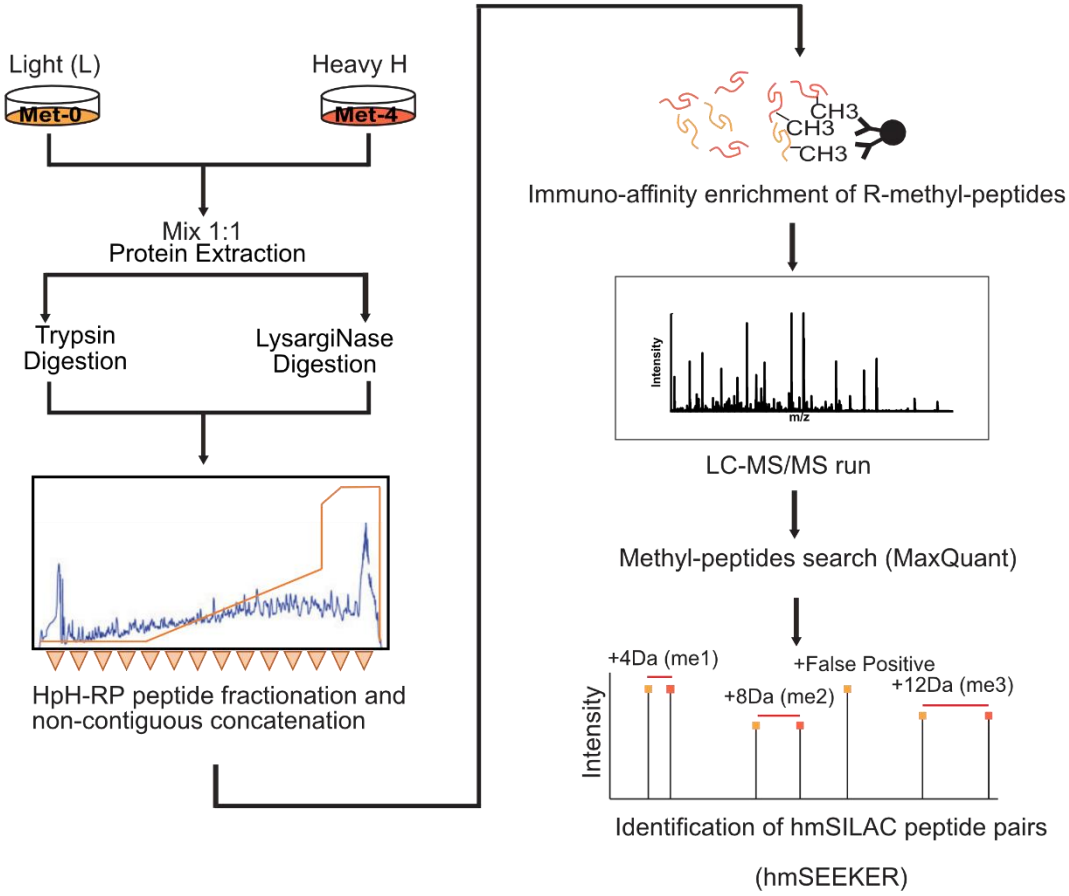

Figure 9: Schematic workflow for in-depth analysis of R-methyl sites

Cells are grown in light (Met-0) and heavy (Met-4) methionine-containing medium and mixed in 1:1 proportion. Proteins are extracted and subjected to digestion with trypsin or LysargiNase in parallel and fractionated by off-line HpH-RP liquid chromatography by collecting 60 fractions, finally concatenated into 14 fractions. R-methyl-peptides are enriched by anti-pan-R-methyl antibodies and analyzed by LC-MS/MS. Raw MS data are processed by MaxQuant algorithm for peptide and PTM identification. MaxQuant output data are then submitted for analysis by hmSEEKER bioinformatic tool, for the heavy and the light methyl-peptide association. Adapted from doi:10.3791/62409 (2022).

For what concern the improvement in the bioinformatics analysis, in the last 2 years our group worked on improving hmSEEKER algorithm by the inclusion of a machine learning model to recognize hmSILAC doublets and implemented in a novel version of the bioinformatic tool (hmSEEKER 2.0). This new version was then used to reanalyze all the hmSILAC experiments collected in our laboratory so far in order to generate the most comprehensive dataset of high-confidence protein methylations annotated in human cancer cells, thus generating the ProMetheus database (ProMetheusDB) , now published and freely accessible to navigation to

the scientific community (Massignani et al., 2022) (https://bioserver.ieo.it/shiny/app/prometheusdb).

2.6 Functional studies about the role of R-methylation in specific biological processes: response to genotoxic stress

In 2020 (in a work that I co-authored), our group investigated global protein R-methylation remodeling in the context of cisplatin (CDDP)-induced replicative stress, in a cellular model of ovarian cancer (Musiani et al., 2020). Applying a proteomic approach including SILAC metabolic labeling with HpH RP chromatographic fractionation of the peptides, and peptide immuno-affinity enrichment, we reproducibly quantified 441 R-methyl peptides that were orthogonally validated by the hmSILAC strategy. Interestingly, when we linked the CDDP-regulated R-methyl sites to their respective proteins, we observed various chromatin-associated factors among the proteins whose R-methylation was increased, while the proteins whose R-methylation was reduced were largely represented by RNA-binding proteins (RBPs) (**Fig.10**).

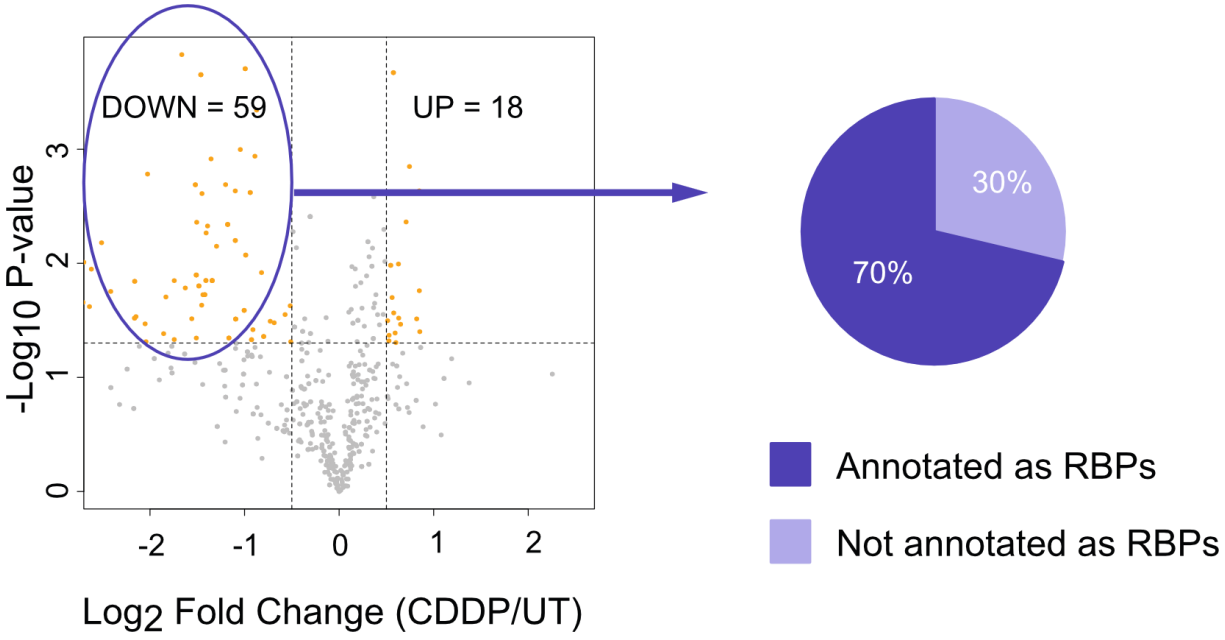

Figure 10: Most of the CDDP-downregulated R-methyl sites belong to RBPs

Volcano plot displaying the R-methyl-peptides significantly changing in response to CDDP treatment. To calculate the significantly regulated peptides, only R-methyl-peptides owing an Andromeda score >25 and a localization probability > 0.75 were considered. Methyl-peptide SILAC ratios were normalized over the corresponding protein SILAC ratios. To define significantly up- and down-regulated peptides, the cut-offs FDR< 0.05 and CDDP/UT SILAC fold change >0.5 were applied. Then, the list of proteins whom R-methyl sites resulted down-regulated were intersected with the list of proteins annotated as RNA-binding proteins (RBPs) in the EuRBP database. Adapted from (Musiani et al., 2020)

This interesting evidence represented the foundations of my research project as it prompted us to investigate more systematically the impact of R-methylation on the RBP-RNA dynamics and its functional implication in cancer cell biology (see "AIM OF THE PROJECT" section).

2.7 RNA-Binding proteins and possible methods to globally study protein-RNA interactions and their dynamics

RNA-Binding Proteins (RBPs) comprise a large class of proteins (almost 2.000 in mammals) (Quattrone & Dassi, 2019), capable to bind both single-strand and double-stranded RNA and in turn to regulate a plethora of RNA-related biological processes, including RNA nucleus-cytosol transport, RNA splicing mRNA polyadenylation to RNA translation and regulation of non-coding RNA. The structures and mechanisms by which RBPs bind and regulate RNA are extremely diverse. RBPs typically contain RNA-Binding Domains (RBDs), which differ for the purpose of binding: Cold Shock Domain (CSD), double-stranded RNA Binding Domain (dsRBD), dead/deah or helicase domain, Intrinsically Disordered Region (IDR), K Homology (KH) domain, P-element Induced Wimpy Testis (PIWI) domain, pseudouridine synthase, and archaeosine transglycoslyase (PUA) domain, Pumillo-like repeat (PUM) domain, RNA Recognition Motif (RRM), Ribosomal S1-like (S1) domain, Sm and Like-sm (Sm / Lsm) domain, YT521-B homology (YTH) domain and Zinc Finger (ZnF) domain (Corley et al., 2020).

Given the importance of characterizing how RBPs and RNA interact, different strategies for RNA-RBP interactions investigation have been proposed that can be summarized into two major categories: RNA-centric and protein-centric methods (**Fig.11A and 11B**). Among the RNA-centric procedures, A.Castello and colleagues described a technique named RBDmap, for identifying the regions of RBPs hooked up in native interactions with RNA (Castello et al., 2017). This represents an extension of the strategy previously described by the same group to identify poly(A)-mRNA-interacting RBPs and named RNA Interactome Capture (RIC) (Castello et al., 2013a). Cultured cells are UV-irradiated to fix RBP-RNA binding covalently and the resulting RBP–RNA complexes are isolated through oligo(dT) magnetic beads. After elution, RBPs undergo partial proteolysis, in which the protein regions are still bound to and protect portion of RNA, while RNAs released to the supernatant are separated by a second oligo(dT) affinity purification. After sample preparation and mass spectrometric analysis, peptide intensity ratios between the RNA-bound and released fractions are used to determine the RNA-binding regions. Variants of the RIC strategy, such as quantitative RIC (Vieira-Vieira et al., 2022), and enhanced RIC (eRIC) (Perez-Perri et al., 2018a), were also described. Still, the major limitation of these RNA-centric strategies namely that it allows the purification of only RNA with poly(A) tails, remains. To overcome this limitation, the chemistry-assisted RIC (CARIC) (R. Huang et al., 2018) variant was designed. It enriches both poly(A)-RNAs and non-poly(A)-RNAs through metabolic labeling of RNAs with photoactivatable and "clickable" nucleoside analogs 4-thiouridine (4SU) and 5-ethynyluridine (EU). However, since the copper (Cu) used as the catalyst in click reactions can cause the fragmentation of RNAs, the maintenance of RNA integrity is a possible problem of this approach.

Protein-centric methods, such as RNA immunoprecipitation (RIP) (Gagliardi & Matarazzo, 2016) or cross-linking and immunoprecipitation (CLIP) (Hafner et al., 2021), were designed. In the RIP approach, a specific antibody against the RBP of interest is required to pull down the RBP-RNA complexes. Subsequently, RNA associated with this protein can be isolated

and analyzed by polymerase chain reaction (PCR)-based methods or RNA-sequencing (RNA-seq). The RIP approach purifies the RBP-RNA complexes both under native conditions and using formaldehyde cross-linking. The CLIP techniques follow different reasoning: after UV-crosslinking to irreversibly fix RBP-RNA binding, protein-immunoprecipitation and the following limited RNase treatment leads to isolating RNA fragments protected by the RBP, while sequencing of these fragments permits the identification of RNA-binding sites. Despite numerous CLIP variants being implemented, in all cases, the immunoprecipitation of the protein of interest remains a required step, thus limiting the investigation to one protein at a time.

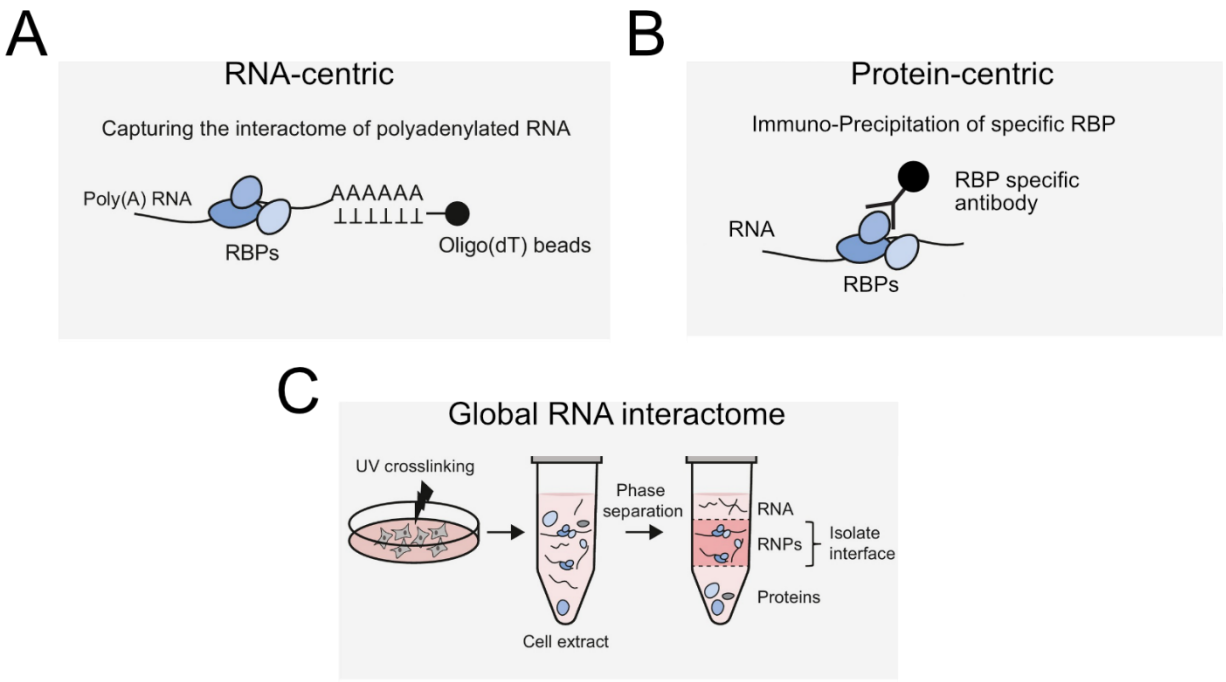

Figure 11: Schematic overview of the possible methods to study RB-RNA interaction

A) Example of an RNA-centric method: poly(A)-mRNA pulldown and subsequently RBP analysis. **B**) Example of a protein-centric method: specific RBP immunoprecipitation and subsequent analysis of associated RNA. **C**) Example phase separation-based strategy for a global and unbiased RNA interactome analysis. Adapted from DOI:https://doi.org/10.1016/j.tibtech.2020.11.011

To overcome these limitations, in the last years, some unbiased strategies exploiting the physicochemical properties of the RBP-RNA complexes were proposed, such as the Orthogonal Organic Phase Separation (OOPS) (Queiroz et al., 2019), the protein-crosslinked RNA extraction (XRNAX) (Trendel et al., 2019), and the Phenol Toluol extraction (PTex) (Urdaneta et al., 2019). With some variation, these methods are all essentially based on a similar rationale: upon irradiation with UV light at 254 nm to induce covalent RBP-RNA cross-links, the cells are subjected to organic extraction by acid guanidinium thiocyanate-phenol (commercially known as TRIzol™)- chloroform mixture. This leads to the separation of three different parts: an upper part (the aqueous phase) containing free RNAs, a small interface containing RBP-RNA complexes, and a lower part (the organic phase) containing free proteins (**Fig. 11C**). To characterize these interactions from a system-wide perspective the interface-enriched RBP-RNA complexes are subsequently digested with RNase and proteins can be analyzed by MS. Alternatively, proteins can be digested with proteinase to allow the analysis of RNAs by RNA-sequencing (RNA-seq).

One difference between the three strategies is the phase partition step: in the OOPS strategy, the purification of RBP-RNA complexes is achieved by three sequential rounds of TRIzol™-chloroform phase partitions. The XRNAX uses a single TRIzol™-chloroform phase separation, followed by DNA digestion, and partial protease digestion, which results in RNA-peptide adducts enrichment that can be isolated using silica-based columns. The PTex uses an initial pH 7.0 phenol:toluol phase partition, which separates DNA and lipids from the proteins and the RNA in the aqueous phase. The aqueous phase is then recovered and subjected to two rounds of TRIzol™-chloroform phase separation to enrich RBP-RNA adducts at the interface (**Fig. 12**).

These unbiased strategies provide global information with no need of an antibody-based affinity enrichment of specific RBP or poly(A)-mRNA pulldown; hence, non-poly(A)-RNA classes (tRNA, rRNA, pre-mRNA) can also be analyzed. Moreover, compared to the previously described RNA-centric and protein-centric methods, which require a considerable amount of

starting material, strategies based on physicochemical phase-partition require lower starting material (OOPS ~3×10^6 cells, PTex ~5×10^6 cells, and XRNAX ~8×10^7 cells), facilitating comparative analyses in different functional conditions (multiplexing).

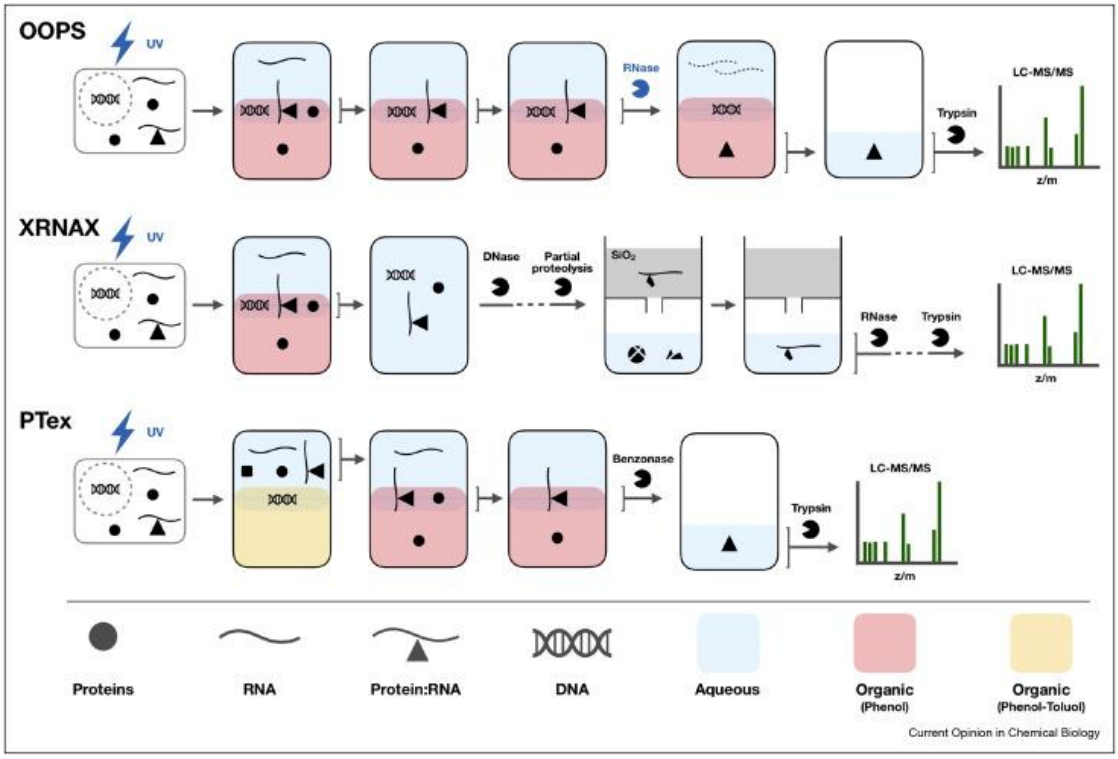

Figure 12: Phase separation–based approaches to enrich RNA-binding proteins

Graphic representation of the major differences between the three phase separation-based approaches: Orthogonal Organic Phase Separation (OOPS), protein-crosslinked RNA extraction (XRNAX), and Phenol Toluol extraction (PTex). Taken from https://doi.org/10.1016/j.cbpa.2020.01.009

2.8 Intrinsically Disordered Regions, Liquid-Liquid Phase Separation, and Stress Granules formation

Thanks to the above-mentioned methods to study RBP-RNA interaction, numerous new putative RBPs were identified. Many of these newly identified RBPs do not contain structured RBDs, but rather contain Intrinsically Disordered Regions (IDRs), which are

defined as protein sequences that lack a defined 3D structure under physiological conditions (Calabretta & Richard, 2015). Even if IDRs are not folded or partially folded, it has been shown that they can mediate RBP-RNA interactions. IDRs include Short Linear Motifs (SLiMs), Molecular Recognition Features (MoRFs), and Low Complexity (LC) regions. Among LC regions, the RGG/RG motifs are highly abundant in RBPs and represent one of the most frequent RNA-binding sequences (Castello et al., 2012). The importance of RGG-repetitive regions as putative RNA-binding regions was first described in 1992, when it was demonstrated that the RGG/RG motif of hnRNPU mediated its interaction with RNA (Kiledjian & Dreyfuss, 1992). The IDRs are evolutionarily conserved, which emphasizes the functional importance of these regions.

In the last years, the presence of IDRs in RBPs was linked to the formation of dynamic RBP-RNA complexes termed “Membrane Less Organelles (MLOs)”, also described as “bodies, puncta, granules, droplets, or biomolecular condensates”. The term MLOs describes local subcellular compartments, both in the cytosol and in the nucleus, which are not physically separated by a membrane and are composed of RBPs and RNA that aggregate as a consequence of the Liquid-Liquid Phase Separation (LLPS) phenomenon. Stress Granules (SGs), Processing bodies (P-bodies), and P-granules have been described as cytosolic MLOs. In contrast, nucleoli, PML bodies, Paraspeckles, and Cajal bodies gave been identified in the nucleus. Due to their liquid-like nature and the lack of physical separation through a membrane, MLOs formed by LLPS can dynamically change in composition, being created and disintegrated in response to various external or internal signals. Among the different MLO types, SGs are the best characterized as key regulators of cellular response to different types of stress stimuli, such as oxidative stress, hypoxia, endoplasmic reticulum stress, heat shock, starvation, the presence of translation-blocking drugs, and viral infection. SGs are considered temporary mRNA storages and translational regulators. The best described SG assembly pathway involved the phosphorylation of the eukaryotic translation initiation factor 2 subunit alpha (eIF2α) as a consequence of a

stimulus, which leads to translational arrest and accumulation of mRNAs, RBPs, and other proteins into SGs. However, SG formation can be independent of eIF2α phosphorylation. For instance, it was shown that inhibition of the eukaryotic translation initiation factor 4A (eIF4A), an RNA helicase required for ribosome recruitment during translation initiation, induces SG formation independently on eIF2α phosphorylation (Mazroui et al., 2006). Different models of SG assembly and disassembly have been proposed: the most supported theory involves the formation of an SG core constituted by nucleating RBPs such as Ras GTPase-activating protein-binding protein 1 (G3BP1), T-cell intracellular antigen-1 (TIA-1), and fragile X mental retardation protein (FMRP). The SG core then grows rapidly and includes a second shell, whose protein composition is variable and depends on the type of stress. When the stress conditions stop, SGs are either disassembled by molecular chaperons or removed by autophagy (Marcelo et al., 2021).

Within the mechanisms driving SGs formation, RNAs can also play relevant roles. Transcriptomic analysis of isolated SGs revealed that over 80% of SG-enriched RNAs are long, poorly translated mRNAs, with also the presence of some non-coding RNAs (Khong et al., 2017). It was shown that free mRNA in excess served as a scaffold for SG formation (Bounedjah et al., 2014) and that the presence of multiple N6-methyladenosine (m6A) modifications on mRNA enhances LLPS (Ries et al., 2019).

Importantly in the context of our study, post-translational modifications occurring on RBPs can also regulate interactions with RNAs and in turn, SG formation (**Fig. 13**). For instance, phosphorylation of serine 51 on eIF2α, a marker of translation arrest, leads to SG formation (Ohn & Anderson, 2010). SUMOylation of eIF4A2 was shown to regulate SG formation (Jongjitwimol et al., 2016) and, remarkably, loss of R-methylation of UBAP2L (C. Huang et al., 2020), FUS (Qamar et al., 2018) and G3BP1 (Tsai et al., 2016) was also been shown to enhance SG formation.

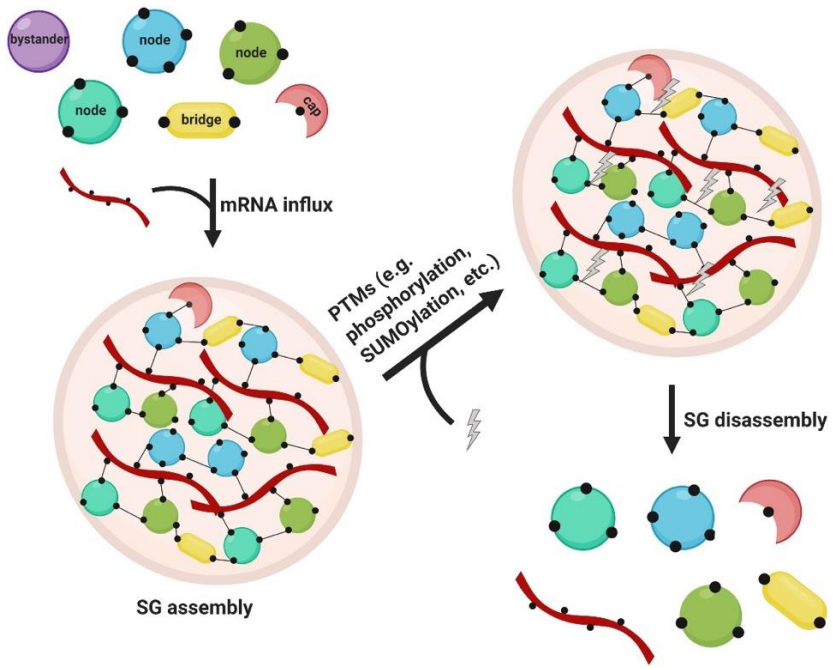

Figure 13: Molecular mechanisms of SG assembly and disassembly through PTMs

Model illustrating how different PTMs can regulate both assembly and disassembly of SGs. Taken from https://doi.org/10.1016/j.bbamcr.2020.118876

In summary, all the pieces of evidence collected experimentally by our group in the last years and integrated with published literature, led us to formulate a model whereby different types of stress (in our case platinum-based chemotherapy) can influence the activity/localization of PRMTs thus impacting globally the methylation-state of RBPs. This can modulate RBP-RNA interaction and -in turn- their propensity to form MLOs through phase separation. This hypothetical model represented the foundations of my Ph.D. project and will be more extensively discussed in the next section.

3. AIM OF THE PROJECT

Elaborating on the hypothesis that the modulation of the R-methylation state of some RBPs may affect their capability to bind cognate/target RNAs and that this may have implications in the cancer cell's response to various types of stress conditions, with my Ph.D. project I aim at carrying out the first systematic characterization of the role of protein-R-methyltransferases (PRMTs) in regulating protein-RNA interaction dynamics, through the modulation of the R-methylation states of specific RBPs. This aim will be achieved through a combination of biochemical and cell biology assays, coupled with quantitative MS-based proteomics and modification proteomics.

First, I plan to investigate the impact of R-methylation remodeling on RBP-RNA interaction directly through the pharmacological inhibition of PRMTs (**Fig. 14A**), and then, indirectly, by assessing the effect of the chemotherapeutic drug cisplatin on global protein-R-methylation modulation, protein-RNA dynamics and formation of membrane-less organelles (MLOs) through phase-separation (**Fig. 14B**).

In this way, I plan to shed light on the multi-layer effect of PRMTs on the activity, interaction, subcellular localization, and biological role of specific RBPs in the context of cancer cell's stress response to chemotherapy, ultimately paving the way to the development of possible strategies to tackle the onset of chemoresistance through combinatorial treatment including PRMT inhibitors.

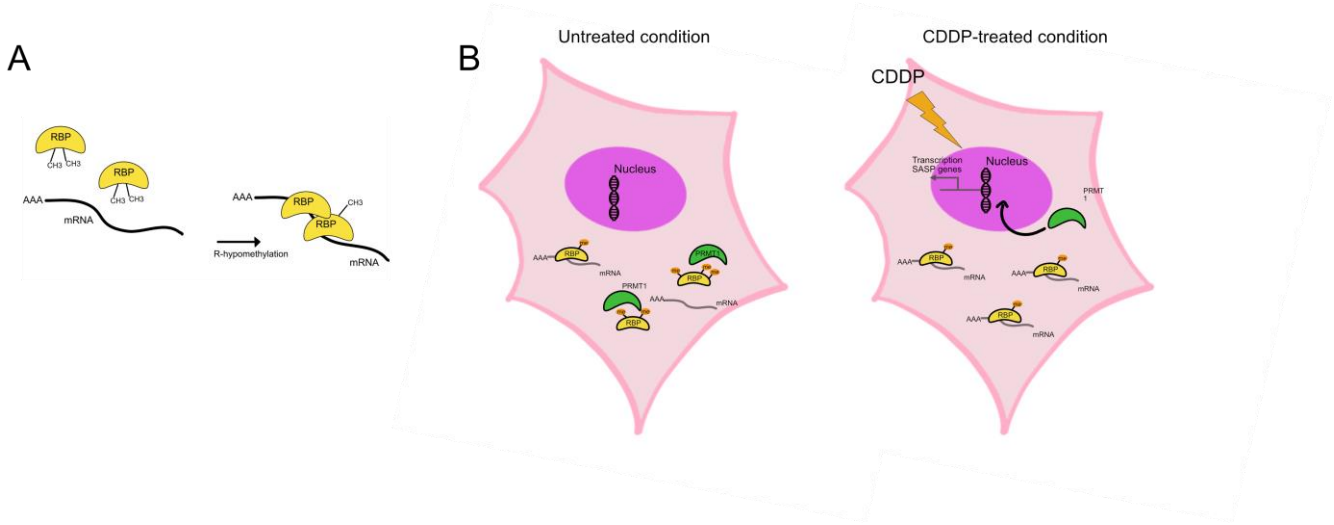

Figure 14: RBP R-methylation remodeling impact RBP-RNA interactions

A) PRMT pharmacological inhibition leads to R-hypomethylation and consequent increase of RBP-RNA interactions. **B**) Upon CDDP treatment, PRMT1 accumulates on the chromatin, causing the increase of H4R3me2a and the transcriptional activation of SASP-related genes, while in the cytosol, RBP targets of PRMT1 remain R-hypomethylated and this result in increased affinity for cognate RNAs.

4. MATERIALS AND METHODS (M&M)

4.1 Cell culture and drug treatments

HeLa, A2780, and COV362.4 cells were grown in Dulbecco's modified Eagle's medium (DMEM) High Glucose with Stable L-glutamine (Euroclone Spa, ECM0103L) supplemented with 10% Fetal Bovine Serum South American (FBS_SA, Microtech Srl S1860-500). Caov-3 cells were grown in DMEM High Glucose with Stable L-glutamine (Euroclone Spa, ECM0103L) supplemented with 10% Fetal Bovine Serum North American (FBS_NA, Fisher Scientific, 12389802). SK-O-V3 cells were grown in Roswell Park Memorial Institute (RPMI) 1640 With Stable L-glutamine (Euroclone Spa, ECM2001L) supplemented with 10% Fetal Bovine Serum North American (FBS_NA, Fisher Scientific, 12389802). OVCAR3 cells were grown in RPMI 1640 With Stable L-glutamine (Euroclone Spa, ECM2001L) supplemented with 10% Fetal Bovine Serum North American (FBS_NA, Fisher Scientific, 12389802). OV90 cells were grown in Medium 199 and MCDB 131 mixed in 1:1 proportion and supplemented with 2mM L-glutamine and 15% Fetal Bovine Serum North American (FBS_NA, Fisher Scientific, 12389802). All the media were supplemented with 100 U/ml penicillin and 100 mg/ml streptomycin. All the cells were cultured at 37°C in a 5% CO_2 humidified atmosphere and tested free of mycoplasma contamination. MS023 was purchased from Cayman chemical; GSK591 was purchased from Sigma-Aldrich. Both PRMT inhibitors were used for 48h, together with DMSO as control, at 10μM (MS023) and 5μM (GSK591), respectively. 17-(Allylamino)-17-demethoxygeldanamycin (17-AAG, HSP90 inhibitor) was purchased from Sigma-Aldrich and used at 1μM for 24h. Cisplatin (CDDP) was obtained from the hospital pharmacy at the European Institute of Oncology (Milan, Italy) and used at 20μM for 24h.

4.2 Stable-isotope labeling by amino acids (SILAC) of HeLa cells

For triple SILAC, HeLa cells were grown in ‘‘Light’’, ‘‘Medium’’ and ‘‘Heavy’’ SILAC DMEM (Thermo Fisher Scientific), supplemented with either L-arginine (Arg0, R0, Sigma-Aldrich), L-lysine (Lys0, K0, Sigma-Aldrich) or their medium (Arg6, R6, Sigma-Aldrich; Lys4, K4, Sigma-Aldrich) or heavy (Arg10, R10, Sigma-Aldrich; Lys8, K8, Sigma-Aldrich) isotope-counterparts. Arginine and lysine were added at a concentration of 84mg/L and 146mg/L, respectively. SILAC media were supplemented with 10% dialyzed FBS (GIBCO, Life Technologies), 100U/ml penicillin, and 100mg/ml streptomycin. HeLa cells were grown in the respective heavy-isotopes containing media for at least 9 replication cycles, to ensure full incorporation of isotope-encoded amino acids, with careful monitoring of growth rate, viability, and overall morphology by growing in parallel HeLa cells in a normal medium.

4.3 Cell lysis and protein extraction

For the preparation of whole cell extracts (WCE), cell pellets were lysed in 2 volumes of UREA lysis buffer (9M UREA, 20mM HEPES (pH 8.0)) supplemented with fresh 1X protease inhibitors cocktail (Roche), 1X phosphatase inhibitors cocktail (Roche) and 1mM DTT. Lysates were then sonicated by ultrasonic cell disruptor (Brandson) for 3 cycles (each cycle 30sec ON and 30sec OFF), centrifuged for 10 min at 12000 g at room temperature (RT) to precipitate cell debris and then supernatant loaded on SDS-PAGE for subsequent protein separation.

4.4 Enrichment of protein-RNA complexes through the Orthogonal Organic Phase Separation (OOPS) strategy

The OOPS strategy was firstly described in (Queiroz et al., 2019). This method is based on the physicochemical properties of the Trizol^{TM}-chloroform mixture which, upon UV-crosslinking to covalently stabilize protein-RNA binding, enables unbiased recovery of all

RNA species and associated RNA-Binding-Proteins (RBPs). More in detail, cells were exposed to UV radiation (254nm) at a dose of 40 J/m^2 using a Stratalinker 2400 UV cross-linker (Stratagene, La Jolla, CA). Immediately after crosslinking, cells were scraped in 5mL PBS 1x supplemented with 2mM EDTA and centrifuged for 10 min at 350 g. The obtained pellets were snap-frozen using dry ice and saved at -80°C until all the required biological replicates were collected. Biphasic extraction was performed by Trizol™ (Fisher Molecular Biology) and chloroform (Fisher Scientific) in the proportion of 1mL: 200µL. The obtained mixture was vortexed and centrifuged for 15 min at 12000 g at 4°C. The interface fraction (containing the protein-RNA complexes) was subjected to two additional phase separation cycles and precipitated by the addition of 9 volumes of cold propan-2-olo and centrifuged for 15 min at 12000g at 4 °C.

For protein: the precipitated interface fraction was re-suspended in 100µL of RNA digestion buffer (100mM TEAB, 1mM MgCl2, 1% SDS) incubated at 95ºC for 20 min, cooled down, and digested with 4µg RNase A, incubating overnight at 37ºC. The following day, after a final Trizol™-chloroform phase partition, proteins in the organic phase were precipitated by the addition of 9 volumes of propan-2-olo, centrifuged for 15 min at 12000 g at 4°C, and re-suspended in UREA lysis buffer (9M UREA, 20mM HEPES (pH 8.0)).

For RNA: the precipitated interface fraction was re-suspended in 100µL of protein digestion buffer (30mM TrisHCl pH 8, 10mM EDTA, 18U Proteinase K (Sigma-Aldrich)) and boiled for 2h at 50°C. After new precipitation by propan-2-olo, each pellet was washed with 1mL of 75% ethanol. Finally, each sample was centrifuged for 5 min at 7500 g, the supernatant discarded and the pellet re-suspended in 30µL of nuclease-free water.

4.5 Enrichment of protein-mRNA complexes through the RNA Interactome Capture (RIC) strategy

The RNA Interactome Capture (RIC) experiment was firstly described in (Castello et al., 2013) as an unbiased strategy to enrich RBP associated with poly(A)-mRNA. After UV-

crosslinking in live cells to covalently stabilize protein-RNA interaction, poly(A)-mRNAs and associated RBPs were enriched by using oligo(dT)-conjugated beads. For our purpose, SILAC-labelled HeLa cells were treated with DMSO or 10μM MS023 or 5μM GSK591 for 48h and UV-crosslinked at 254nm at a dose of 40J/m2 using a Stratalinker 2400 UV cross-linker (Stratagene, La Jolla, CA). An aliquot corresponding to 10% of each condition was saved for WB analysis while the remaining cells were mixed in 1:1:1 proportion. Cells were then lysed (Lysis buffer: 20mM Tris-HCl (pH 7.5), 500mM Lithium chloride (LiCl), 0.5% lithium dodecyl sulfate (LiDS) (wt/vol, stock 10%), 1mM EDTA and 5mM DTT) and passed through the narrow needle for homogenization. Poly(A)-mRNAs were pulled down 3 times (each time using the flow-through from the previous pull-down) using Dynabeads® oligo(dT) 25 (Thermo Fisher Scientific). The Dynabeads-mRNA-proteins complexes were then washed with 3 different buffers in a consecutive manner (Buffer 1: 20mM Tris-HCl (pH 7.5), 500mM LiCl, 0.1% LiDS (wt/vol), 1mM EDTA and 5mM DTT; Buffer 2: 20mM Tris-HCl (pH 7.5), 500mM LiCl, 1mM EDTA and 5mM DTT; Buffer 3: 20mM Tris-HCl (pH 7.5), 200mM LiCl, 1mM EDTA and 5mM DTT) that led to an efficient removal of polypeptides associated with the mRNA template non-covalently or via protein-protein interactions, while poly(A) tail and oligo(dT) bind remains stable.

4.6 Western Blot Analysis

Western Blot analysis was performed starting from proteins from WCE obtained as previously described in paragraph 4.3, or from the interface isolated through the OOPS strategy as previously described in paragraph 4.4, or from protein eluted from oligo(dT)-poly(A)mRNA-RBPs complex in the RIC experiment as previously described in paragraph 4.5. In each condition, the protein amount was quantified using the Pierce™ BCA Protein Assay Kit (Thermo Fisher Scientific). Equal protein amounts were separated by SDS-PAGE electrophoresis and transferred on the transfer membrane (Immobilon-P, Merck Millipore)

by the wet-transfer method. Not specific signals were blocked by incubating the membranes with 10% BSA/TBS 0.1% Tween-20 for 1h at room temperature (RT). After overnight incubation with the primary antibodies and subsequent incubation with the HRP-conjugated secondary antibodies for 1h (Cell Signaling Technology), proteins were detected by enhanced chemiluminescence (ECL, Bio-Rad). The following primary antibodies were used: anti-vinculin (V9131, 1:5000) was purchased from Merck Life Science; anti-RPS2 (A303-794A, 1:5000), anti-CCT5 (A300-421A, 1:5000), anti-LDHB (A304-7070A 1:5000), anti-FUS (A300-293A,1:2000), anti-RPL7A(A300-749A, 1:5000), anti-RPL27A (A305-380A, 1:1000), and anti-PRMT4 (A300-421A 1:5000) were purchase from Bethyl Laboratories; anti-NONO (SC-376865, 1:500), anti-hnRNPH3 (SC-376416, 1:500), and anti-hnRNPA1 (SC-32301, 1:500) were purchase from Santa Cruz Biotechnology; anti-HSP90AA1 (AB2928, 1:1000), anti-HuR (AB136542, 1:1000), anti-HMGB1 (AB79823, 1:5000), anti-TIA1 (AB140595, 1:2000), anti-H4R3me2s (AB5923, 1:1000), anti-H3R2me2a (AB9147061:1000), anti-H3R17me2a (AB8284 1:1000), anti-PRMT6 (AB 47244 1:1000), anti-PRMT1 (ab73246, 1:1000), and anti-total histone 4 (AB7311 1:2000) were purchase from Abcam; anti-H4R3me2a (61988, 1:500) was purchase from Active Motifs; anti-ADMA (ASYM24 07-414, 1:1000) and anti-SDMA (SYM10 07-412, 1:2000) were purchase from Millipore; anti-MMA (D5A12; 1:1000) was purchase from Cell Signaling Technology; anti-pan -14-3-3 (MA5-1224, 1:2000) was purchase from Thermo Fisher Scientific.

4.7 Strategy of normalization for WB profiling of candidate RBPs from the interface of OOPS and RIC

For the WB analysis each band intensity in each condition was measured with FiJi software (http://www.yorku.ca/yisheng/Internal/Protocols/ImageJ) and subsequently normalized at four different levels:

1. In the WCE, each band was normalized on the vinculin as loading control;

2. In the interface or RIC fractions, each band was normalized on HuR or NONO, selected as loading controls for the interface/RIC, because they resulted unchanging from quantitative proteomics analyses;

3. For each treatment, the intensity in the interface/RIC was normalized over the corresponding in the WCE, to discern the different abundance within these fractions from mere protein expression changes;

4. After the previous three normalizations, the intensity for each treatment was normalized over DMSO.

4.8 Protein Arginine Methyltransferase 1 (PRMT1) Knock-Down by short hairpin RNA (shRNA) strategy

PRMT1 knock-down in HeLa cells was obtained using a second-generation pLKO lentiviral vector, in which two distinct short hairpin RNAs (shRNAs) targeting PRMT1 were cloned:

5′-CCGGCAGTACAAAGACTACAA-3′ (shPRMT1 #1)

5′-GTGTTCCAGTATCTCTGATTA-3′ (shPRMT1 #2)

The pLKO scramble shRNA was used as a negative control. To obtain PRMT1 depletion, HeLa cells were transduced using lentiviruses whose stocks were produced by transient transfection of HEK293T cells with 120mM CaCl2, 5µg of the packaging plasmid pCMV-DR8.74, 5µg of the envelope plasmid pMD2G-VSVG and 10µg of the respective transfer gene-carrying vector. After 15 min 20µM chloroquine was added to inhibit lysosomal degradation of exogenous DNA. After 2 hours the medium of HEK293T packaging cells was replaced with the fresh medium. 48h post-transfection, the supernatant containing the virus was ultra-centrifuged at 32000 rpm for 2h and subsequently added to the HeLa medium. Transduced HeLa cells were then selected by incubation with 1µg/ml puromycin for 48h and subsequently used for the downstream applications.

4.9 Protein Immunoprecipitation coupled to Western Blot analysis (IP-WB) upon PRMT inhibitor treatment

Protein Immunoprecipitation coupled to Western Blot (IP-WB) was performed starting from 500µg of HeLa protein extract, 5% of which was saved as input. 30×10^6 HeLa cells were harvested, washed twice with cold PBS, and re-suspended in 2 volumes of RIPA Buffer (10mM Tris pH 8, 150nM NaCl, 0.1% SDS, 1% Triton X-100, 1mM EDTA, 0.1% Na-Deoxycholate), supplemented with 1mM PMSF,1mM DTT, 1x Proteases and Phosphatase Inhibitors cocktail (Roche) and 10K U of Benzonase (Merck Life Science). The suspension was rotated on the wheel for 45 min at RT (vortex every 10 min), centrifuged at 12000 g at 4°C for 1h and the supernatant was transferred into a new Eppendorf tube. Proteins were quantified by BCA colorimetric assay (Pierce BCA Protein assay kit). The protein lysate was rotated at 4°C overnight with 8µg of anti-pan-14-3-3 (MA5-1224 Thermo Fisher Scientific) or with 5µg of anti-LDHB (A304-770A Bethyl Laboratories) for 500µg of protein extract. In parallel, 50µL of slurry G-protein-coupled magnetic beads (Dynabeads, Thermo Fisher Scientific) for each IP were blocked with a blocking solution (0.5% BSA in TBS supplemented with 1% Triton X-100) and rotated at 4°C overnight. The following day, the beads were added to the lysate in 1:100 proportion with a primary antibody and incubated at 4°C on a wheel for 3h; the captured immuno-complexes were washed 3 times with the RIPA Buffer and then incubated for 10 min at 95°C with LSD sample Buffer supplemented with 100mM DTT in order to elute the immuno-precipitated proteins for subsequent WB analysis, as previously described (paragraph 4.6).

4.10 Protein Affinity Purification coupled to Mass Spectrometry (AP-MS) upon CDDP treatment

Total protein extracts from both untreated SK-O-V3 or treated with 20µM CDDP were obtained by RIPA buffer (10mM Tris HCl pH 8, 150mM NaCl, 0.1% SDS, 1% Triton, 1mM EDTA, 0.1% Na Deoxycholate) supplemented with 1mM PMSF, 1x Proteases and

Phosphatase Inhibitors cocktail (Roche) and 10kU of Benzonase (Merck Life Science)). The experiment of protein AP-MS was performed starting from 3mg of total protein extract for each condition. The extracts were precleared by incubation on a rotating wheel at 4°C for 1h with 50µl of slurry Dynabeads protein G (Thermo Fisher Scientific) and then incubated overnight on a rotating wheel at 4°C with 24µg of the primary antibody (8µg for each mg of protein extract) against RPL27A (Bethyl Laboratories, A305-380A). The following day, 100µL of slurry Dynabeads protein G pre-equilibrated in PBS supplemented with 0.5% BSA were added to the extract and incubated for 3h on a rotating wheel at 4°C. Beads were then washed 4 times with RIPA buffer and then bound proteins were eluted by incubation with LSD Sample Buffer supplemented with 100mM DTT at 95°C for 10 min. One-tenth of eluted proteins were saved for WB analysis of RPL27A protein, while the remaining 9/10 were loaded on SDS-PAGE and visualized with InstantBlue Coomassie (Abcam) staining, for subsequent protein in gel-digestion prior to MS analysis, as described in the following paragraph.

4.11 "In-gel" and "in-solution" tryptic protein digestion prior to MS analysis

In-gel protein digestion was performed as previously described in (Shevchenko et al., 2006). Briefly, proteins (40µg) extracted by UREA lysis buffer (9M UREA, 20mM HEPES (pH 8.0)) were loaded onto a 4–12% Invitrogen NuPAGE Bis-Tris precast polyacrylamide gel. The gel was then stained with InstantBlue Comassie (Abcam) and 8 bands for each line were excised and subsequently cut into 1mm^3 pieces. Reduction and subsequent alkylation of the thiol groups of proteins were performed by incubation of the bands with 10mM dithiothreitol (DTT) at 56°C for 1h and with 55mM iodoacetamide (IAA) at RT in the dark for 45 min, respectively. The gel bands were then washed with the digestion buffer (50mM NH4HCO3) and dehydrated with 100% EtOH twice. Speed-vac dried samples were rehydrated with trypsin solution (12,5 ng/µL of modified sequencing grade trypsin

(Promega) in 50mM NH4HCO3) and protein digestion was performed at 37°C overnight. The following day, 5% trifluoroacetic acid (TFA) was used to stop the reaction and digested peptides were extracted by two subsequent incubations with extraction buffer (3% TFA / 30% acetonitrile (ACN)) followed by 100% ACN. Finally, extracted peptides were desalted and concentrated through reversed-phase (RP) chromatography on C18 stage tips micro-columns (Rappsilber et al., 2007). In RP C18 micro-columns, concentration and desalting were based on the hydrophobic interaction between the peptides resuspended in the mobile phase and the immobilized stationary phase, which was composed of hydrophobic C18 resin, allowing small interfering molecules to be washed off. The solid phase resin consists of eighteen carbon atoms (C18) and is suitable for binding and separation of tryptic peptides. Stage tips were prepared by placing two disks of Empore™ C18 47mm extraction disks (Model 2215, 3M) in a P200 pipette tip without filters. The resin was activated with 100% methanol (CH3OH) and equilibrated twice with buffer A (0.1% TFA). Tryptic digested samples were re-suspended in buffer A (0.1% TFA) and loaded on the stage tips. Samples were then eluted from the stage tips with high organic solvent (80% ACN, 0.1% TFA), lyophilized by vacuum concentrator (Speed Vac) and re-suspended in 0,1% formic acid (FA) for LC-MS/MS analysis.

For in-solution protein digestion, 40µg of proteins were extracted by UREA lysis buffer (9M UREA, 20mM HEPES (pH 8.0)) supplemented with fresh 1X protease inhibitors cocktail (Roche), 1X phosphatase inhibitors cocktail (Roche), and 1mM DTT. In this case, reduction and alkylation of the thiol groups of proteins were performed with 4.5mM DTT at 56 °C for 30 min and with 10mM IAA at RT in the dark for 15 min, respectively. Then the samples were diluted with 20mM HEPES pH 8.0 to reduce the UREA concentration from 9M to 2M, which is a concentration of the chaotropic agent compatible with the protease activity. Proteins were digested with modified sequencing grade trypsin (Promega) at 37°C for 16h at a protein-to-enzyme ratio of 100:1 (wt/wt). The following day, 1% TFA was used to stop the reaction and digested peptides were loaded on an already conditioned cartridge for high

pH reversed-phase chromatography (Pierce™ High pH Reversed-Phase Peptide Fractionation Kit). According to a principle similar to the C18 RP stage tips, the tryptic peptides were first re-suspended in a high pH buffer (0.1% triethylamine) and loaded into small columns with C18 resin as stationary phase. Then, the elution was achieved through a gradient of increasing percentages of organic solvent (ACN) in high pH buffer (0.1% triethylamine), which led to the separation of peptides into 8 fractions differing for their hydrophobicity.

4.12 Liquid Chromatography-tandem Mass Spectrometry (LC-MS/MS) analysis

Peptide mixtures obtained from either in-gel digestion or in-solution digestion of proteins extracts derived from different protocols (e.g. direct WCE extraction, interface from OOPS, protein affinity- enriched by either RIC or protein-IP) were analyzed by online nano-flow liquid chromatography-tandem mass spectrometry (nLC-MS/MS) using an EASY-nLC™ 1200 (Thermo Fisher Scientic) connected to a quadrupole/Orbitrap mass spectrometer (Q Exactive, Thermo Fisher Scientific) through a nanoelectrospray ion source. Solvent A was 0.1% formic acid (FA) in ddH2O and solvent B was 0.1% FA in 80% ACN. Peptides were injected into a 25-cm analytical column (75µm inner diameter, 350µm outer diameter) packed with C_{18} RP resin (ReproSil, Pur C18AQ 1.9µm, Dr. Maisch, Germany) at a flow rate of 300 nl/min and separated with a gradient of 5–40% solvent B over 80 min, followed by a gradient of 40–60% for 15 min and 60–80% over 5 min at a flow rate of 300 nl/min. The Q Exactive was operated in the data-dependent acquisition (DDA) mode to automatically switch between full scan MS and MS/MS acquisition. Survey full scan MS spectra (from m/z 300-1150) were analyzed in the Orbitrap detector with resolution R = 35,000 at m/z 400. The 15 most intense peptide ions (Top15) with charge states 2+ were sequentially isolated to a target value of 3×10^6 and fragmented by Higher Energy Collision

Dissociation (HCD), with a normalized collision energy setting of 25%. The maximum allowed ion accumulation times were 20 ms for full scans and 50 ms for MS/MS and the target value for MS/MS was set to 10^6. The dynamic exclusion time was set to 20 s.

4.13 MaxQuant settings for MS raw data analysis for protein identification and quantification

Acquired raw data were analyzed using the integrated MaxQuant software v1.6.2.10, using the Andromeda search engine (Cox & Mann, 2008). The 2020_06 version of the UniProt Human sequence database (UP000005640), which includes both the canonical forms of the proteins and the isoforms, was used for peptide identification. In the "Global parameters" section, enzyme specificity was set to trypsin/P, meaning that trypsin cleavage occurs also in the presence of proline after lysine or arginine residues; the estimated false discovery rate (FDR) of all peptide identifications was set to a maximum of 1%; the main search was performed with a mass tolerance of 4.5 ppm; a maximum of 3 missed cleavages in the SILAC experiment or a maximum of 2 missed cleavages in the label-free experiment were permitted, and the minimum peptide length was fixed at 6 amino acids. The SILAC protein quantification from MS raw data was performed automatically by the MaxQuant software, using the general parameter setting described above and changing the "group-specific parameters". In the group-specific parameters section, we indicated K8+R10 and/or K4+R6 as SILAC labels. N-terminal acetylation (+42.01 Da), M oxidation (+15.99 Da), mono-methyl-K/R (+14.02 Da), di-methyl-K/R (+28.03 Da), and tri-methylation of K (+42.04 Da) were specified as variable modifications. Carbamidomethylation of cysteine was set as a fixed modification. Output data from MaxQuant software were manually filtered starting from the "*proteinGroups.txt*" file as follows: proteins were accepted if identified with at least two peptides, of which at least one unique; potential contaminants (e.g. keratins) and reverse sequences (consisting of all protein sequences read from the end to the beginning in the target-decoy database strategy) were removed and all accepted identified proteins

should display an Andromeda score ≥ 25. Proteins identified according to these criteria were considered for further quantitative analysis only if they had a SILAC ratio count equal to or greater than 1 (RC≥ 1). Last, protein SILAC H/L and M/L ratios in the interface were normalized on the respective protein SILAC H/L and M/L ratios in the WCE, both extracted from the "*proteinGroups.txt"* MaxQuant output file. This normalization allowed us to discriminate between changes in protein level within the interface fraction (as the hypothetical consequence of a different interaction with cognate RNAs) and mere protein expression changes, following transcriptional induction/repression induced by drug treatments. To define up- or down-regulated proteins by MS023 or GSK591, we calculated the mean (μ) and the SD (σ) of the distribution of the protein SILAC ratios over the DMSO, calculated separately in the forward and reverse experiments, and applied a μ±1σ cut-off to the protein SILAC ratios distribution in each replicate. To determine whether the abundance of the proteins in the interface was significantly affected by PRMT inhibitors compared to their expression level in the corresponding WCE, supervised clustering analysis was performed by Perseus (Tyanova & Cox, 2018), a bioinformatics platform for the analysis of proteomics data that works downstream to MaxQuant software (Tyanova et al., 2016). Clusters of regulated proteins were defined with Ward's method (Ward, 1963).

4.14 Gene Ontology (GO) enrichment analyses for characterization of the proteins emerging as dynamically regulated from the OOPS-MS experiment

Given a set of genes that are dynamically regulated under certain conditions, a Gene Ontology (GO) enrichment analysis will find which functional GO terms are over-represented or under-represented, using annotations regarding the molecular function, biological processes, and cellular components of that gene set. To evaluate the percentage of biological processes correlated with the proteins dynamically regulated in the interface

of OOPS, we performed GO enrichment analysis with GOrilla (Eden et al., 2009) and REVIGO (Supek et al., 2011) using as target the list of dynamic proteins in the interface and as background the list of proteins in the WCE. A GO term was considered significantly enriched when displaying a False Discovery Rate (FDR) lower than, or equal to, 0.05 (FDR <0.05). Analysis of the most enriched protein domains and characterization of the possible protein-protein interactions network among the most enriched RBPs in the interface upon MS023 treatment were done through the STRING (Szklarczyk et al., 2019) plugin of Cytoscape (Shannon et al., 2003). Motif analysis was performed using the pLogo web application (O'Shea et al., 2013): for each "R" in the human protein sequences, a 5-amino acid sequence window centered on that R was extracted from the 2020_06 version of the SwissProt human database. Sequence windows from proteins in the Interface and in the WCE were then provided to pLogo as foreground sequences, while sequence windows from the remaining proteins were used as background.

4.15 Confocal immunofluorescence (IF) experiments to evaluate protein sub-cellular localization and possible Membrane Less Organelles (MLOs) formation

HeLa cells were plated on glass coverslips for 24h and grown with DMSO or 10µM MS023 or 5µM GSK591 for 48h or 400µM NaAsO2 for 30 min and 0.8mM modified uridine (EU) for 48h. For MS023 and NaAsO2 treatments, each experiment was carried out in duplicate and one of the two experiments was subsequently treated with 5% 1,6-Hexanediol for 10 min. Next, cells were washed with 1x PSB, fixed in 4% paraformaldehyde for 20 min at RT, permeabilized with 0.1% Triton X-100 in PBS for 5 min on ice, and the "click" reaction was carried out to conjugate the incorporated EU with Alexa 594 Fluor, according to the manufacturer's instruction (Click-iT™ RNA Alexa Fluor™ 594 Imaging kit, Thermo Fisher Scientific). Then, cells were incubated with 2% BSA in PBS for 30 min at RT and then with the primary antibody in PBS containing 2% BSA overnight at 4°C. After washes, primary

antibodies were removed and cells were incubated with the antibody anti-G3BP1 (BD 611126, 1:400) for 3h at RT. After three additional washes, cells were stained with Rabbit Alexa Fluor 488 secondary antibody (for the protein of interest) or with Mouse Alexa Fluor 647 secondary antibody (for G3BP1) (Molecular Probes, Eugene, OR, United States), both diluted 1:400 in PBS containing 2% BSA for 1h at RT. Nuclei were stained with DAPI (Invitrogen). Images were acquired with a Leica TCS SP8 confocal microscope (Leica Microsystems, Heerbrugg, Switzerland).

4.16 Confocal image analysis to assess the stress granule formation and co-localization with target RBPs

To evaluate the percentage of cells with stress granules, samples were acquired with a Nikon CSU-W1 spinning disk using a 60X/1.4NA objective lens, a 50 um-pinhole disk, solid-state lasers, a multiband dichroic mirror, and a fast-rotating emission filters wheel. Eighty-one fields of view (FOV) were automatically acquired for each sample with an autofocus routine on the DAPI channel. A Z-stack of 7 optical sections with a step size of 0.6µm together with the emissions from the 4 fluorophores (DAPI, AlexaFluor488, AlexaFluor594, and AlexaFluor647) were acquired in each FOV with a pixel size of 108 × 108 nm (2048 × 2048 pixels per FOV). The acquired images were analyzed with a custom-made FiJi/ImageJ (Schindelin et al., 2012) macro. Briefly, the DAPI channel was used to identify the relevant area of each cell (cell area) using the Voronoi filter on the maximum intensity projections. In each cell area, the presence of a nucleus was evaluated, and the cell areas without any nucleus or with more than one were discarded. Then, a band of 12 microns was created around each nucleus (cytoplasmic area), the G3BP1 signal was used to segment the stress granules using a fixed threshold in all samples and the objects inside the cytoplasmic area (stress granules) were counted in each cell. For each sample, the number of cells with at least one stress granule was considered. To evaluate the co-localization between G3BP1 and the RBP signals, single optical sections per sample were

acquired with a Leica SP8 laser scanning confocal microscope equipped with 405nm and 561 solid-state lasers, an Argon and a Helium–Neon (HeNe) lasers, Hybrid detectors, and a motorized stage. More than 15 FOV per sample were acquired using a 63X/1.4NA objective lens with a pixel size of 45nm (2048 × 2048 pixels per FOV). Co-localization indices were calculated in a 10um-thick band around each nucleus (cytoplasmic area) thanks to a custom-made FiJi/ImageJ macro and the JaCoP plug-in (Bolte & Cordelieres, 2006). In all experimental conditions, the M1 coefficient (the fraction of RBP signal co-localizing with G3BP1 signal) was used as an indication of co-localization between RBP and stress granules. The Huang and the Max Entropy algorithms were used to automatically find the thresholds for RBP and G3BP1 signals, respectively.

4.17 Total and interface-RNA extraction and sequencing for the analysis of global and interface-specific transcriptomic changes

Total RNAs from SK-O-V3 cells, both untreated and treated with 20µM CDDP (biological replicate n=3) were extracted using Quick-RNA Miniprep kit (Zymo Research), according to the manufacturer's instructions and eluted in 60µL nuclease-free water. Following the same approach as for the proteomics analysis, RNA levels from total extracts were used to normalize the levels of corresponding RNAs in the interface, in order to distinguish RNA enrichment in OOPs from mere transcriptional changes, due to the CDDP treatment. RNAs from the interface from SK-O-V3 untreated and treated with 20µM CDDP (biological replicate n=3) were isolated as described in (Queiroz et al., 2019), with minor adjustments. Briefly, after 3 consecutive Trizol^{TM}-chloroform phase partitions, the isolated interface was incubated for 2h at 50°C in protein digestion buffer (30mM Tris HCl pH8, 10mM EDTA and 18U of proteinase K (Sigma-Aldrich)). Samples were cooled and washed with 1mL of 75% ethanol twice. After centrifugation for 5 min at 7500 g at 4°C, DNAse (Zymo Research) treatment of RNA was performed according to the manufacturer's instructions and finally, the pellets were re-suspended in 30µL nuclease-free water. Both total and interface-RNA

were carefully quantified by Quibit (Thermo Fisher Scientific) and assessed for RNA integrity by Bioanalyzer 2100 system (Agilent) before RNAseq analysis. 800ng of total and interface- RNAs were used as input for libraries preparation with the TruSeq Stranded Total RNA Library Prep Gold (Illumina), following the manufacturer's instructions. Sequencing was performed on an Illumina HiSeq2000 at 50bp single-read mode and 35 million read depth.

4.18 RT-qPCR analysis

One μg of RNA from each sample (WCE or interface) and from each condition (untreated or treated with 20μM CDDP) was reverse transcribed using OneScript® Plus cDNA Synthesis Kit and random primers (abmgood), according to the manufacturer's instruction. Real-time quantitative PCR reactions were prepared using fast SYBER™ Green reaction mix (Thermo Fisher Scientific) and performed on ViiA7 Real-Time PCR system (Applied Biosistems). The relative expression level was calculated with the $2^{-\Delta\Delta Ct}$ method and expressed as fold change. The data were normalized to housekeeping gene (18S) expression and compared to the untreated condition. The primers used to profile mRNA expression levels are the following:

18S FWD CCGATTGGATGGTTTAGTGAG

18S REV AGTTCGACCGTCTTCTCAGC

GRP94 FWD CTGGAAATGAGGAACTAACAGTCA

GRP94 REV TCTTCTCTGGTCATTCCTACACC

GRP78 FWD CAACCAACTGTTACAATCAAGGTC

GRP78 REV CAAAGGTGACTTCAATCTGTGG

4.19 Cell death assay to verify possible cell death induction by PRMT inhibition

HeLa cells were grown for 48h in the presence of DMSO, 10µM MS023, and 5µM GSK591; upon harvesting, the percentage of apoptosis was measured by evaluation of FITC-conjugated Annexin V (Thermo Fisher Scientific) and propidium iodide (Thermo Fisher Scientific), following the manufacturer's protocols. Cells were measured using the FACSCalibur platform (BD Bioscience) and analyzed using the FlowJo software. Statistical analysis was performed using ANOVA (GraphPad Prism software, version 9.3.1) collecting data from 3 biological replicates per each condition.

4.20 Cell viability evaluation by CellTiter-Glo assay to determine the EC50 of CDDP in ovarian cancer cell line

S-KO-V3, OV90, COV-362.4, Caov-3, A2780, and OVCAR3 cells were grown for 24h in a 96 multi-well in untreated condition or in the presence of growing doses of CDDP: 1.25µM, 2.5µM, 5µM, 10µM, 20µM, 40µM, and 80µM. Cell viability was calculated indirectly by measuring the ATP content of each condition through the CellTiter-Glo® luminescent assay (Promega). The rationale behind the assay is that the amount of ATP is directly proportional to the number of metabolic active cells present in the culture. The luminescence intensity was recorded by GloMax® Discover Microplate Reader (Promega). All the acquired luminescence intensities were normalized over the corresponding untreated condition and the EC50 for each cell line was calculated through a dose-response non-linear regression analysis through the GraphPad Prism software (version 9.3.1).

5. RESULTS

5.1 Optimization of sample preparation protocol prior to MS-based analysis of RBP-RNA interaction dynamics

5.1.1 Evaluation of PRMTs inhibition impact on cell viability

To investigate the effect of R-methylation remodeling on RBP-RNA interaction dynamics, we decided to take advantage of the use of MS023 (PRMT type I inhibitor) and GSK591 (PRMT5 selective inhibitor) drugs, in combination with the OOPS strategy for RBP-RNA complexes enrichment and MS-based proteomic analysis of the dynamically enriched RNA-Binding Proteins (RBPs). First, we evaluated whether PRMT pharmacological inhibition could impair cell viability in our cell model: the growth curve of HeLa cells treated in parallel with 10μM MS023 or 5μM GSK591 or DMSO, as control, showed that the growth rate among the three conditions was comparable for the first 48h of treatment, while after 72h both MS023- and GSK591-treated cells started to grow slower than in the DMSO condition (**Fig. 15A**). The time frame required for R-methylation remodeling depends on several factors. Typically, PTMs are deposed and removed by enzymes known as “writers”, and “erasers”, respectively. In the case of R-methylation, the existence of erasers is still debated (see paragraph 2.1.1 of the Introduction) and, compared to other PTMs, it is considered significantly less dynamic. However, some considerations about the time required for deposition can be done. First, R-methylation is a time-dependent process, so that by increasing the time will increase the number of R sites fully methylated. Second, PRMTs and their substrates could be confined within a subcellular location and this could result in a rapid increase in the local concentrations of PRMTs and substrates, which could not be detected at the global level. Third, PRMTs utilize a sequential ternary complex mechanism to catalyze arginine methylation, in which both SAM and the R substrate are required to bind to the active pocket of PRMTs and also this combination requires time. In light of all these considerations, we selected the 48h as the time window which enables a complete

R-methylation turnover and in parallel, cell viability is still comparable to the control condition. As additional check that the selected drug concentrations do not induce cell death (neither apoptosis nor necrosis) after 48h of treatment, we performed a cell death assay by flow cytometry analysis detecting annexin V and propidium iodide (PI) staining: in all tested conditions the percentage of cell death was comparable to DMSO and in any case lower than 10% (**Fig 15B**).

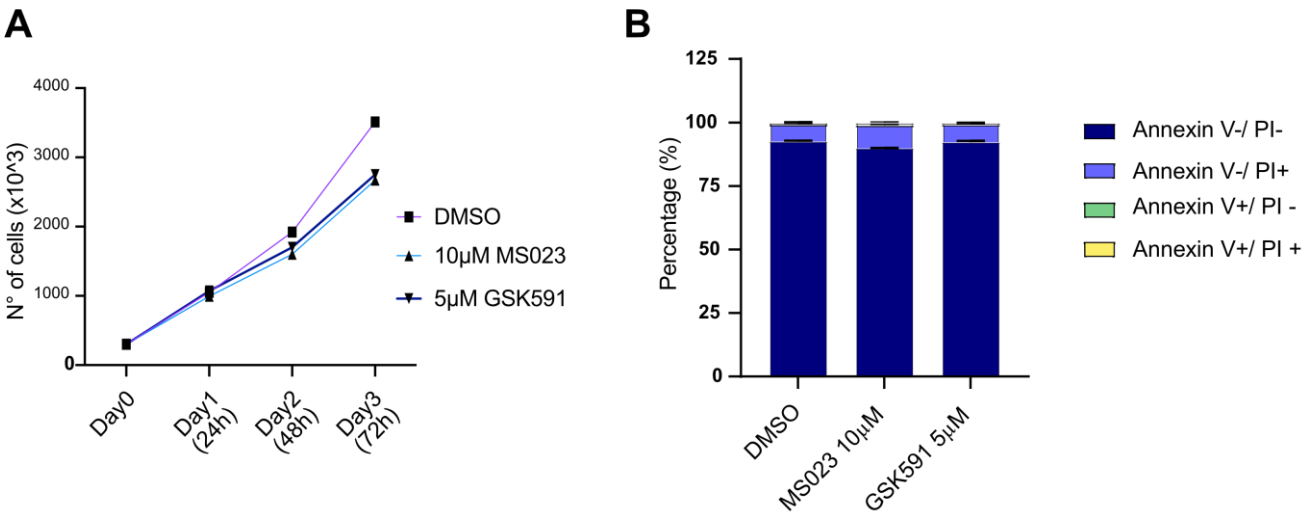

Figure 15: Impact of PRMTs inhibition on cell viability

A) Counts of living cells by trypan blue staining at the different time points (0h, 24h, 48h, 72h) upon DMSO, 10µM MS023, and 5µM GSK591 treatment. ***B)*** Cell death assay, performed by flow cytometry analysis of Annexin V and Propidium Iodide (PI) expression upon DMSO, 10µM MS023, and 5µM GSK591 treatment for 48h, in triplicate. Annexin V+ cells represent apoptotic cells, PI+ cells represent necrotic cells

5.1.2 RNA-Binding Proteins (RBPs) enrichment through the Orthogonal Organic Phase Separation (OOPS) strategy

The Orthogonal Organic Phase Separation (OOPS) method was published as an unbiased way to enrich RNA-Binding protein (RBP)-RNA complexes and to study their dynamics in different conditions, with no need for molecular tagging specific proteins, or capturing poly-adenylated RNAs (Queiroz et al., 2019). Therefore, we decided to adopt this protocol to globally analyze the impact of protein R-methylation state on the modulation of RBP-RNA

interactions. First, we tested the efficiency of RBP enrichment by OOPS. As described in the M&M section (paragraph 4.4) and schematically illustrated in **Fig.16A**, cells were first UV-crosslinked at 254nm and subsequently phase-partitioned through a Trizol™ - chloroform mixture: this allowed to separate an upper part (the aqueous phase), a small intermediate interface and a lower part (the organic phase), which are expected to be enriched in free RNA, RNA-RBP complexes, and free/soluble proteins, respectively. For the analysis of the interface-enriched proteins, after 3 consecutive phase-partition rounds, the interface was treated with RNase A, and the RNA-depleted interface was used to detect the protein content. Another crucial step of this strategy is the UV-crosslinking at 254 nm: this type of crosslinking stabilizes irreversibly RNA–RBP binding so that RBPs are retained more in the interface fraction. Hence, in order to verify the importance of this step, we performed the phase partition both with and without the UV-crosslinking step. When we monitored the presence of a set of known RBPs (FUS, HuR, and hnRNPA1) in the interface by Western Blot (WB) in the two conditions, we could detect their significant enrichment upon UV-crosslinking, which confirmed that UV-crosslink is a crucial step in the protocol (**Fig. 16B**).

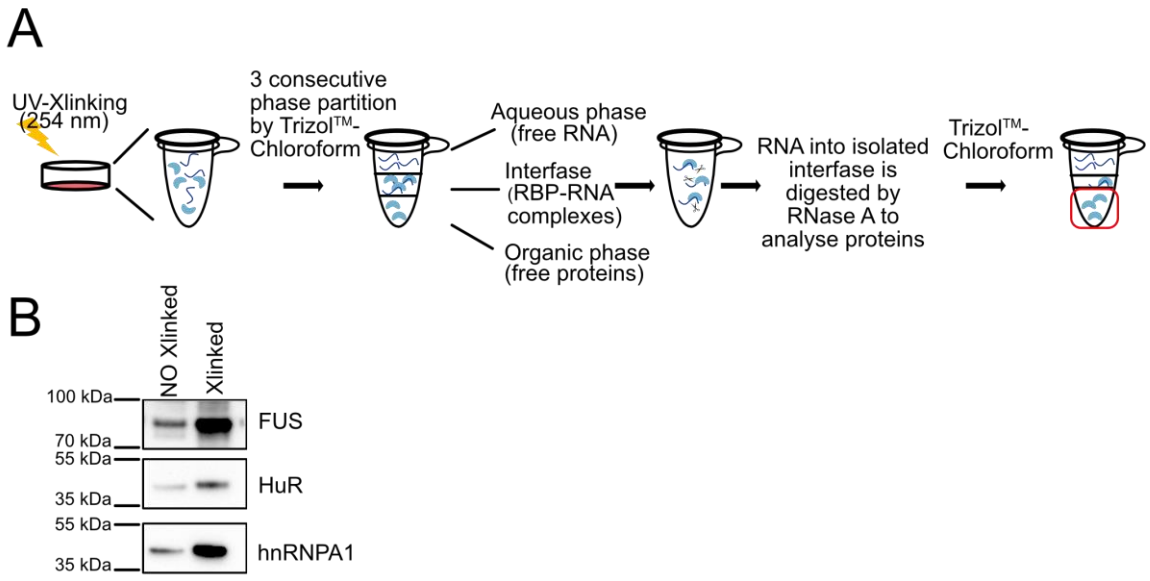

Figure 16: RBP enrichment through the OOPS strategy

A) Schematic representation of the OOPS strategy: cells are UV-crosslinked (UV-Xlinking) at 254nm to covalently stabilize RBP-RNA binding. Subsequently, through three consecutive Trizol-chloroform mixture phase partitions, the purified interface is enriched for RBP-RNA complexes. Finally, the RNA in the interface is digested by RNaseA, new Trizol-chloroform phase partition e the RBPs in the organic phase are analyzed by MS or WB. ***B)*** WB analysis of three RBPs (FUS, HuR, and hnRNPA1) to evaluate the impact of UV-Xlinking on their enrichment in the OOPS

5.1.3 Comparison of different protein digestion strategies prior to LC-MS/MS analysis to maximize the interface proteome coverage

As the next step, we set to optimize the sample preparation protocol for protein separation and digestion prior to LC-MS/MS, to determine which strategy would lead to the highest number of proteins identified downstream of OOPS.

To this aim, we performed in parallel either an "*in-gel protein digestion*" protocol (Shevchenko et al., 2006) and an "*In-solution protein digestion*" protocol (Maniaci et al., 2022), coupled to high pH (HpH) reversed phase (RP) chromatography for peptide fractionation according to their hydrophobicity, as schematized in **Fig. 17A** and described in M&M section (Paragraph 4.10).

For the in-gel digestion protocol, 40µg of proteins both from WCE and interface were separated on SDS-PAGE, and each line was cut into 8 gel slices which in turn were cut into 1mm^3 cubes for further processing. Reduction of the thiol groups of proteins trapped in the gel cubes was achieved by incubation with 10mM DTT at 56°C for 60 min, while their alkylation was obtained upon incubation with 55mM IAA at RT in the dark for 45 min and finally, trypsin-digestion was performed at 37°C overnight, prior to MS analysis (more technical detail in the M&M section at paragraph 4.10). The major advantage of this digestion is that SDS-PAGE separation helps reducing sample complexity by separating denatured proteins according to their molecular weight; in addition, this strategy allows the removal of sample contaminants such as detergents, salts or nucleic acids.

For the in-solution protein digestion protocol, 40µg of proteins both from WCE and interface extracted in UREA lysis buffer (9M UREA, 20mM HEPES (pH 8.0)), directly reduced (with

4.5mM DTT), alkylated (with 10mM IAA) and overnight digested with trypsin directly in the same buffer of protein extraction, upon UREA dilution at 2M with 20m HEPES pH 8.0, in order to obtain a concentration of UREA at which trypsin is still active (E. I. Chen et al., 2007). By coupling the in-solution protein digestion with high pH (HpH) RP chromatographic separation of peptides, we could fractionate peptides according to their hydrophobicity by sequentially eluting them with increasing concentration of organic solvent (in this case ACN) in the HpH mobile phase solution. It has been demonstrated that HpH RP peptide fractionation reduces sample complexity by providing an efficient separation that increases the proteome coverage upon MS (F. Yang et al., 2012), and this is particularly effective when carrying out proteomics analysis of PTMs(Batth et al., 2014; Maniaci et al., 2022).
This comparison highlighted that most RBPs enriched by the OOPS own similar molecular weight, so the separation of protein according to their molecular weight in the in-gel protein digestion protocol resulted ineffective, whereas the strategy of peptide separation by hydrophobicity in the in-solution protein digestion protocol was significantly more efficient. As a matter of fact, while the total number of proteins identified within the WCE by the two protocols was similar (1435 proteins in the in-gel digestion versus 1536 proteins in the in-solution coupled to HpH chromatography), a significant increase could be appreciated in the number of proteins identified within the interface fraction with the second approach (212 proteins in the in-solution versus 72 form in-gel digestion, **Fig. 17B**). The in-solution protein digestion protocol followed by HpH-RP fractionation was therefore adopted prior to MS analysis for the subsequent OOPS experiments.

A

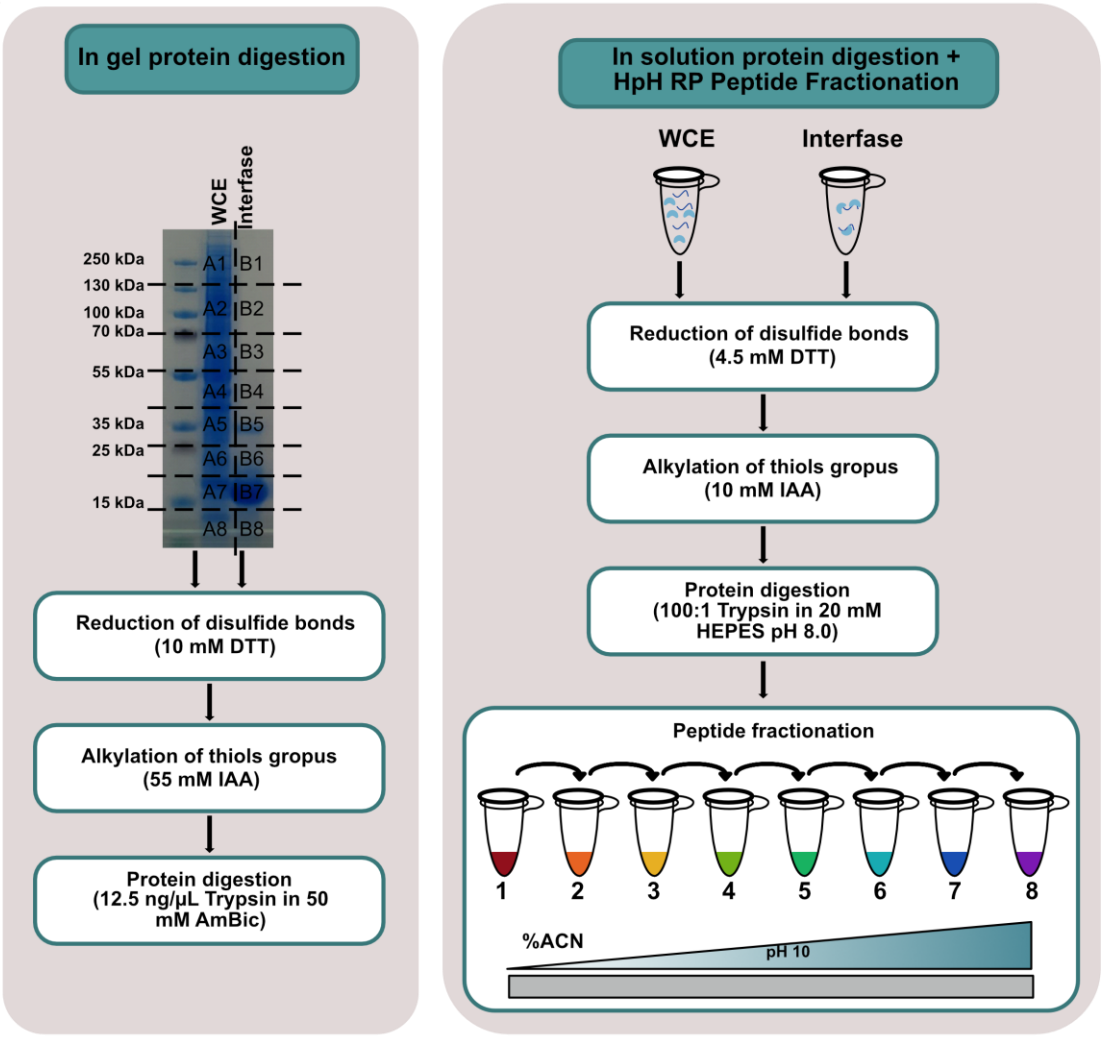

B

Tot n° of identified proteins	1548
Tot n° of identified protein in the WCE after in gel-digestion	1435
Tot n° of identified protein in the WCE after in solution-digestion +HpH fractionation	1536
Tot n° of identified protein in the interface after in gel-digestion	72
Tot n° of identified protein in the interface after in solution-digestion +HpH fractionation	212

Figure 17: Optimization of the protein digestion prior LC-MS/MS analysis

A) Scheme highlighting the main differences between the “in-gel” protein digestion and the “in-solution” protein digestion coupled to RP chromatography protocols **B*)*** Summary table of identified proteins, both in the whole cell extract (WCE) and in the interface from OOPS experiment, comparing in-gel and in-solution digestion methods. For each condition, the identified proteins respect the following filtering criteria: a) reverse sequences and potential contaminants were removed; b) proteins were identified by at least two peptides, one of which unique; c) Andromeda score was>25.

5.1.4 SILAC labeling of HeLa cells and SILAC amino acid incorporation analysis

In order to achieve a robust protein quantification in the OOPS experiment, we adopted the Stable-Isotope Labeling by Amino acids in Cell culture (SILAC) metabolic labeling strategy (See paragraph 2.3.2 of the introduction and paragraph 4.2 of M&M). HeLa cells were cultured in SILAC DMEM media, supplemented with light (L) arginine (R0) and lysine (K0) and either medium-heavy (M, R6 and K4) or heavy (H, R10 and K8) amino acids, in parallel. The substitution of normal with dialyzed fetal bovine serum (FBS) in the SILAC medium ensures that the isotope-encoded amino acids counterparts represent the only source available for incorporation in newly synthesized proteins, during cell replication. Cells were grown in the respective heavy, medium and light media for about 2 weeks, in parallel with the normal medium, and carefully checked for the rate of growth and morphology. Both doubling time and growth curves of HeLa cultured in the differentially isotopic-encoded media are comparable **(Fig. 18A** and **18B)**, indicating that cell viability is not influenced by the different amino acid composition of the media. When up to about nine cell replications were achieved, cells were harvested, protein extracted and amino acids incorporation efficiency into proteins was assessed in each condition by LC-MS/MS and data analysis with the MaxQuant algorithm.

Peak detection and peptide identification are two of the algorithms within the MaxQuant suite, thus after we stated that the samples were SILAC-labeled, the MaxQuant output file named "*peptides.txt*" was used to determine the number of R0K0, R6K4, or R10K8 intensity for each channel and thus to calculate incorporation percentage of each isotope-encoded amino acid. The incorporation efficiency of medium and heavy amino acids in the corresponding channel was calculated between 97.7-98% **(Fig. 18C)**. Hence, these SILAC-labeled cells were used for the subsequent OOPS-MS experiment.

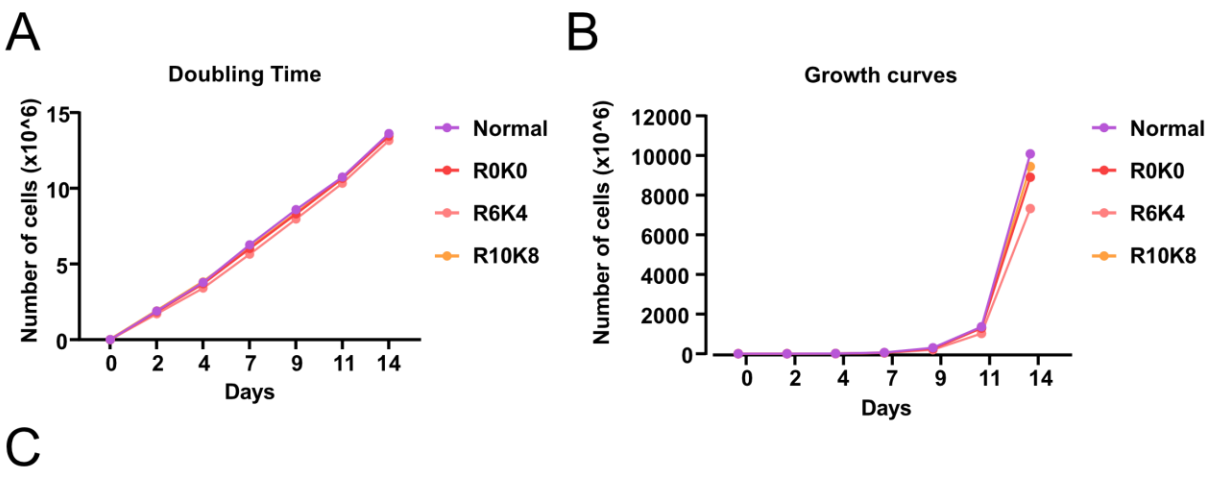

C

	Light	Medium	Heavy
Only R0	97,7%	0,1%	0,05%
Only R6	0,06%	98,05%	0,04%
Only R10	0,08%	0,01%	97,58%

	Light	Medium	Heavy
Only K0	98,08%	0,11%	0,05%
Only K4	0,06%	98,29%	0,04%
Only K8	0,05%	0,02%	97,58%

Figure 18: amino acid SILAC incorporation in HeLa cells

A*)* Counts of living HeLa cells by trypan blue staining for two weeks in normal, light (R0K0), medium (R6K4), and heavy (R10K8) SILAC media**. B*)*** HeLa growth curves in the four conditions to monitor growth rate over the two weeks required to achieve around 9 cell replications. **C*)*** Summary tables of the number of R and K, both light and isotope-encoded amino acids counterparts, for each SILAC channel.

5.2 Implementation of the proteomic workflow to evaluate the impact of R-methylation on RBP-RNA interaction dynamics

In order to evaluate how protein R-methylation can affect globally RBP-RNA interactions, we applied a proteomic workflow that combines RBP-RNA complexes enrichment by OOPS with SILAC metabolic labeling of cells, pharmacological inhibition of PRMTs, and in-solution protein digestion coupled with HpH RP chromatography prior to high-resolution MS analysis. The workflow adopted is outlined in **Fig. 19A**. To achieve robust protein quantification, we used HeLa cells metabolically labeled with the three isotopic variants (light (L), medium (M), and heavy (H)) of both lysine and arginine. Fully SILAC-labeled HeLa

cells were treated for 48h with either 10μM PRMT type I inhibitor (MS023) or 5μM PRMT5 selective inhibitor (GSK591) or DMSO as control.

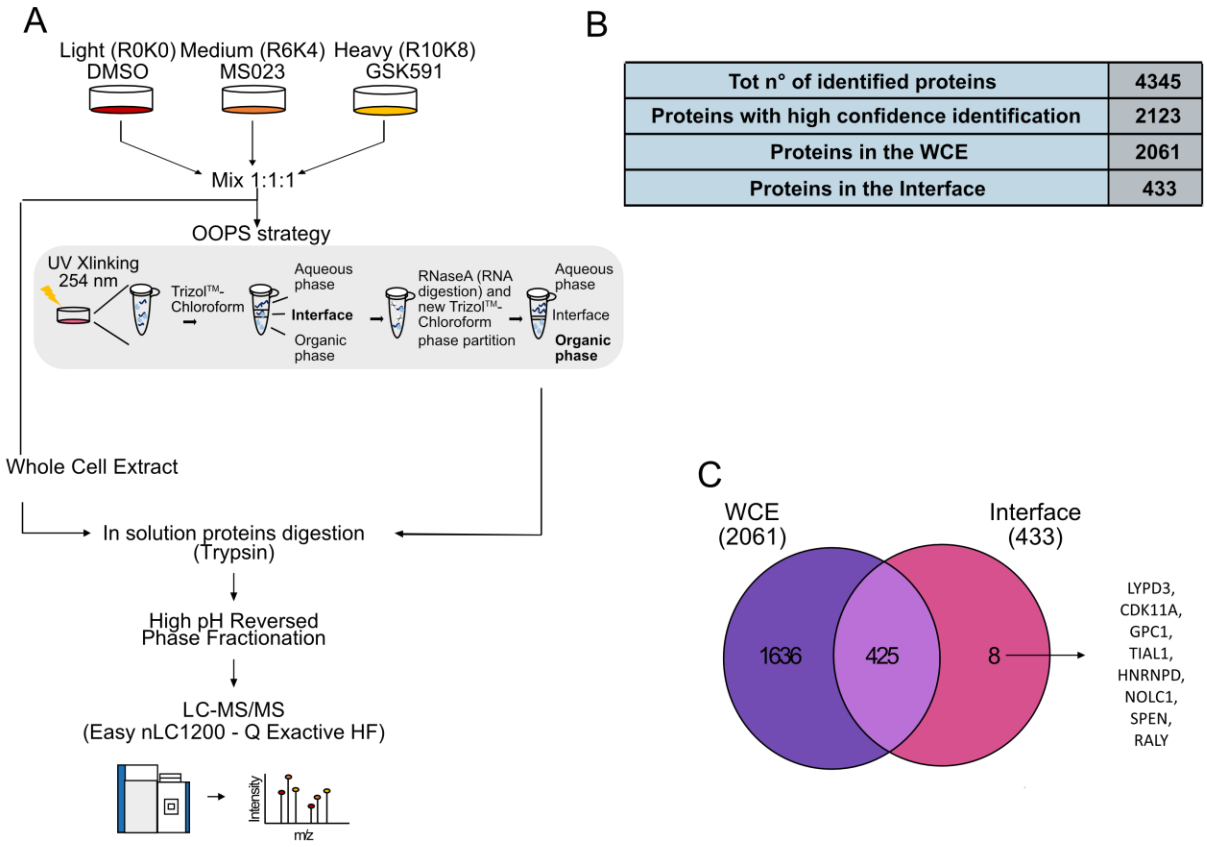

Figure 19: Proteomic approach to profile RBP-RNA complexes in dependence on PRMT activity

A) Representative workflow of the SILAC OOPS-MS approach. HeLa cells were grown in light (R0K0), medium (R6K4), and heavy (R10K8) SILAC medium and treated with DMSO, 10μM MS023, and 5μM GSK591 for 48h. Aliquots from the light-, medium- and heavy-labeled cells were mixed in 1:1:1 proportion and saved as whole cell extract (WCE), while the remaining cells were UV-crosslinked and phase-partitioned through Trizol™-chloroform mixture. Proteins from both WCE and interface were subjected to in-solution protein digestion and fractionation by off-line HpH-RP chromatography. Tryptic peptides were analyzed by high-resolution LC-MS\MS. **B)** Table summarizing the number of proteins identified by MaxQuant, upon application of filtering criteria: a) removal of reverse hits and contaminants; b) Andromeda score ≥25 and at least two peptides, one of which unique, for each experiment (high-confidence identification), both in the WCE and interafce; c) the number of proteins identified with high confidence in the WCE; d) the number of proteins identified with high confidence in the interface fraction. **C)** Intersection of the number of proteins identified with high confidence in the WCE and in the interface fraction from OOPS. *Adapted from* (Maniaci et al., 2021).

WB analysis of asymmetric and symmetric R-methylation on arginine 3 of histone 4 (H4R3me2a and H4R3me2s, respectively), normalized over the total amount of histone 4, were used as control of the drug efficacy in inhibiting the respective PRMT type (**Fig. 20A**). Indeed, reduction of H4R3me2a upon MS023 treatment and reduction of H4R3me2s upon GSK591 treatment, indicated a reduced activity of PRMT1 and PRMT5, respectively. The triple SILAC experiment was carried out in two biological replicates, in “Forward” (FWD) and “Reversed” (REV) mode, whereby the treatments in the medium and heavy SILAC conditions were swapped among the channels, to increase the confidence in the discrimination of true outliers from random variations.

About 20% from each channel was collected, saved, and mixed in 1:1:1 proportion prior to OOPS, as whole cell extract (WCE). The remaining cells were UV-crosslinked and another small fraction (around 10%) of the cells from each individual channel was saved and phased-partitioned according to the optimized OOPS protocol, for subsequent WB profiling of specific proteins. The rest of the UV-crosslinked cells were mixed in 1:1:1 proportion and phased partitioned for the large-scale OOPS-MS quantitative experiment. Here, the interface fraction (enriched in RNA-RBP adducts) was collected, proteins were extracted in UREA lysis buffer (9M UREA, 20mM HEPES (pH 8.0)), and subjected to in-solution protein digestion. Tryptic peptides were separated by HpH RP chromatography prior to nanoLC-MS/MS analysis, as described in paragraph 5.1.3 of the Results and paragraph 4.10 of the M&M sections. For the OOPS-WB, the proteins from the interface fraction were extracted by 9M UREA lysis buffer and subsequently used for WB analysis: the enrichment of known RBPs (RPS2 and HuR) in the interface and the parallel absence of non-RBP proteins (Vinculin and total H4) confirmed the efficiency of the OOPS protocol (**Fig. 20B**). During sample preparation, the efficacy of in-solution trypsin digestion was tested by loading on SDS-PAGE gel a small fraction (around 1%) of both undigested and digested samples, and staining of the gel with InstantBlue Coomassie. As illustrated in **Fig. 20C**, complete protein digestion was achieved both for WCE and interface and both for the FWD and the REV experiment.

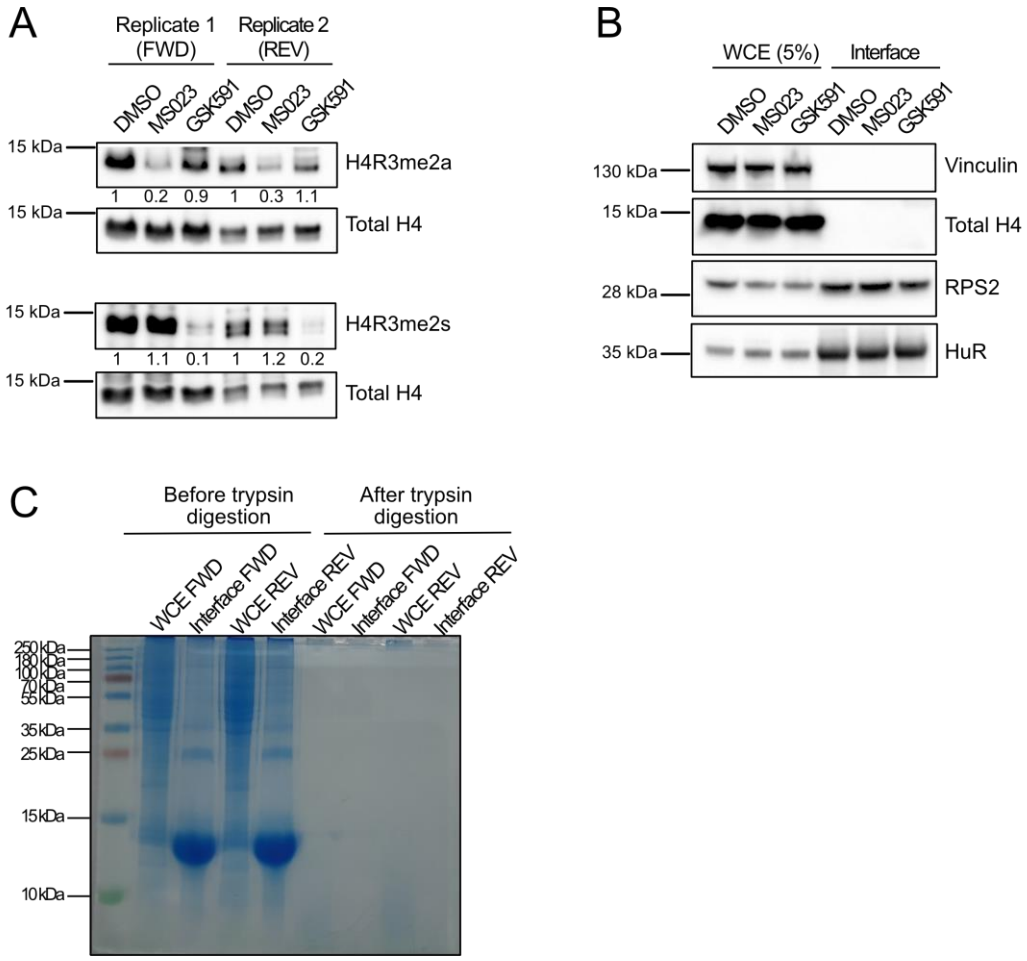

Figure 20: Technical controls to asses PRMT inhibition, RBP enrichment, and protein digestion

A) Western Blot (WB) validation of the PRMT pharmacological inhibition. Before mixing in 1:1:1 proportion as described in panel A, an aliquot of each condition was used to test specific histone R-methylation marks deposed by PRMT1 and PRMT5, both in the forward (FWD) and in the reversed (REV) experiment. Reduction of asymmetric di-methylation of arginine 3 on histone 4 (H4R3me2a) was observed upon MS023 treatment; the total unmodified H4 was used as loading control. The reduction of symmetric di-methylation of arginine 3 on histone 4 (H4R3me2s) was observed upon GSK591 (with H4 as loading control). Quantification of the signal intensity for each modified R-methyl site normalized over the total H4 is reported for each replicate. **B)** WB validation of RBPs enrichment by OOPS. WB analysis of the RNA binding proteins RPS2 and HuR confirms their enrichment in the interface fraction, while the absence of non-RBP proteins Vinculin and H4 from the same fraction confirmed the selectivity of the method. **C)** SDS-PAGE gel stained with Instant Blue Coomassie to evaluate protein content before and after in-solution trypsin digestion, from WCE and interface fractions, both for the FWD and REW experiment. *Adapted from* (Maniaci et al., 2021).

Subsequently, fractionated peptides were re-suspended in solvent A (0.1% FA) and analyzed by nanoLC ultra-high-pressure HPLC system directly coupled online to a Q

Exactive HF mass spectrometer. Peptides were separated with a gradient of 5–40% solvent B (0.1% FA in 80% ACN) over 80 min, followed by a gradient of 40–60% for 15 min and 60–80% over 5 min at a flow rate of 300 nl/min. The Q Exactive was operated in the data-dependent acquisition (DDA) mode to automatically switch between full scan MS and MS2 acquisition and peptide fragmentation in the MS2 was achieved by HCD (see M&M, paragraph 4.11).

The MS raw data acquired were processed with the MaxQuant software package, using the Andromeda Search Engine (Tyanova et al., 2016)as described in M&M (paragraph 4.12) for protein identification and SILAC-based quantification. MaxQuant produced several output files including "*proteinGroups.txt*" that was used to evaluate the number of proteins identified in total and for each experiment, as described in the table in **Fig. 19B**. Upon filtering the data by removing reverse sequences and contaminants (technical details in paragraph 4.12 of M&M), we identified a total of 4345 proteins, including both WCE and interface. To nail down a list of more confident identifications, we applied more stringent filtering criteria, such as: a) each protein should be identified by at least two peptides, one of which is unique; b) each protein should be identified with an Andromeda score ≥ 25. A total of 2123 protein identifications, comprising both WCE and interface, satisfied these criteria and were annotated as "high confidence identifications"; among them, 2061 were identified in the WCE and 433 in the interface. The majority (425, ±98%) of the interface proteins were in common with the WCE, with only 8 proteins exclusively found in this fraction (**Fig. 19C)**, among which TIAL1, hnRNPD, NOLC1, SPEN and RALY are well-known RBPs.

5.3 Qualitative analysis of the interface-enriched proteins from OOPS-MS

Before assessing the effect of PRMT inhibition on RBP-RNA dynamics, we set to thoroughly evaluate the extent of RBP enrichment from the OOPS experiment. First, we compared the

list of the putative RBPs enriched in our interface with the list of proteins annotated in Queiroz et al., 2019 where the OOPS was applied for the first time. In this case, the overlap was small (**Fig. 21A**), probably because of the use of different cell lines: the list of proteins annotated by Queiroz et al., 2019 results from the combination of three distinct OOPS experiments carried out in three different cell lines, one of which is non-tumorigenic (U2OS, HEK293, and MCF10A). Instead, our dataset represents the dynamic RBP proteome from HeLa cells only. Then, we intersected the list of putative RBPs in our dataset with three online available RBP database named “EuRBPDB” (Jian-You Liao et al.2019), “RBP2go” (Maiwen Caudron-Herger et al. 2020) and “RBPDB” (Kate B Cook et al. 2011), which include both “canonical” RBPs, with an RBD, and “non-canonical” ones, identified through different large-scale experiments. Overall, 418 over 433 (around 96.5 %) of our candidates had been previously annotated as RBP (**Fig. 21B**), which indicates the effectiveness of our enrichment. Among the remaining 15 proteins, the majority are components of the extracellular matrix. Consequently, it cannot be ruled out that these are true RBPs or simply RBP interactors. As an additional control, we performed a functional analysis of the most enriched GO biological process emerging from our dataset: as expected, terms describing RNA metabolism, RNA processing, RNA splicing, RNA translation, and assembly of ribonucleoprotein complexes emerged (**Fig. 21C**).

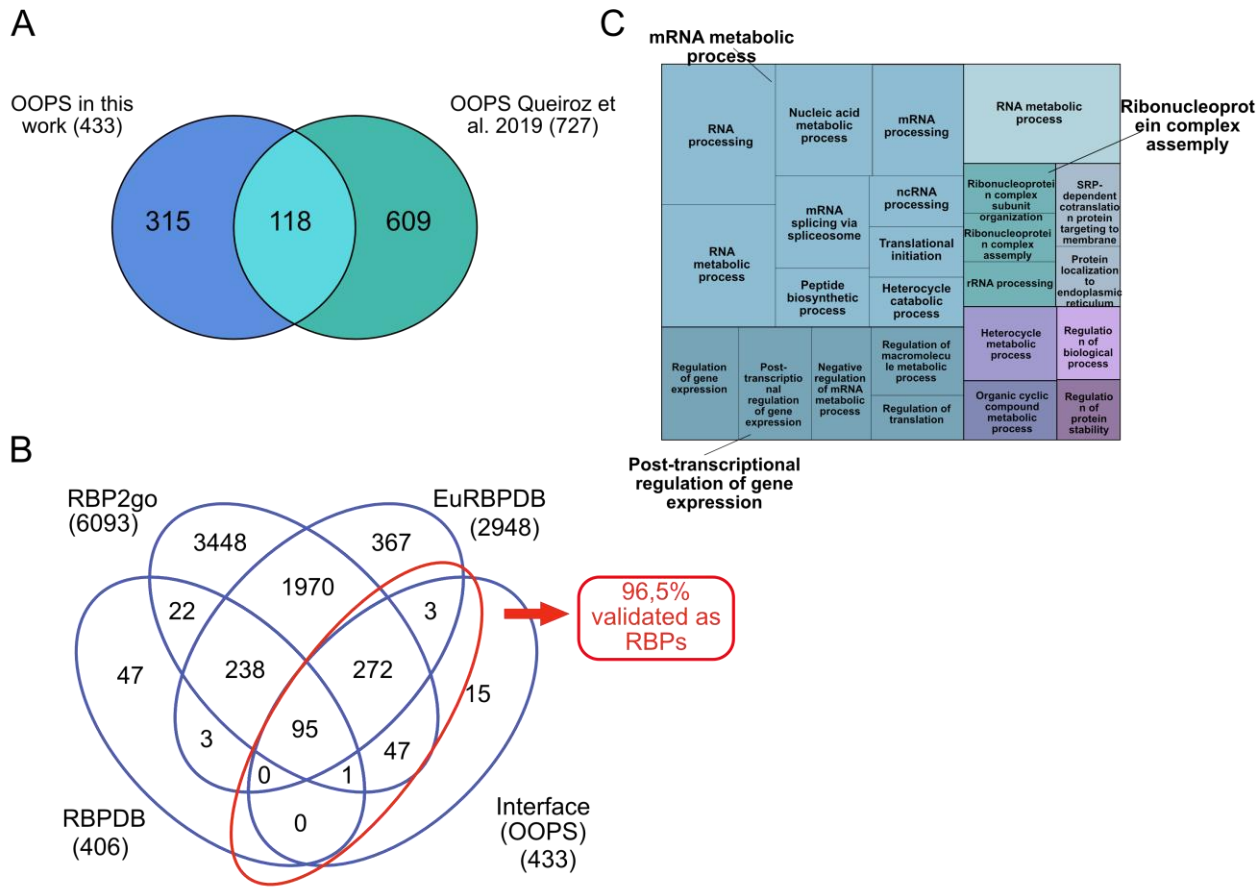

Figure 21: Functional characterization of the interface fraction upon OOPS

A)Comparative validation of RBPs enrichment in the interface fraction. Comparative analysis was performed the list of putative RBPs identified in our study and the RBPs identified in Queiroz et al., 2019 **B)** TreeMap representation of the GO enriched terms in the interface fraction. GO analysis performed by GOrilla and REVIGO indicates the most enriched GO terms in the interface proteins. **C)** Intersection between our datased of putative RBPs form interface of OOPS and the three online available RBP databases EuRBPDB, RBPDB and RBP2go
Adapted from (Maniaci et al., 2021).

Furthermore, domain enrichment analysis of the same dataset highlighted a strong over-representation ($-Log_{10}$ p-value= 60) of RNA-binding domains (RBDs), RNA recognition motives (RRMs), and nucleotide-binding domains. Although to a minor extent, we also found specific types of RBDs, such as the SAP domain (Aravind & Koonin, 2000), the DEAD/DEAH box for RNA helicase (Gilman et al., 2017), and the K homology (KH) domain (Valverde et al., 2008)

(**Fig. 22A**). Of particular interest for our study, these RBDs had been previously described as R-methylated and, in specific cases, it was reported that this PTM could affect - either positively or negatively- binding to RNA (Bedford & Richard, 2005; Blackwell & Ceman, 2012). Indeed, in a recent publication from our group (Massignani et al., 2022), we demonstrated not only that RBPs are in general hypermethylated (bearing up to five or more R-methyl-sites) but also that two categories of R-methyl-sites may co-exist: “structural” or “constitutive”, methyl-sites that are overall refractory to modulation, and “dynamic” methyl-sites, frequently located into RBD, whose changes may affect protein-protein or protein-RNA interactions.

Considering that glycine-arginine-rich (GAR) domains and RG/RGG box could mediate nucleic acid-protein interactions (Chong et al., 2018) and that arginine located in RGG domains are preferred targets of PRMTs (Bedford & Richard, 2005), we asked whether the specific enrichment of this motif could be observed in our interface-enriched protein list. Remarkably, when we analyzed the amino acids surrounding each arginine in search of emerging motifs, we found a strong enrichment of the RG\RGG-repeated region in the interface proteins, but not in the WCE dataset (**Fig. 22B**). This result in our opinion suggests that RBPs are main targets of PRMTs and that modulation of their R-methylation state may be directly linked to their RNA-binding capability.

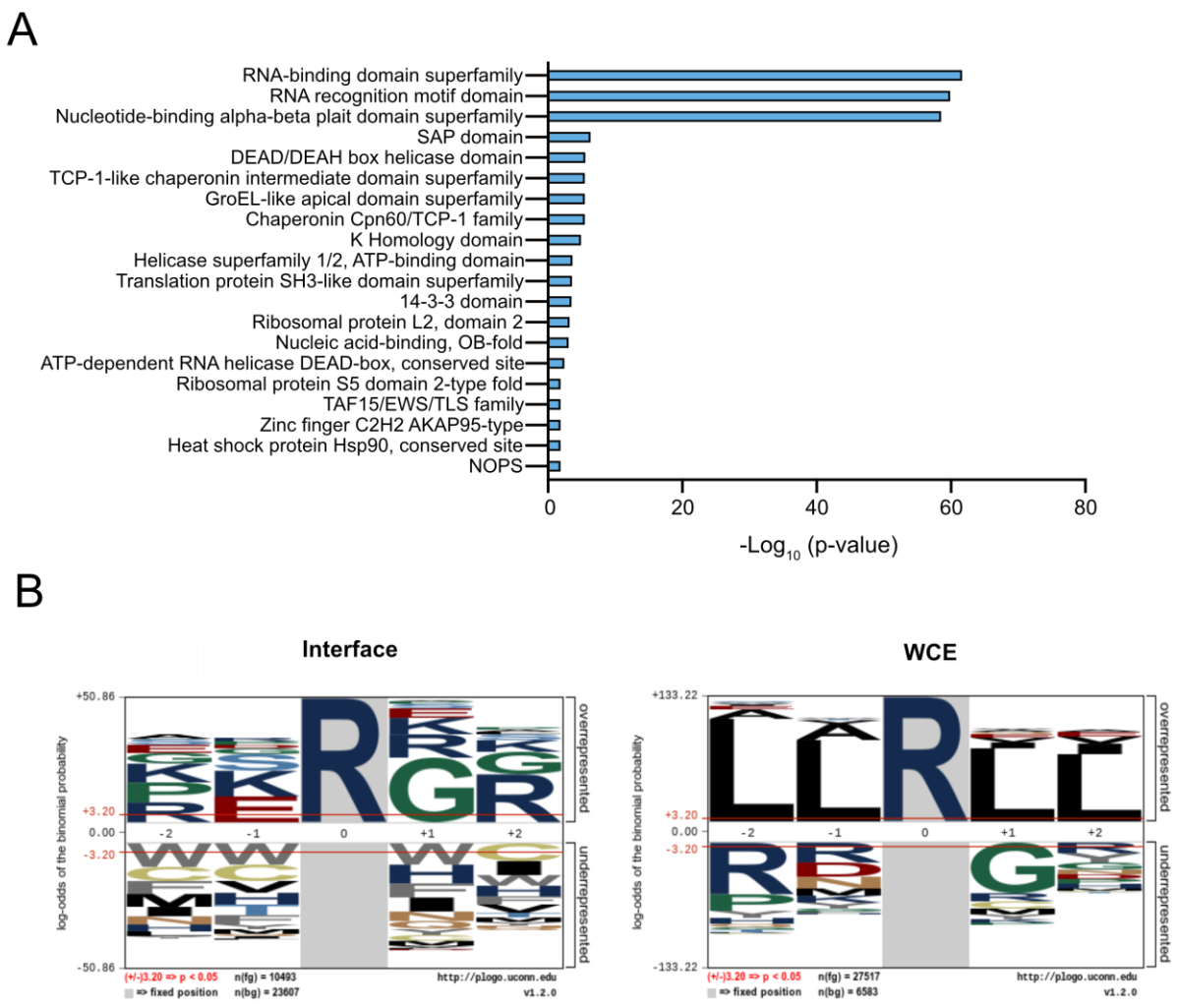

Figure 22: Further characterization of the interface-enriched proteins

A) Domain enrichment analysis of the interface-enriched proteins performed by STRING database on the list of the interface proteins. **B)** Over-representation analysis of the R-centered sequences, performed with the pLogo software, comparing the interface and the WCE proteins. *Adapted from* (Maniaci et al., 2021).

5.4 Quantitative analysis of OOPS-MS data highlights the impact of R-methylation state on RNA binding capability

We then took advantage of the implemented proteomic approach to identify and robustly quantify the global proteomic changes both in the interface and in the WCE, in dependence on R-methylation remodeling. Overall, our quantitative OOPS experiment generated information at different levels. First, thanks to the use of MS023 and GSK591 normalized

over DMSO, we could appreciate differential protein expression and the capability to bind RNA specifically associated with asymmetric or symmetric R-di-methylation remodeling. Second, the comparison between the interface and the WCE allowed distinguishing changes in the interface that represented differential interaction to RNA from changes that merely reflected the protein expression modulation by the drugs. To retrieve and display such information, we performed a supervised clustering analysis of the MS023/DMSO and GSK591/DMSO Log_2 SILAC ratios from the "proteinGroups. txt" file generated by MaxQuant (see M&M paragraph 4.12). We selected only proteins whose SILAC ratio count (RC) was ≥ 1 in all conditions, both in the interface and in the WCE. From 416 proteins profiled according to this criterion, four different clusters emerged (**Fig. 23**). Cluster 1, consisting of 53 proteins (red), and Cluster 2, consisting of 85 proteins (blue), represent proteins enriched in the interface fraction (+1 and +1.5 Log_2 SILAC ratio, respectively) but not in WCE upon MS023 treatment. This pattern suggests that MS023, by modulating MMA/ADMA balance in a set of RBPs, positively influenced their interaction with RNAs and that, since the same trend was not observed in the WCE, this effect is not the consequence of increased protein expression. Cluster 3, including 206 proteins (green), represents proteins that are not significantly modulated by MS023 or GSK591, neither at the level of RNA binding capability nor of protein expression. Finally, Cluster 4, constituted by 65 proteins (yellow), represents proteins whose expression is overall not significantly changing upon PRMT inhibition, but that display minor down-regulation in the interface upon GSK591 treatment. Two proteins, MANF and HMGB1 are of interest because they are significantly down-regulated in the interface, but not in the WCE, upon both MS023 and GSK591 treatment. This suggests that modulation of both types of R-di-methylation reduces their interaction with RNAs, independently from protein expression.

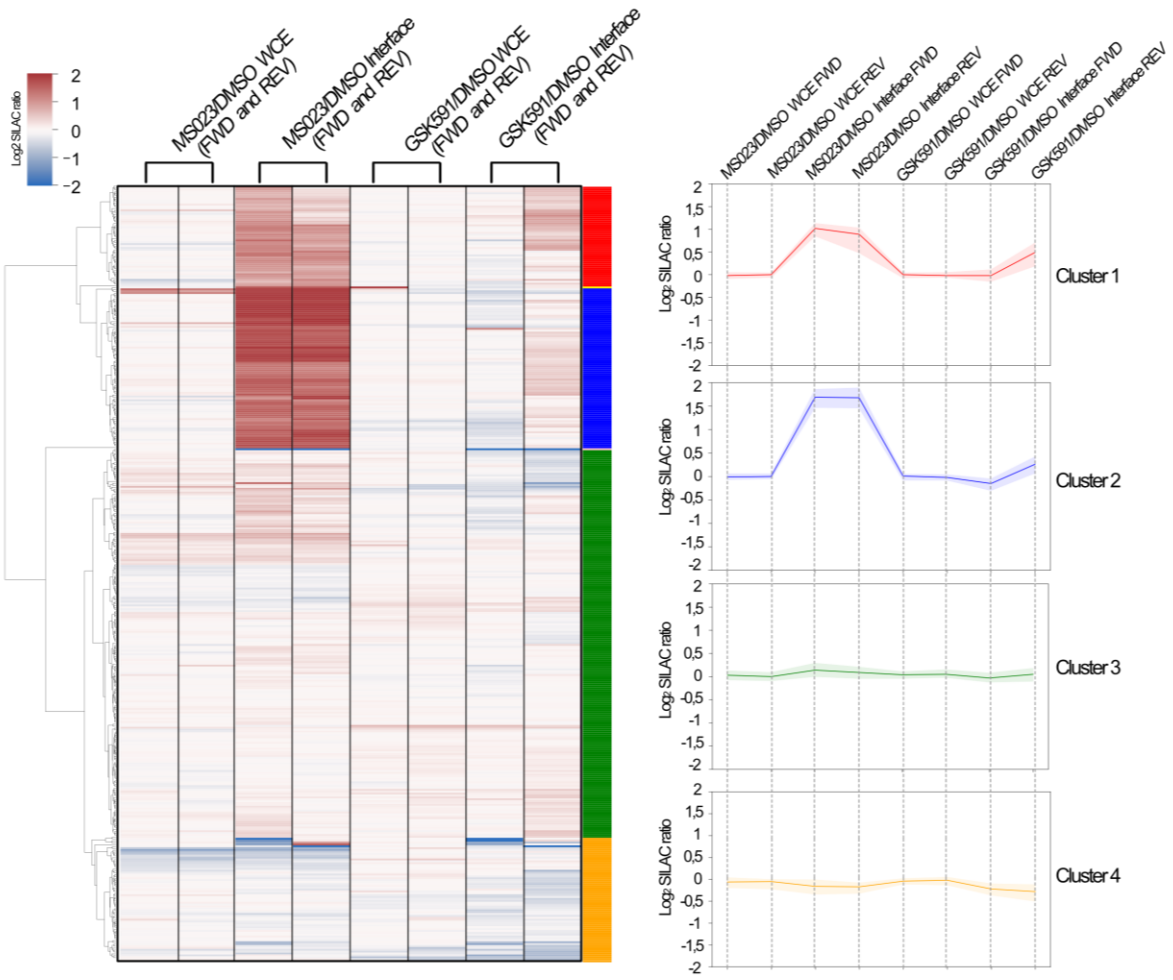

Figure 23: Dynamics of RBP-RNA interactions in dependence on PRMT pharmacological modulation

Supervised clustering analysis of the SILAC-OOPS proteomics data. Supervised clustering analysis of differential protein expression or differential RNA-binding after MS023 and GSK591 treatment, normalized on DMSO led to the definition of four representative clusters: Cluster 1 and Cluster 2 contain proteins with Log2 SILAC ratio MS023/DMSO +1 and +1.5, respectively, only in the interface fraction; Cluster 3 and Cluster 4 contains proteins overall not significantly modulated in the interface, with Cluster 4 displaying a mild down-regulation in the interface upon GSK591 (-0.3 Log2 SILAC ratios). *Adapted from* (Maniaci et al., 2021).

To better highlight the different abilities to bind RNA in dependence on the type of PRMT inhibitor, we normalized the MS023/DMSO and GSK591/DMSO SILAC ratios over the same ratios in the WCE and plotted the Log_2 of each normalized SILAC ratio in the forward versus the reverse experiment. For each scatterplot, we defined significant outliers considering the

mean(μ) ± 1 standard deviation(σ) as the cut-off of a normal distribution of the SILAC protein ratios. Thus, we identified 77 proteins up-regulated (+1σ) and 4 down-regulated (−1σ) upon MS023 (**Fig. 24A**). The same analysis carried out with the GSK591/DMSO SILAC ratio led to the identification of only 4 proteins significantly down-regulated (−1σ), two of which (MANF and HMGB1) were also down-regulated by MS023. No proteins appeared to be up-regulated in the interface fraction upon GSK591 treatment (**Fig. 24B**). Overall, this analysis robustly indicated that the modulation of MMA/ADMA balance consequently to MS023 treatment is the main regulator of the RBPs-RNA interaction.

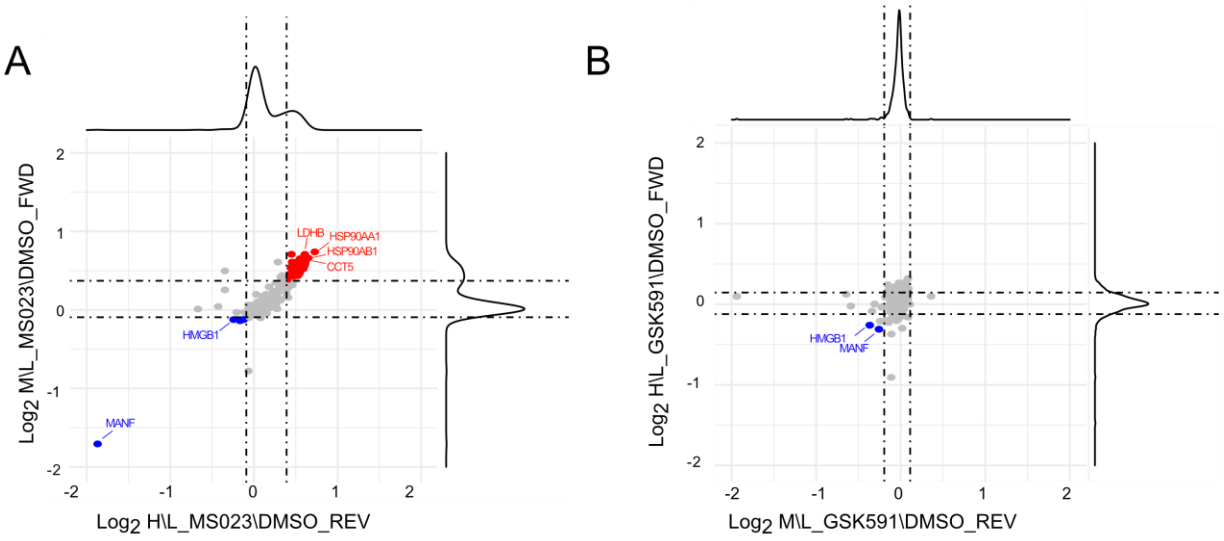

Figure 24: MS023 has a higher impact than GSK591 on RBP-RNA interactions

A) Scatter-plot representation of the normalized Log2 SILAC ratio in MS023-treated condition. Scatter-plot of the Log2 MS023/DMSO SILAC ratio of interface proteins, normalized on the respective protein SILAC ratio in the WCE, in FWD versus REV experiment. Dashed lines indicate μ±1σ of the respective SILAC protein ratio distributions; proteins up- or down-regulated are displayed in red and blue, respectively. **B)** Scatter-plot representation of the normalized Log2 SILAC ratio in GSK591 treated condition. The scatter plot displays the Log2 GSK591/DMSO SILAC ratio of interface proteins, normalized on the respective SILAC ratio in the WCE in the FWD versus the REV experiment. Dashed lines indicate μ±1σ of the respective SILAC protein ratio distributions; proteins down-regulated are displayed in blue. *Adapted from* (Maniaci et al., 2021).

5.5 Complementary validations of the OOPS-MS data

The proteomics data revealed significant modulation of the RNA-binding capability of a set of proteins upon treatment with MS023, suggesting that the balance between MMA/ADMA of these proteins may be a player in modulating this process. To strengthen our data, we performed various validating experiments: a) we performed OOPS followed by WB profiling of selected proteins upon the same treatment; b) we repeated the OOPS-WB analysis upon PRMT1 protein depletion using short hairpin RNAs (shRNAs) targeting PRMT1, instead of the pharmacological treatment, to confirm the dependency on PRMT1; c) we assessed the effect of PRMT inhibition on RBP-RNA interactions by using an alternative strategy to enrich RBPs, named RNA Interactome Capture (RIC), which provide information about protein association to poly(A)-mRNAs.

5.5.1 OOPS-WB analysis upon PRMT pharmacological inhibition of selected candidates

We selected a few proteins representative of the different responses to PRMT inhibitors to validate the proteomics data by WB analysis (**Fig. 25A**). In particular, we chose: as loading control of interface NONO and HuR (gene name ELAV1) proteins, whose SILAC ratios were unchanged in the interface fraction upon the two treatments; HSP90AA1 and HMGB1 as representative of proteins significantly (up- and down-) regulated in the interface upon MS023 treatment, with no change at the protein expression level; hnRNPH3 and TIA1 because dynamically regulated both in the interface and WCE, so we interpreted their dynamic behavior more likely due to protein expression changes. WB profiling confirmed all the expected behaviors in the interface fraction when normalized on NONO and HuR levels in the corresponding functional states. In particular, upon MS023 treatment, HSP90AA1 and HMGB1 were up- and down-regulated, respectively, only in the interface. hnRNPH3 and TIA1 were up- and down-regulated, both in WCE and in the interface (**Fig. 25B**).

A

Protein ID	Protein Names	Gene Names	WCE				Interface			
			MS023/ DMSO FWD	MS023/ DMSO REV	GSK591/ DMSO FWD	GSK591/ DMSO REV	MS023/ DMSO FWD	MS023/ DMSO REV	GSK591/ DMSO FWD	GSK591/ DMSO REV
P07900	Heat shock protein HSP90-alpha	HSP90AA1	-0.02	0.05	-0.03	0.00	2.05	2.01	0.24	-0.19
P63104	14-3-3 protein zeta/delta	YWHAZ	-0.08	-0.07	-0.06	0.02	1.97	1.97	0.08	-0.21
P62258	14-3-3 protein epsilon	YWHAE	-0.06	0.00	0.04	0.01	1.90	1.90	0.02	-0.22
P27348	14-3-3 protein theta	YWHAQ	0.01	-0.05	0.05	0.03	1.88	1.82	0.27	0.17
P61981	14-3-3 protein gamma	YWHAG	-0.06	-0.03	-0.03	-0.12	1.78	1.72	-0.03	-0.22
A0A5F9Z	L-lactate dehydrogenase B chain	LDHB	-0.07	0.01	-0.03	0.04	2.05	2.27	0.09	-0.36
P48643	T-complex protein 1 (TCP1) subunit epsilon	CCT5	-0.06	0.00	0.07	0.06	1.98	2.06	0.44	0.02
P31942	Heterogeneous nuclear ribonucleoprotein H3	HNRNPH3	0.60	0.54	0.05	-0.12	0.67	0.58	0.02	-0.10
Q15233	Non-POU domain-containing octamer-binding protein	NONO	-0.05	-0.05	0.00	0.00	-0.24	-0.15	-0.10	-0.03
Q15717	ELAV-like protein 1 (HuR)	ELAVL1	-0.11	-0.15	0.16	0.07	-0.17	-0.17	-0.12	0.06
F8W8I6	Nucleolysin TIA-1 isoform p40	TIA1	-0.61	-0.73	0.36	-0.05	-0.94	-0.92	-0.35	-0.22
P09429	High mobility group protein B1	HMGB1	-0.07	-0.01	0.04	0.03	-0.89	-0.53	-0.97	-0.53
A8K878	Mesencephalic astrocyte-derived neurotrophic factor	MANF	-0.04	-0.12	-0.01	-0.18	-6.64	-5.64	-5.06	-6.64

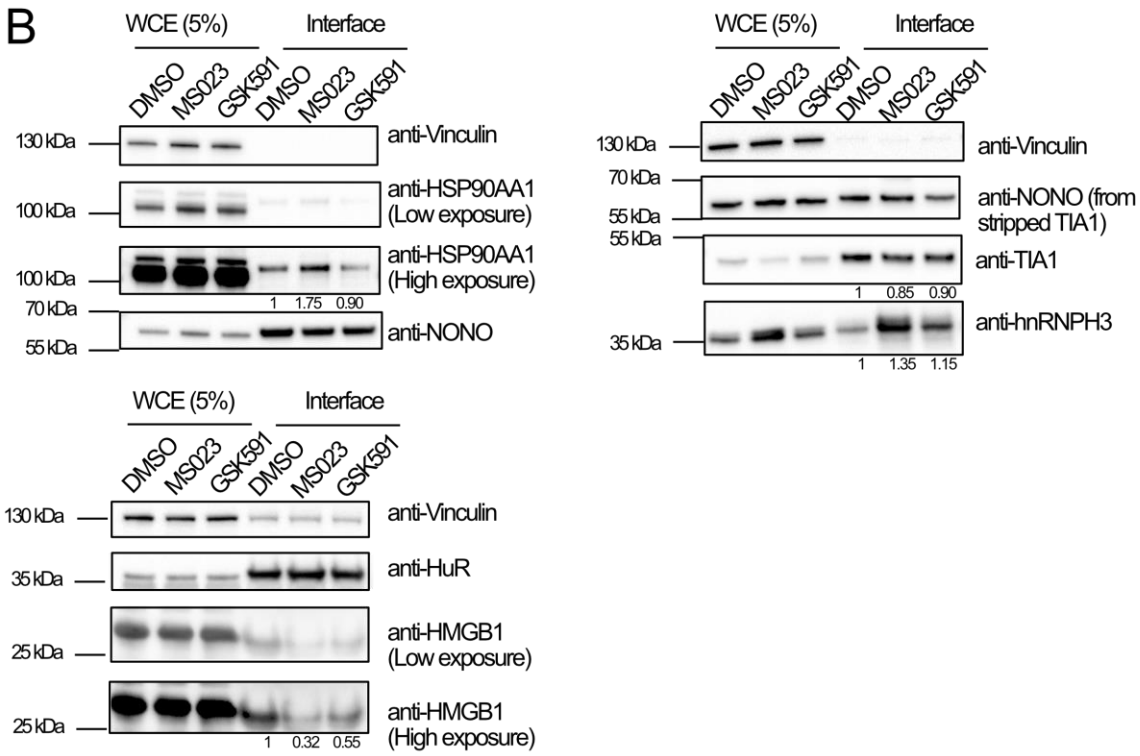

Figure 25: WB validation of the MS-based proteomics data

A) Overview of representative RBPs quantified by OOPS-MS data. The table summarizes the MS023/DMSO and GSK591/DMSO SILAC protein ratios of representative proteins, both in the WCE and in the interface fraction, both in FWD and REV experiments. **B)** WB validation of the differential protein response to PRMT inhibitors in the interface. WB profiling of representative protein, whose MS023/DMSO SILAC protein ratio is summarized in panel A: HSP90AA1 and HMGB1 were selected as examples of proteins up-regulated and down-regulated, respectively, in the interface but not in WCE upon MS023; hnRNPH3 was selected as an example of protein up-regulated upon MS023 in the interface as a consequence of a similar modulation in WCE; TIA1 was selected as an example of protein down-regulated upon MS023 treatment as a consequence of a similar modulation in WCE; NONO and HuR, displaying a SILAC protein ratio around 1 in the interface, were selected as loading controls for the interface fraction. Protein abundance in the interface upon different treatments was evaluated upon multiple normalizations of band intensities as described in the M&M section paragraph 4.7. (Replicate n=2) *Adapted from* (Maniaci et al., 2021).

5.5.2 OOPS-WB analysis upon PRMT1 silencing by RNA interference

To confirm the relevant role of PRMT1 in governing these dynamics, we used RNAi to deplete this enzyme in place of MS023-triggered PRMT1 inhibition. We transfected HeLa cells with two different short hairpin RNA (shRNA) constructs specifically targeting PRMT1 (shPRMT1 #1 and shPRMT1 #2); a scrambled shRNA (shScramble) was designed as negative control (see Material and Methods section 4.8). The choice of using two distinct shRNAs allows for controlling for potential off-target effects (Taxman et al., 2010). WB analysis confirmed that both shPRMT1 effectively silenced PRMT1, without off-target effects on other PRMT types I, like PRMT4 or PRMT6 (**Fig. 26A**), while the PRMT1 levels was unaffected in cells transduced with shScramble. OOPS-WB was carried out in upon shScramble and PRMT1 KD, both in the WCE and in the interface fraction from OOPS. We observed a specific increase of HSP90AA1 and a parallel decrease of HMGB1 in the interface when PRMT1 was depleted, without associated protein expression changes in the WCE (**Fig. 26B**). These results corroborated the data obtained upon pharmacological inhibition of PRMT1 and confirmed its dominant role - among the PRMT type I family- in modulating RBP-RNA interactions.

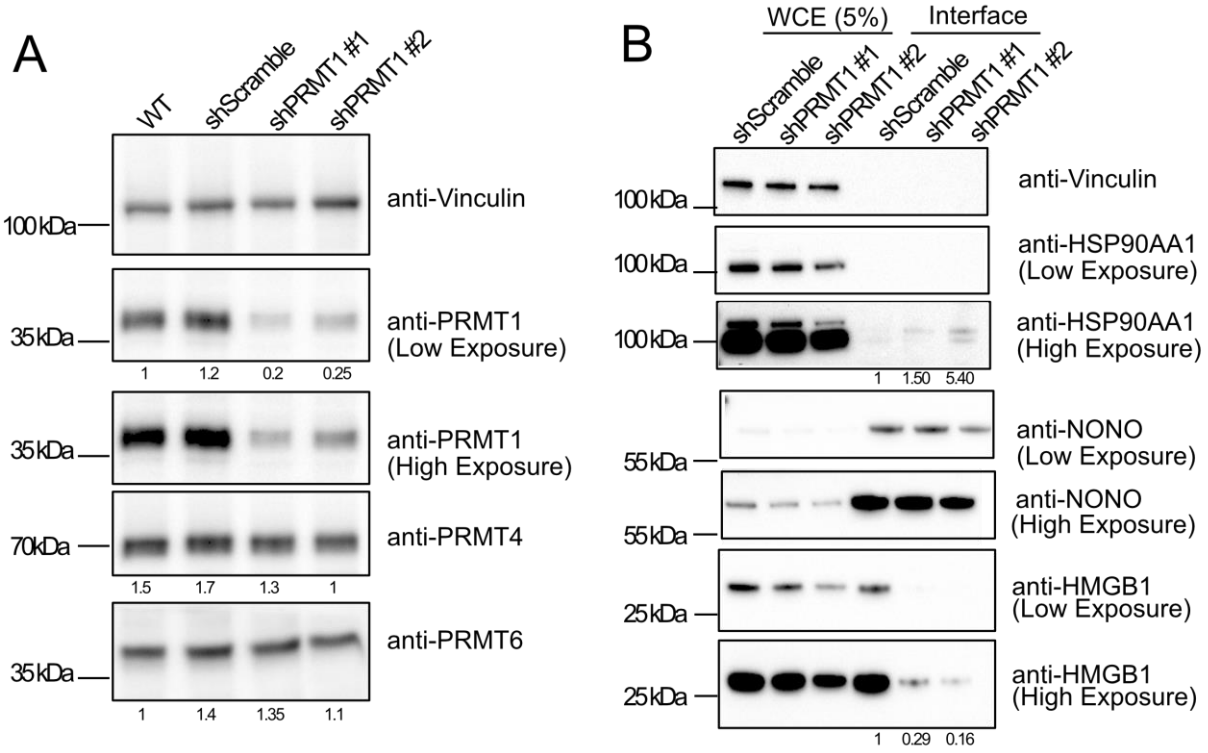

Figure 26: Validation of the PRMT1-mediated RBP-RNA binding dynamicity

A) WB profiling of PRMT1, PRMT4, and PRMT6 upon PRMT1 knock-down by two distinct shRNA constructs. (Replicate n=1) **B)** WB profiling of HSP90AA1 and HMG1 protein in WCE and interface fraction following OOPS in PRMT1 KD and control (scramble shRNA) cells. Protein abundance in the interface upon different treatments was evaluated upon multiple normalizations of band intensities as described in the M&M section paragraph 4.7. (Replicate n=1) *Adapted from* (Maniaci et al., 2021).

5.5.3 RNA Interactome Capture (RIC)-MS analysis corroborates OOPS-MS data

To corroborate the OOPS-MS data with a complementary method to dissect protein-RNA interactions, we performed the RNA Interactome Capture (RIC) experiment, which enables pull-down poly(A)-mRNAs and co-associating RBPs by using oligo(dT)-conjugated beads (Castello et al., 2013, 2016; Perez-Perri et al., 2018). The RIC approach still requires UV-crosslinking to covalently stabilize RBP-RNA binding but, in contrast to OOPS, it only allows for the enrichment of RBPs associated with poly(A)-mRNAs due to the immuno-affinity enrichment obtained by oligo(dT)-conjugated beads. Indeed, poly(A)-mRNAs represent

only a small fraction of the total cellular RNA, and RBPs associated with non-poly(A)-mRNA, such as rRNA processing proteins, are loosed. On the contrary, the OOPS strategy is based on the physicochemical phenomenon of phase-partition through the use of a Trizol™-Chloroform mixture, which allows the analysis of proteins associated with all RNA types. With this difference in mind, we set to couple RIC with triple SILAC labeling, PRMT pharmacological inhibition, and MS analysis for protein identification and profiling, to assess the impact of R-methylation remodeling on RBP-poly(A)-mRNA interaction dynamics.

Upon poly(A)-mRNA pull-down, protein extraction, digestion, LC-MS/MS analysis and MaxQuant processing of the MS data, we obtained a list of 130 RBPs identified in at least one of the two replicates, in all three conditions (DMSO, MS023, and GSK591), both in the RIC and in the corresponding WCE. Similarly to the strategy undertaken in the OOPS-MS experiment, we normalized the protein SILAC ratios in the RIC over the corresponding values in the WCE (used as input), to discriminate changes in protein-mRNA interactions from mere protein expression variations. When we compared the list of proteins detected in the interface with the protein list from the RIC experiment, we observed a rather limited overlap (**Fig. 27A**), with 18% of the OOPS proteins also identified in the RIC experiment, whose dataset was much smaller (130 versus 433 in the OOPS). The limited overlap and the dissimilar size of the two proteomes can be explained in light of the following considerations: first, the different rationale of the two techniques that implied a more limited type of RBPs enriched by RIC given that the baits are represented by poly(A)-mRNAs only, while OOPS enriches proteins interacting with all RNA types. Second, the larger amount of starting material required for RIC imposed to work in 50mL falcon tubes which may have compromised the efficiency in capturing poly(A)-mRNAs of the small oligo(dT)-conjugated beads. Third, the higher number of washes before protein elution from the RIC beads could lead to lower recovery of interacting protein. When we carried out GO analysis on proteins identified only in the OOPS, terms like nucleus-cytosol transport, nuclear ribonucleoprotein complex, spliceosome, or mRNA 3'-end maturation emerged. On the other hand, when we

carried out the same analysis of the list of RBPs identified only in the RIC experiment, few terms related to translation emerged, and with a smaller p-value (-Log_{10} p-value less than 5) (**Fig. 27B**). Focusing on the proteins in common, we observed that a large proportion of proteins (61 out of 85, corresponding to 71% of the RIC dataset), comprising the hnRNP family proteins, the ribosomal protein RPS2, and HuR, resulted unchanged both in the OOPS and in the RIC experiment. More interestingly, proteins MANF and HMGB1, which showed less RNA binding capability upon MS023 treatment in the interface of OOPS, resulted also significantly down-regulated in the RIC experiment (**Fig. 27C**). Unfortunately, none of the proteins up-regulated in the OOPS experiment was detected within the RIC experiment, so their dynamic behavior could not be validated by MS.

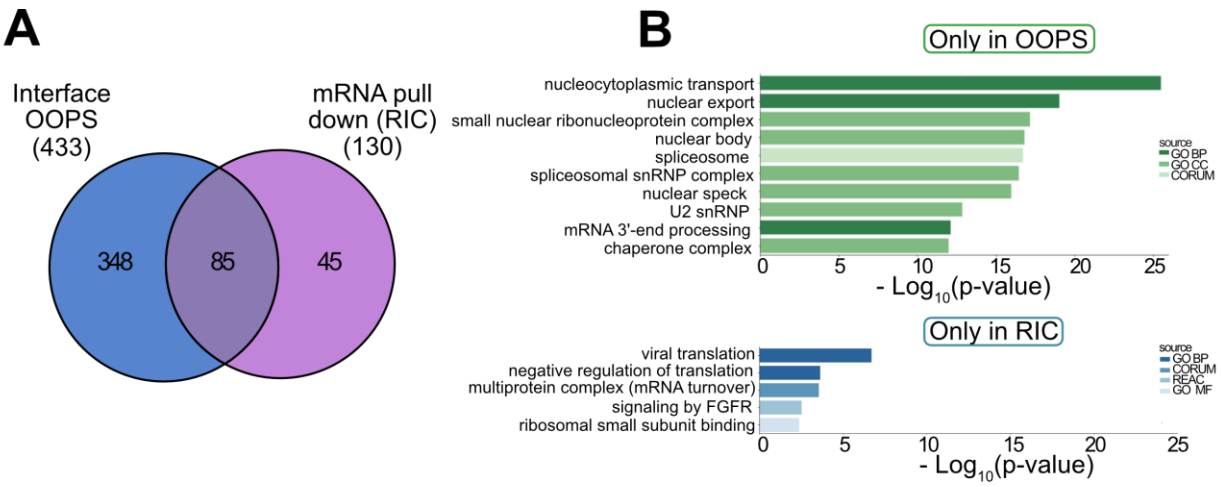

C

	Protein name	Gene name	Log2 MS023\DMSO RIC FWD	Log2 MS023\DMSO RIC REV	Log2 MS023\DMSO OOPS FWD	Log2 MS023\DMSO OOPS REV
G8JLB6	Heterogeneous nuclear ribonucleoprotein H	HNRNPH1	-0.13	0.01	0.00	0.02
O43390	Heterogeneous nuclear ribonucleoprotein R	HNRNPR	-0.29	-0.04	-0.19	-0.10
P51991	Heterogeneous nuclear ribonucleoprotein A3	HNRNPA3	-0.08	-0.18	-0.03	-0.05
G3V4C1	Heterogeneous nuclear ribonucleoprotein C	HNRNPAC	-0.09	0.21	-0.08	-0.01
P15880	40S ribosomal protein S2	RPS2	-0.45	-0.35	-0.01	-0.15
Q15717	ELAV-like protein 1 (HuR)	ELAVL1	-0.49	-0.13	-0.07	-0.02
A8K878	Mesencephalic astrocyte-derived neurotrophic factor	MANF	-5.82	N.D.	-6.21	-5.67
P09429	High mobility group protein B1	HMGB1	-3.40	-4.77	-0.81	-0.41

Figure 27: RIC experiment as OOPS-complementary strategy

A) Intersection between the protein in the interface fraction from OOPS-MS and those identified by RIC-MS validates 85 proteins identified in both experiments upon stringent filtering of MS-data (Andromeda score ≥25, identified by at least two peptides, one of which unique, for each experiment). **B)** Comparative GO analysis of the most enriched biological process terms from proteins identified in either OOPS only or RIC only. **C)** Table summarizing the MS023/DMSO SILAC protein ratios of representative unchanging and down-regulated proteins, both in the OOPS and in the RIC, both in FWD and REV SILAC experiments. *Adapted from* (Maniaci et al., 2021).

To expand the possible overlap between the OOPS and RIC datasets and to be more explorative, we relaxed the filtering criteria and considered as valid hits all proteins identified in at least one of the two replicates, regardless of the Andromeda score value. The intersection of these relaxed datasets led to a higher number of shared proteins, from 85 to 108 (**Fig. 28A**), the majority of which (75%) were not significantly changed either in RIC nor in OOPS experiments upon drug treatment. Among the significantly down-regulated, nine proteins were annotated (TCEA1, NQO1, HISTH1E, RPL26, RPS19, RPS27A, RRBP1, H2AFV and FKBP3) in addition to MANF and HMGB1. Noteworthy, the protein RALY emerged as significantly up-regulated upon MS023 treatment in both OOPS and RIC experiments. As further validation of our data, for the CCT5 protein, that was up-regulated in the interface upon MS023 in OOPS but not identified in the RIC-MS experiment, we carried out RIC followed by WB analysis in untreated and drug-treated cells and could confirm its increased association with mRNA induced by MS023 treatment. The HuR protein, which from RIC-MS analysis emerged unchanging despite the treatments, was used as loading control for the RIC fraction (**Fig. 28B**). Taken together, these results support our previous hypothesis that -at least for a subset of proteins- the MS023-mediated modulation of PRMT1 activity entailed modulation of RBP-RNA interaction, probably through a change of their MMA/ADMA level.

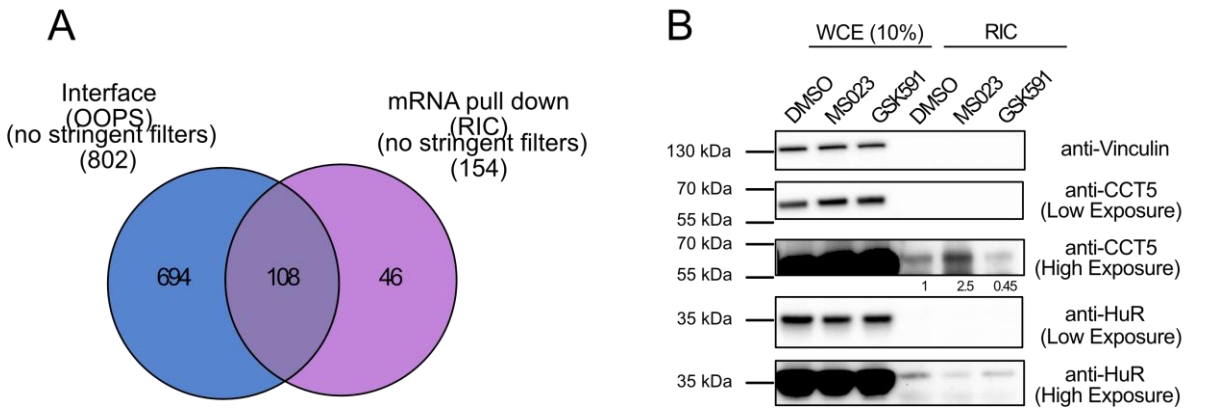

Figure 28: Less stringent criteria for the RIC analysis

A)Venn diagram displaying the intersection of proteins identified in OOPS and RIC when filtering criteria were relaxed, as described in the text. **B)** WB analysis of CCT5 protein upon MS023 treatment in the RIC experiment confirms its increased binding to RNA. Vinculin and HuR were used as loading control for WCE and interface, respectively. Protein abundance in the interface upon different treatments was evaluated upon multiple normalizations of band intensities as described in the M&M section paragraph 4.7. (Replicate n=1). *Adapted from* (Maniaci et al., 2021).

5.6 R-methylation profiling of candidate RBPs by IP-WB suggests a link between the modulation of MMA and RNA-interaction

It is described that R-methylation is an abundant and common PTM and that it is crucial in the regulation of several biological processes (Fulton et al., 2019; F. Zhang et al., 2021). To understand in which proportion MMA/ADMA and MMA/SDMA balance impact on RNA-binding capability, we compared the number of proteins significantly modulated in the WCE and in the interface upon PRMT inhibition. In the WCE, 258 over 2061 (12%) proteins are significantly modulated upon MS023, while in the interface 89 over 433 (21%) **(Fig. 29A**). Fisher's exact test applied to these numbers confirmed that the increased percentage is statistically significant (p-value<0.0001). This indicated that the MS023-mediated modulation of the MMA/ADMA balance influences the protein-RNA binding more than the gene expression regulation. On the other hand, when we performed the same type of analysis upon the GSK591 treatment, we noted 365 proteins modulated in the WCE over

2061 (18%) while only 10 proteins over 433 (2%) in the interface. This confirmed that the modulation of MMA/SDMA balance has a role in modulating protein expression stronger than that in regulating RNA-binding. Applying the same rationale, we carried out WB profiling of global R-methylation by using pan-antibodies against MMA, ADMA, and SDMA upon MS023 and GSK591 treatment, both in the WCE and in the interface fraction from the OOPS experiment. As previously described (Eram et al., 2016), MS023 treatment in the WCE induced reduction of ADMA and a concomitant increase of MMA (**Fig. 29B**) and SDMA (**Fig. 29C**). Along the same line, although to a lesser extent, GSK591 induced a reduction in SDMA but without any compensatory effect on MMA and ADMA. A possible explanation for the observed phenomenon may be the so-called “substrate scavenging effect”: when PRMT1 is lost, other PRMTs could methylate the PRMT1 substrate sites that remain free. The massive MMA increase was neither observed with the loss of other PRMT type I, such as PRMT3, PRMT4/CARM1, or PRMT6, nor with the loss of PRMT5, the major PRMT type II (Dhar et al., 2013). This difference can be explained by the fact that PRMT1 is the most active PRMT, accounting for 85% of PRMT activity in the cell (Tewary et al., 2019). Interestingly, the described patterns for global MMA, ADMA, and SDMA modulation in dependence on the PRMT inhibitor type, not only were maintained but they looked even more pronounced in the interface (**Fig. 29B** and **Fig. 29C**). This piece of data, confirmed once again that the RBPs represent a class of proteins largely and dynamically R-methylated.

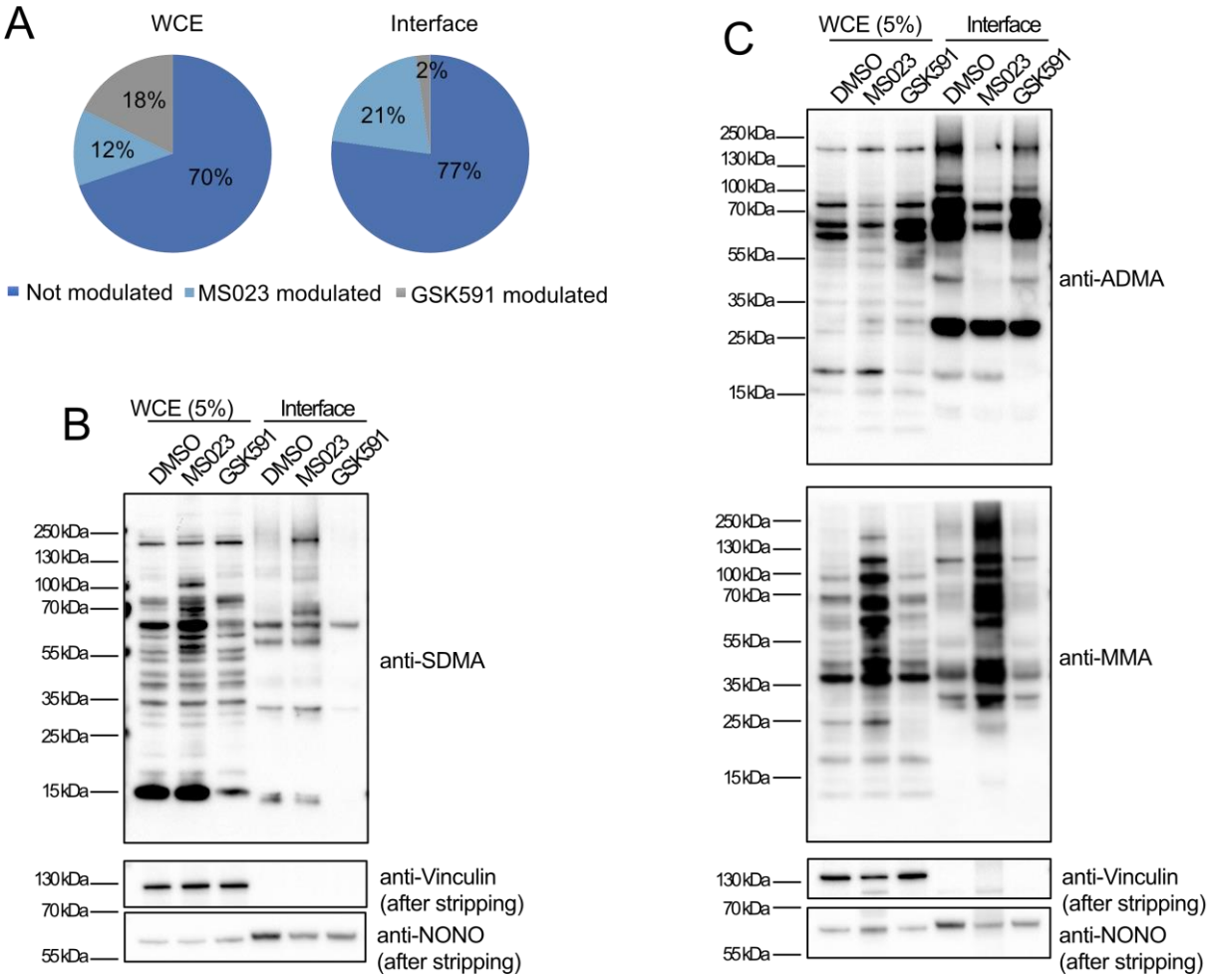

Figure 29: Dynamic RBP-RNA interactions are linked to RBPs R-methylation state

A) Percentage of proteins modulated, depending on drug treatment. The percentage of proteins significantly modulated (±1σ) was calculated in dependence on MS023 or GSK591 treatment, both in the WCE and in the interface fraction. In the WCE the two treatments equally modulate protein expression (12% regulated by MS023 and 18% by GSK591, respectively), whereas in the interface fraction RBP-RNA interactions are almost exclusively regulated by MS023 (21% regulated by MS023 and 2% regulated by GSK591, respectively). **B)** WB profiling of dynamic regulation of global protein symmetric R-di-methylation (SDMA). WB analysis was carried out on aliquots of WCE and interface fraction in control DMSO and upon MS023 and GSK591. Vinculin and NONO proteins were used as loading control for the WCE and the interface, respectively. **C)** WB profiling of dynamic regulation of protein asymmetric R-di-methylation (ADMA) and R-mono-methylation (MMA). WB analysis was carried out on aliquots of WCE and interface fraction in control DMSO and upon MS023 and GSK591. The same membrane was first probed with an anti-ADMA antibody, then stripped and used to detect SDMA. Vinculin and NONO proteins were used as loading control for the WCE and the interface, respectively. *Adapted from* (Maniaci et al., 2021).

To specifically validate the R-methylation state of the most interesting candidates, we set to immuno-precipitate some of them and subsequently profile their MMA, ADMA,

and SDMA levels by WB using pan-antibodies against the three distinct R-methylation states and comparing MS023-, GSK591- and DMSO-treated cells. For this purpose, we selected LDHB and 14-3-3 proteins, which are already annotated in the online database PhosphositePlus (Hornbeck et al., 2012) to be monomethylated. Both LDHB and 14-3-3 proteins from the MS023-treated condition showed alteration of their MMA state compared to DMSO; this effect was not detected or less pronounced upon GSK591-treatment (**Fig. 30A** and **30B**). This is in agreement with our OOPS-MS proteomics data, which indicated that modulation of MMA/ADMA balance is the major player in the regulation of RNA-binding potential. Unfortunately, the signals for ADMA and for SDMA were ambiguous or unchanging upon drug treatments (**Fig. 30A** and **30B**). Overall, these data suggested that the observed differences in RNA-binding capability upon MS023 treatment could be linked to the alteration of the R-methylation state of the candidate RBPs.

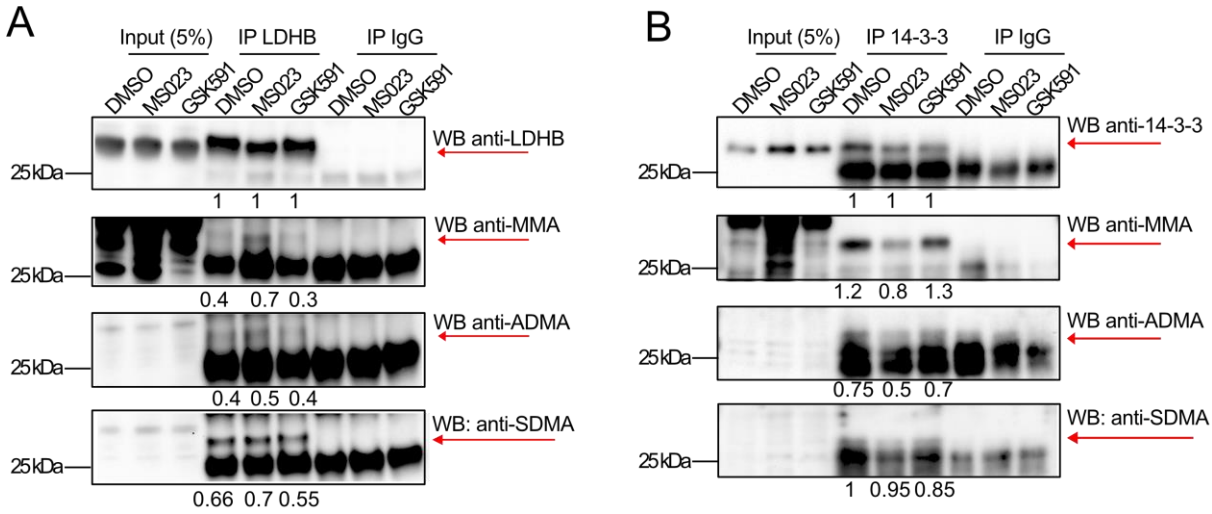

Figure 30: IP-WB analysis of LDHB and 14-3-3 proteins

A) Protein IP followed by WB validation of the R-methylation state of LDHB protein as representative for MS023-modulated RBPs in the OOPS. The R-methylation states of LDHB proteins were assessed upon DMSO, MS023, or GSK591 treatment by protein IP followed by WB with the anti-pan-methyl antibodies against MMA, ADMA, and SDMA. IgGs were used as mock controls for IP. For LDHB MMA and SDMA

are clearly detectable, while the ADMA signal is ambiguous, due to the strong cross-contaminating signals of the light chains of denatured antibodies. Protein abundance in the IP upon different treatments was evaluated upon multiple normalizations of band intensities as described in the M&M section paragraph 4.7. (Replicate n=2) **B)** Protein immunoprecipitation (IP) followed by WB validation of the R-methylation state of 14-3-3 proteins as representative for MS023-modulated RBPs in the OOPS. The R-methylation states of 14-3-3 proteins were assessed upon DMSO, MS023, or GSK591 treatment by protein IP followed by modification analysis by probing with the anti-pan-methyl antibodies against MMA, ADMA, and SDMA. IgGs were used as mock controls for IP. For 14-3-3 MMA is clearly detectable, while the ADMA and SDMA signals are ambiguous, due to the strong cross-contaminating signals of the light chains of denatured antibodies. Protein abundance in the interface upon different treatments was evaluated upon multiple normalizations of band intensities as described in the M&M section paragraph 4.7. (Replicate n=2). *Adapted from* (Maniaci et al., 2021).

We then assessed how many proteins regulated by MS023 in the OOPS-MS experiment are already annotated as R-methylated. To this aim, we compared our protein list with the dataset of R-methylated proteins annotated in the online PTM database PhosphositePlus and in our recently published high-confidence methyl-proteome named (Massignani et al., 2022): 53 out of 103 (51.4%) proteins significantly up-regulated upon MS023 treatment in the WCE and 60 out of 77 (77.9%) enriched in the interface upon MS023 treatment, respectively, are annotated as R-methylated (**Fig. 31A**). Among them, only two of the 60 R-methylated proteins regulated in the interface are also regulated in the WCE, which once again, supports the idea of the mechanistic link between increased RBP-RNA interaction and modulation of RBP R-methylation state.

However, since it is also known that R-methylation modulation has an impact not only on protein-RNA but also on protein-protein interaction, we could not exclude that some proteins were enriched in the interface because they are co-interactors of other RNA-interacting RBPs. To assess this possibility, we carried out a protein-protein interaction analysis on the MS023-up-regulated RBPs from the interface by Cytoscape (https://cytoscape.org/), an open-source software platform for visualizing complex networks. As depicted in **Fig. 31B**, this analysis produced a high-density network in which each protein interacts at least with another partner within the same group.

Interestingly, the RBPs with higher node degrees, such as HSP90AA1, HSP90AB1, or the 14-3-3 protein family YWHAZ and YWHAQ, were also those displaying higher SILAC ratios upon MS023 treatment. These results highlight the importance of considering the possible enrichment of strong co-interactors in our OOPS-MS experiments.

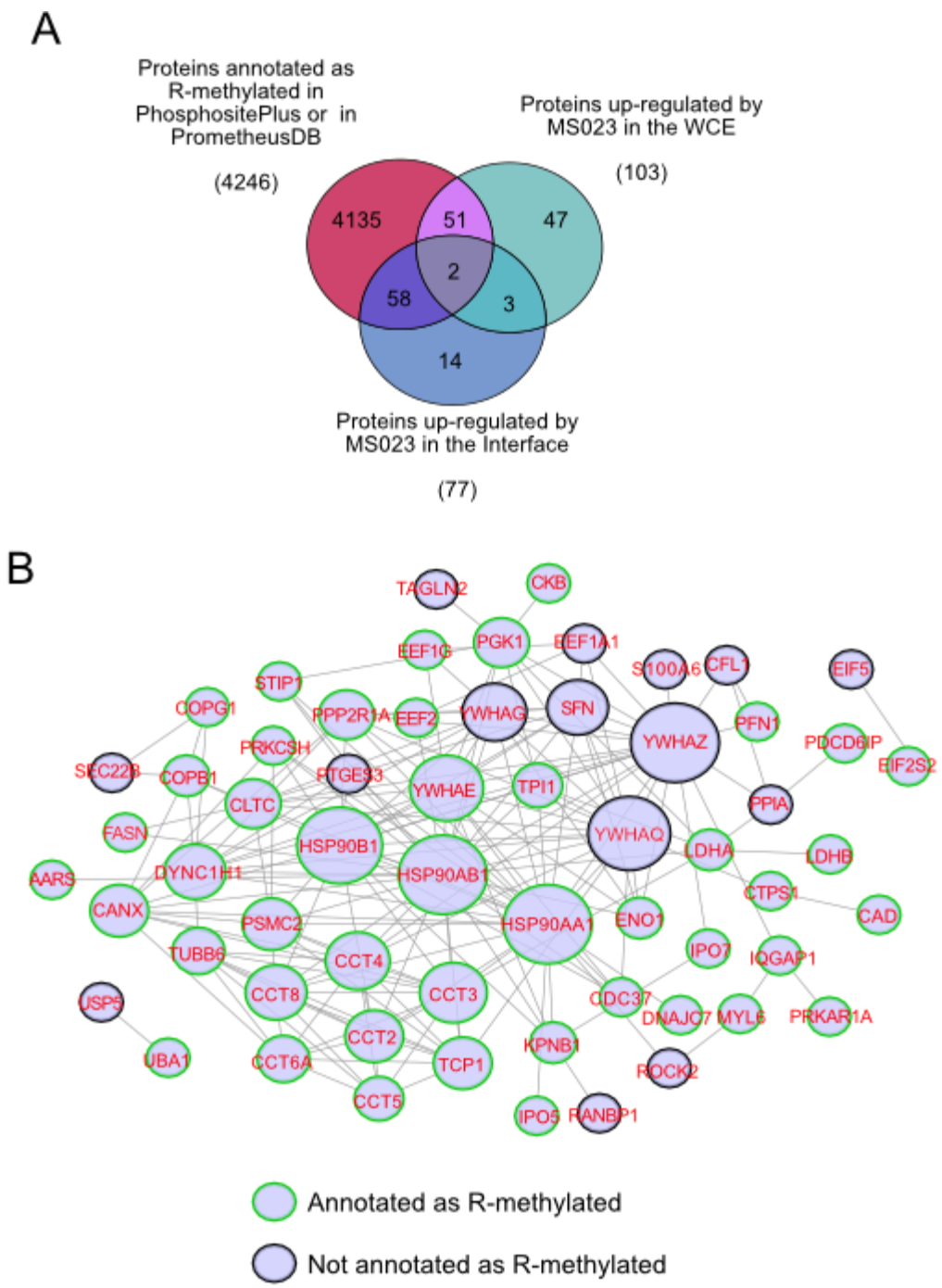

Figure 31: Protein-protein interaction network of MS023-upregulated proteins

A) Venn diagram illustrating the intersection of the proteins up-regulated by MS023 in the WCE, in the interface fraction and annotated as R-methylated in PhospshositePlus Database (Hornbeck et al., 2012) and in our internal high-confidence methyl-proteome dataset “PrometheusDB” (Massignani et al., 2022) **B)** Protein-protein interaction network of proteins modulated in the interface fraction by MS023 treatment. The size of each node is proportional to the number of interacting proteins. Proteins annotated in PhospshositePlus database or in our internal high-confidence methyl-proteome are circled in green;

proteins not annotated in the above-mentioned datasets are circled in black. *Adapted from* (Maniaci et al., 2021).

5.7 Subcellular localization and Liquid-Liquid Phase Separation of candidate RBPs

In light of published evidence connecting modulation of the R-methylation state of a protein with its subcellular localization (Kolb et al., 2018; Sinha et al., 2010), we set out to investigate the subcellular localization of some of the proteins that resulted enriched in the interface upon MS023 treatment by immunofluorescence (IF) analysis. In particular, for some RBPs (e.g. FUS protein), evidence linking its MMA/ADMA modulation with its tendency to undergo "Liquid-Liquid Phase Separation (LLPS)" is published (Yamaguchi & Kitajo, 2012). LLPS is a biophysical phenomenon inducing transient and dynamic RBP-RNA aggregates, usually in response to stress, creating different types of granules that share the feature of not being physically separated by a membrane and are thus called "Membrane Less Organelles (MLOs)" (Gomes & Shorter, 2019). To investigate the possibility that the increased RNA-binding capability upon MS023 treatment could result in LLPS of these proteins, we intersected the list of RBPs up-regulated in the interface fraction upon MS023 with two available databases of proteins undergoing LLPS: the Phase Separation Database (PhaSepDB) (You et al., 2020) and the RNA Granule Database (http://rnagranuledb.lunenfeld.ca/). This intersection analysis highlighted that 42 out of 77 (54.5%) of MS023-upregulated proteins in the interface are indeed annotated as displaying LLPS propensity (**Fig. 32A**). Among them, LDHB and 14-3-3 proteins were selected for assessment. IF analysis was employed to assess their subcellular location and/or co-localization with both RNAs and the G3BP1 protein, commonly used as a marker for cytosolic MLOs named stress granules (SGs) (P. Yang et al., 2020). While proteins were profiled by antibodies, RNA was detected taking advantage of the "click" chemistry strategy,

based on the incorporation of the uridine analog 5-ethynyluridine (EU) into newly transcribed RNA in cultured cells, so that EU-labeled RNA can be detected by IF (Jao & Salic, 2008). Co-IF analysis showed that MS023 treatment induces the formation of cytosolic granules with both LDHB and 14-3-3 proteins and that in such aggregates the two proteins co-localize with both G3BP1 and EU-labelled RNA (**Fig. 32B** and **Fig. 33A**).

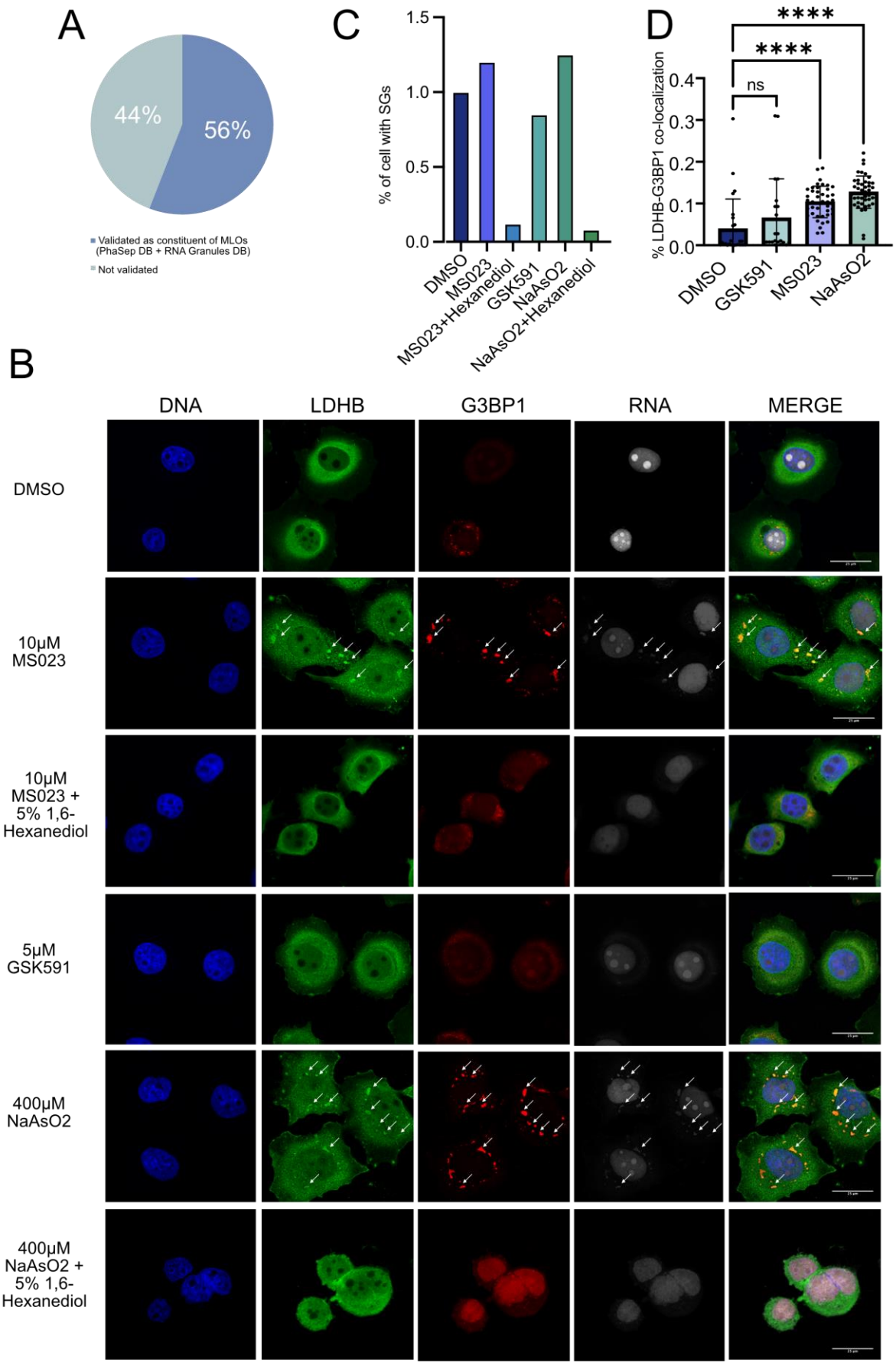
A
44%
56%
Validated as constituent of MLOs (PhaSep DB + RNA Granules DB)
Not validated
C
% of cell with SGs
1.5
1.0
0.5
0.0
DMSO
MS023
MS023+Hexanediol
GSK591
NaAsO2
NaAsO2+Hexanediol
D
% LDHB-G3BP1 co-localization
0.4
0.3
0.2
0.1
0.0
ns
****
****
DMSO
GSK591
MS023
NaAsO2
B
DNA
LDHB
G3BP1
RNA
MERGE
DMSO
10μM MS023
10μM MS023 + 5% 1,6-Hexanediol
5μM GSK591
400μM NaAsO2
400μM NaAsO2 + 5% 1,6-Hexanediol

Figure 32: Immunofluorescence analysis of LDHB protein

A) Among the 77 proteins up-regulated in the interface fraction upon MS023, 43 (56%) were also annotated as proteins undergoing phase separation in at least one of the two PhaSepDB (http://db.phasep.pro/) and RNA Granules DB (http://rnagranuledb.lunenfeld.ca/) databases. 16% of them were annotated in both databases, 33% were annotated only in PhaSepDB and 51% were annotated only in RNA Granules DB. **B)** Immunofluorescence (IF) analysis of LDHB protein in basal condition (DMSO) and in response to different treatments. Representative IF images show LDHB protein subcellular localization in HeLa cells treated with the following compounds: DMSO, 10 μM MS023, and 5 μM GSK591 for 48 hours; 10 μM MS023 for 48 hours, followed by 10 min treatment with 5% 1,6-Hexanediol; 400μM NaAsO2 for 30 min, or 400μM NaAsO2 for 30 min followed by 10 min treatment with 5% 1,6-Hexanediol. Immunostaining of RNA was performed with the Click-iT™ RNA Alexa Fluor™ 594 Imaging Kit. DAPI staining was used for DNA visualization. G3BP1 staining was used as positive control for SGs formation. DNA, LDHB, G3BP1, and RNA staining and the respective merged images are displayed. Images were taken by SP80BS confocal microscopy using a 60× oil objective, and a scale bar of 25 μM is included in the merged figure. White arrows indicate the co-localization of target RBP, G3BP1, and RNA. **C)** Bar-graph representation of the percentage of cells with stress granules. The bar graph shows the percentage of cells with at least 1 G3BP1 positive SGs for the different conditions; all treatments were normalized over DMSO. **D)** Bar-graph representation of the percentage of LDHB-G3BP1 co-localization. The image describes the percentage of co-localization between G3BP1 and LDHB in the SGs in each condition. All treatments were normalized over the DMSO. Statistical significance was calculated by Student's t-test (*$p < 0.05$). *Adapted from* (Maniaci et al., 2021).

Interestingly, such granules were either not observed, or detected to a much lower extent, when cells were treated with DMSO and GSK591. To prove that the observed behavior is really the consequence of LLPS, we designed two additional controls: first, we used 1,6-Hexanediol, an alcohol widely employed to disrupt MLOs (Düster et al., 2021); second, we used $NaAsO_2$ treatment, which is a well-known inducer of SGs formation ((Wheeler et al., 2016). Remarkably, both MS023-induced LDHB- and 14-3-3- granules were dissolved upon treatment with 1,6-Hexanediol, which confirms their LLPS property. Second, co-IF analysis upon $NaAsO_2$ treatment showed stronger and more numerous G3BP1-positive MLOs, co-localizing with both EU-labelled RNA and our proteins of interest, which confirmed that they are *bona fide* associated with SGs. Also in this case, the disassembly of such granules by 1,6-Hexanediol confirmed their LLPS property (**Fig. 32B** and **Fig. 33A**).

Unbiased and automatic quantification of the signal intensities of the acquired images revealed that, upon both MS023 and $NaAsO_2$, the number of cells presenting at least one SG per cell increased significantly and that formation of such granules is almost completely abolished upon 1,6-Hexanediol treatment (**Fig. 32C** and **Fig. 33B**). Furthermore, we calculated the percentage of co-localization between G3BP1 and LDHB and 14-3-3 proteins, we measured a statistically significant increase (p-value<0.001 and <0.05, respectively) upon MS023, but not upon GSK591 and DMSO (**Fig. 32D** and **Fig. 33C**).

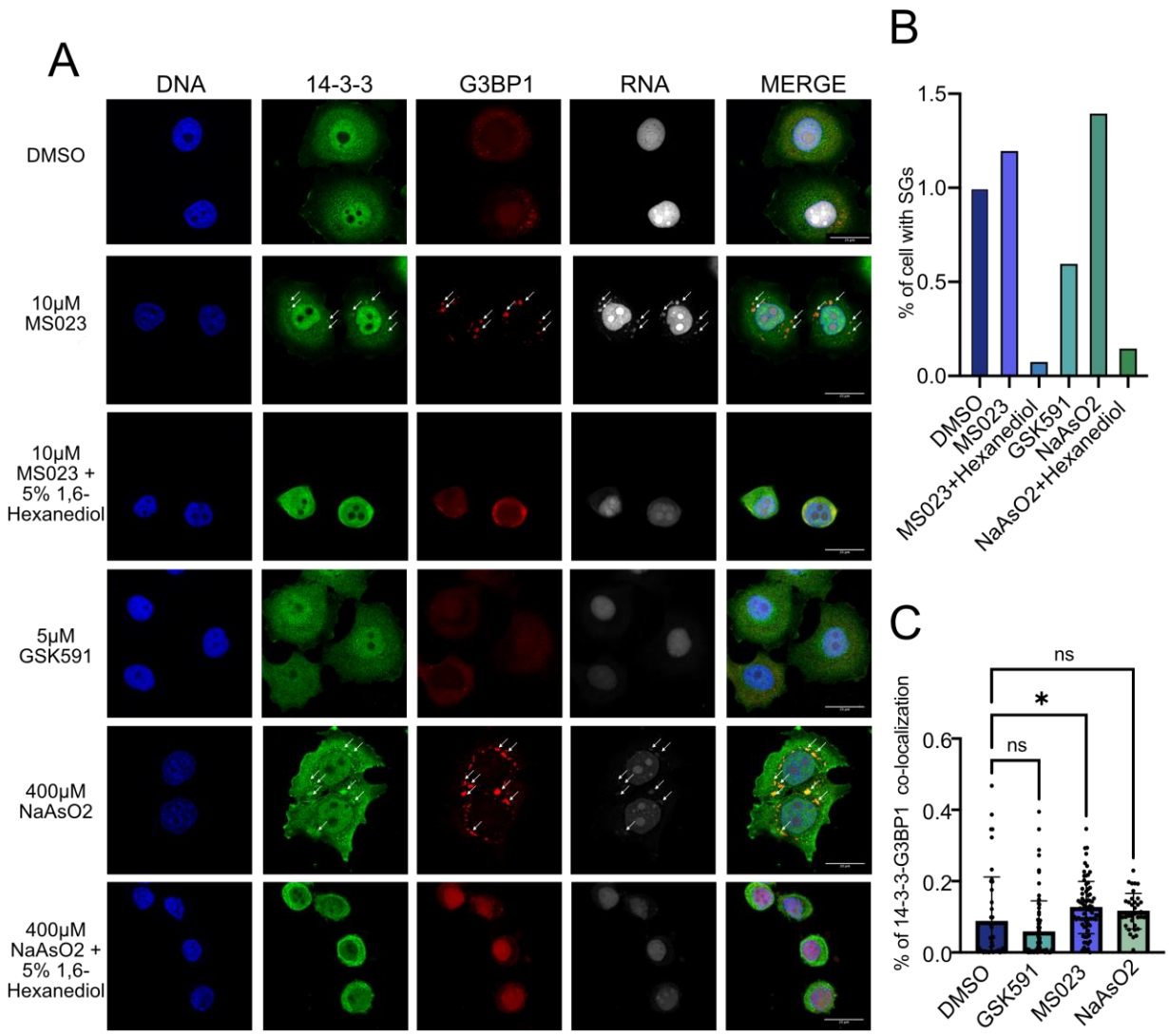

Figure 33: Immunofluorescence analysis of 14-3-3 proteins

A) Representative images of IF analysis of 14-3-3 protein in Hela cells treated with the following compounds: DMSO, 10 μM MS023, and 5 μM GSK591 for 48 hours; 10 μM MS023 for 48 hours, followed by 10 min treatment with 5% 1,6-Hexanediol; 400μM NaAsO2 for 30 min; 400μM NaAsO2 for 30 min followed by 10 min-treatment with 5% 1,6-Hexanediol. Immunostaining of RNA was performed with the Click-iT™ RNA Alexa Fluor™ 594 Imaging Kit. DAPI staining was used for nuclei visualization. G3BP1 staining was used as a positive control for SGs formation. DAPI, LDHB, G3BP1, and RNA staining and the respective merged images are displayed. Images were taken by SP8OBS confocal microscopy using a 60× oil objective, and a scale bar of 25 μM is included in the merged figure. White arrows indicate co-localization of target RBP, G3BP1, and RNA. **B)** The bar graph represents the percentage of cells with more than 1 G3BP1+ granule and all the treatments were normalized on the DMSO. **C)** Bar-graph representation of the percentage of 14-3-3 proteins-G3BP1 co-localization. The image describes the percentage of colocalization between G3BP1 and 14-3-3 proteins in the SGs in each condition. All the treatments were normalized over the DMSO. Statistical significance was calculated by Student's t-test (*$p < 0.05$). *Adapted from* (Maniaci et al., 2021).

When we performed protein-protein interaction analysis of the protein enriched in the interface upon MS023 treatment, we observed that the HSP90 family proteins were central in the network and that they displayed a high degree of nodes (**Fig. 31B**). Thus, we wondered whether the observed LLPS behavior could be driven by their HSP90 family proteins, instead of a direct consequence of MS023 treatment.

To investigate this possibility, we repeated the co-IF analyses of LDHB and 14-3-3 proteins in DMSO- and MS023-treated conditions, but upon 24h pre-treatment with the HSP90 inhibitor 17-AAG. The acquired IF images confirmed that there was no difference in MLOs formation, regardless of HSP90 inhibition (**Fig. 34**). This result ruled out the idea that HSP90 family proteins are the driver of these MLOs formation.

Collectively, our results allowed us to extrapolate a model, according to which PRMT1 inhibition leads to increased interaction between a subset of RBPs with cognate RNAs, which in turn, leads to MLOs formation. These results encouraged us to investigate the impact of R-methylation remodeling on RBP-RNA interaction in a more clinically relevant context.

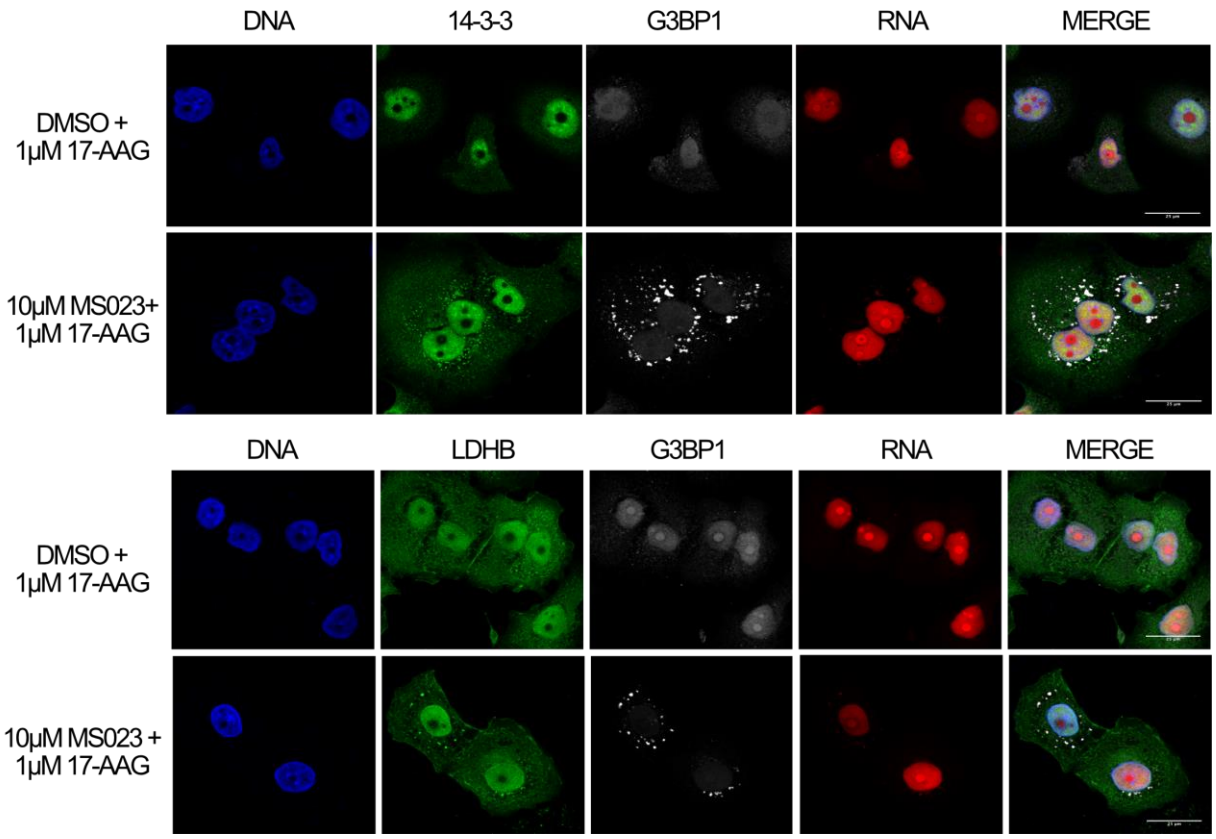

Figure 34: LDHB and 14-3-3 proteins LLPS is independent on HSP90 protein activity

Representative images of IF analysis of both 14-3-3 and LDHB proteins in HeLa cells pre-treated for 24h with 1μM 17-AAG (HSP90 inhibitor) and then treated for 48h with DMSO or 10μM MS023. In both cases, HSP90 inhibition does not impair the MS023-driven MLOs formation. Immunostaining of RNA was performed with the Click-iT™ RNA Alexa Fluor™ 594 Imaging Kit. DAPI staining was used for nuclei visualization. G3BP1 staining was used as a positive control for SGs formation. DAPI, LDHB, G3BP1, and RNA staining and the respective merged images are displayed. Images were taken by SP8OBS confocal microscopy using a 60× oil objective.

5.8 Analysis of RBPs-RNA interaction dynamics in ovarian cancer

Based on the quantitative methyl-proteomic analysis carried out in the context of CDDP-induced replicative stress in S-KO-V3 Epithelial ovarian cancer (EOC) (described in Musiani et al. 2020) and the data that I obtained which indicates that PRMT1 inhibition can modulate RBP-RNA interactions, we hypothesized a model whereby CDDP induces PRMT1-dependent R-methylation remodeling of some RBPs, which in turn, increases the interaction with RNA of a specific subset of RBPs and modulate CDDP-resistance in EOC.

5.8.1 Evaluation of ovarian cancer cell line sensitivity to CDDP

To confirm that S-KO-V3 cells, used in the Musiani et al. 2020 study, truly represent an appropriate model to investigate the RBP-RNA interaction dynamics in response to CDDP, we measured the CDDP half maximal effective concentration (EC_{50}) for a panel of ovarian cancer cell lines displaying different sensitivity to CDDP (S-KO-V3, OV90, COV362.4, Caov-3, A2780, and OVCAR3). Cells were treated with increasing doses of CDDP (1.25µM, 2.5µM, 5µM, 10µM, 20µM, 40µM, and 80µM) for 24h. Cell viability was calculated indirectly, by measuring the ATP content of each condition through the CellTiter-Glo® luminescent assay, and the EC_{50} for each cell line was calculated through dose-response non-linear regression analysis (see M&M paragraph 4.20). This analysis confirmed that S-KO-V3, OV90, and COV362.4 cells are good models of CDDP-resistant cell lines, displaying EC_{50} > 100µM CDDP. On the contrary, the EC_{50} for A2780 and OVCAR3 was < 20µM, so they could be considered models of CDDP-sensitive ovarian cancer cell lines. Caov-3 cells showed an intermediate sensitivity (EC_{50} around 43µM CDDP) (**Fig. 35**). Thus, we decided to carry out experiments in S-KO-V3 cells and to use the other cell lines for future validations of the emerging mechanisms experimentally observed.

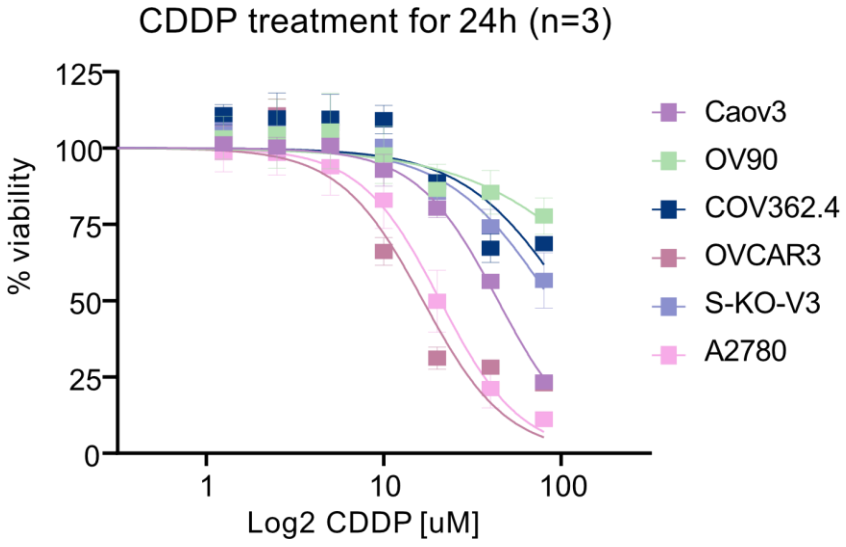

EC50 (µM)

	CDDP
Caov3	43 ± 0.9
OV90	>100
COV362.4	>100
OVCAR3	19 ± 6.2
S-KO-V3	>100
A2780	19 ± 2.3

Figure 35: Calculation of CDDP EC50 in EOC cell lines

On the left, dose-response curves show the different sensitivity to increasing doses of CDDP upon 24h of treatment of the indicated EOC cell lines. The EC_{50} for each cell line is summarized in the table on the right (biological replicates n=3).

5.8.2 OOPS-MS experiment to investigate the impact of CDDP on RBP-RNA interaction dynamics in CDDP-resistant EOC model

RBPs are key regulators of cancer progression and it was described that they regulate CDDP sensitivity (Rogoyski & Gerber, 2021). To assess how CDDP treatment could influence RBP-RNA interaction dynamics, we adopted the already implemented OOPS-MS approach in S-KO-V3 cells. We evaluated the CDDP-modulated RNA binding capability by coupling CDDP treatment with RBP-RNA complexes enrichment by OOPS and in-solution protein digestion by Trypsin, followed by peptide fractionation prior to high-resolution nLC-MS/MS analysis (**Fig. 36**).

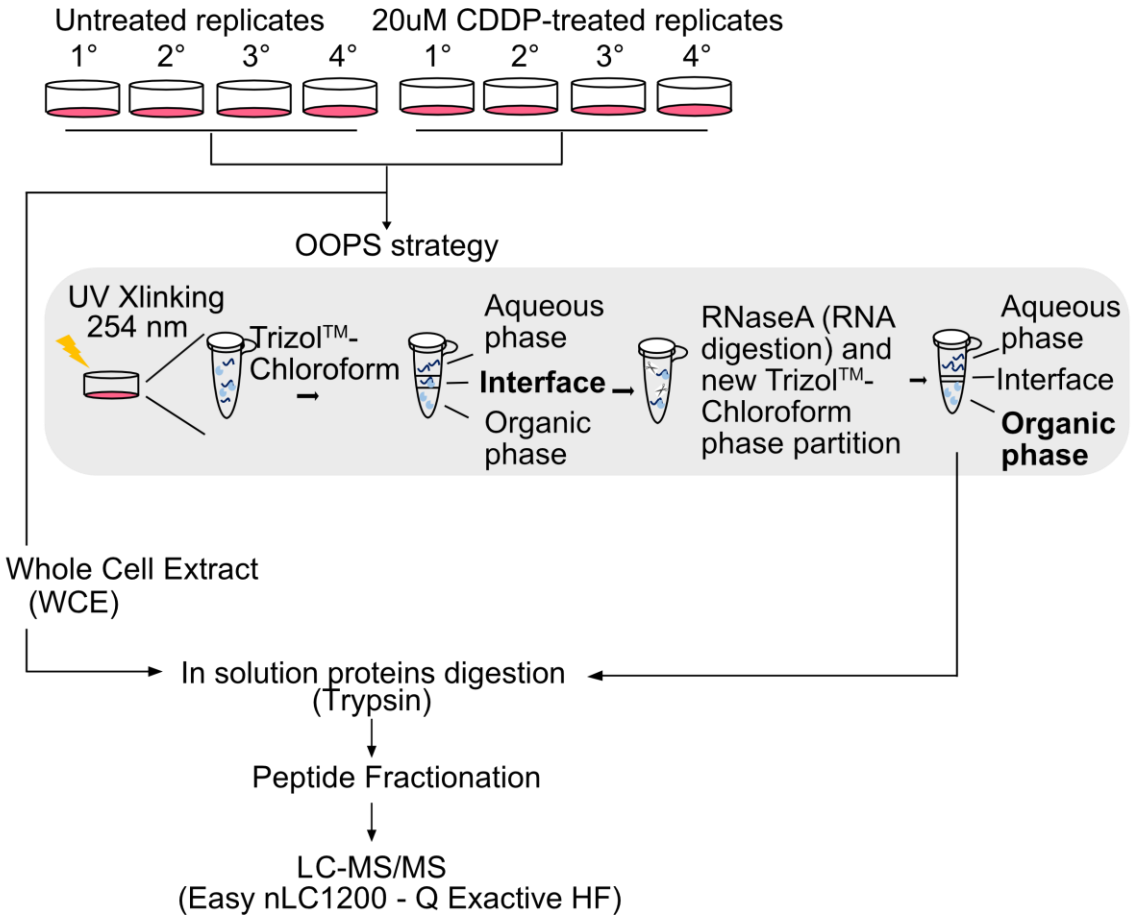

Figure 36: OOPS-MS proteomics to profile RBP-RNA interaction in dependence on CDDP

Workflow of the OOPS-MS approach. S-KO-V3 cells were grown in label-free medium, either untreated or treated with 20µM CDDP for 24 hours (biological replicates n=4). 10% of the sample was saved as whole cell extract (WCE), while the remaining cells were UV-crosslinked and phase-partitioned through the Trizol™-chloroform mixture. Proteins from both WCE and the interface were extracted in 9M UREA buffer, subjected to in-solution protein digestion by trypsin, and peptide fractionated prior to high-resolution MS.

In this experiment, cells were not SILAC-labeled but protein quantification was carried out by a label-free approach (see the introduction, paragraph 2.3.1). For this reason, we prepared four biological experimental replicates, for both untreated and 20µM CDDP-treated conditions, in order to give statistical robustness to the label-free quantitation (LFQ) of proteins. A small fraction (around 5%) of each condition was saved for WB profiling of two positive controls for treatment efficacy (**Fig.37**). In particular, an

increased level of phosphorylated H2A.X (γ-H2A.X) upon CDDP treatment confirmed the efficient induction of DNA damage response (DDR); the increased signal intensity of H4R3me2a, normalized over total H4, corroborated our previous observation that CDDP induces PRMT1 accumulation on chromatin and increased asymmetric R-di-methylation of its major histone target.

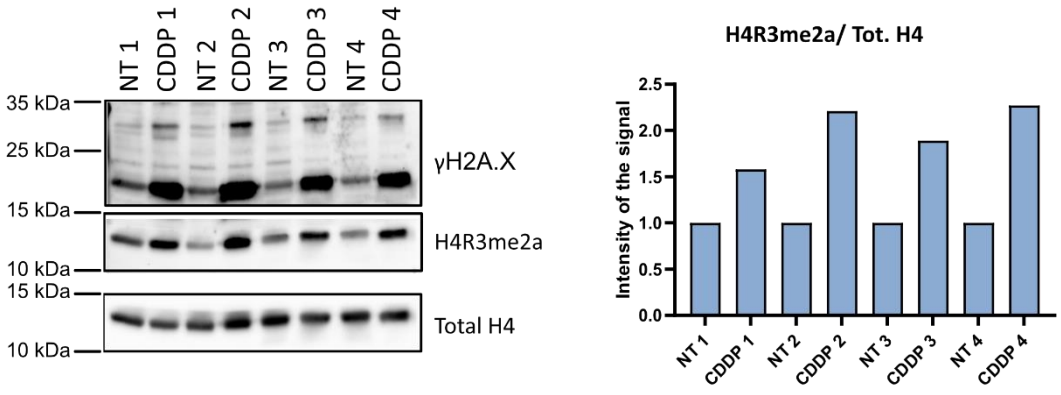

Figure 37: Assessment of CDDP treatment efficacy

Phosphorylated H2A.X (yH2A.X) was used as a positive control for DDR induction, while increased H4R3me2a level over total H4 was used as a readout of increased PRMT1 activity in chromatin (for each condition: biological replicate n=4). The bar graph represents the H4R3me2a/total H4 intensity ratio of WB bands. The ratio of all four CDDP-treated conditions is higher than the untreated counterpart.

Similar to the previous OOPS-MS experiment, a fraction of about 10% from each replicate was collected and saved as WCE. The remaining cells were UV-crosslinked and phased-partitioned through three consecutive Trizol™-chloroform extractions. The resulting interface fraction enriched in RNA-RBP complexes was collected, and proteins were extracted and subjected to in-solution protein digestion. Tryptic peptides were analyzed by high-resolution mass spectrometry. The MS raw data acquired were processed with the MaxQuant software package, as described (M&M, paragraph 4.12). The number of identified and quantified proteins was obtained from the MaxQuant output file “proteinGroups.txt” and is summarized in **Fig. 38.**

Tot n° of identified proteins	5911
Tot n° of quantifiable proteins	4774
Quantifiable proteins in the WCE	4752
Quantifiable proteins in the Interface	1106

Figure 38: Summary of the identified and quantified proteins in the OOPS-MS experiment in CDDP-treated S-KO-V3

Table summarizing the number of proteins identified and quantified by MaxQuant. The total number of identified proteins was obtained upon removal of reverse hits and possible contaminants. The same proteins were considered quantifiable if they own a MaxLFQ value in three out of four replicates, both in the WCE and Interface separately.

Upon data filtering by removing reverse sequences and potential protein contaminants (technical details in paragraph 4.12 of M&M section), we identified a total of 5911 proteins, including both WCE and interface. Since the experiment was performed in label-free conditions, we employed the MaxQuant algorithm for label-free quantification (MaxLFQ)(Cox et al., 2014), which is an XIC-based quantification approach (see Introduction, paragraph 2.3). We considered a protein as quantifiable if an LFQ value in three out of four replicates was detected for that protein. This criterion led to the identification of 4774 quantifiable proteins in total, 4752 specifically in the WCE, and 1106 specifically in the interface. Only the proteins quantifiable in the interface with corresponding LFQ values in the WCE (989 proteins) were taken into consideration for the subsequent quantitative analyses.

5.8.3 Quantitative analysis of the OOPS-MS experiment highlights the CDDP-induced substantial remodeling of RBP-RNA interaction

Following the same analytical strategy applied in the OOPS-MS coupled to PRMT pharmacological inhibition, we normalized the CDDP/NT LFQ intensity ratios in the interface over the corresponding ratios in the WCE, to highlight proteins differentially

enriched in the interface due to changes at the level of RNA-binding capability and not as a mere reflection of protein expression changes. We plotted the fold changes of the CDDP/NT ratios in the interface normalized over the WCE, in dependence on their statistical significance (FDR-adjusted p-value < 0.05) (**Fig. 39**).

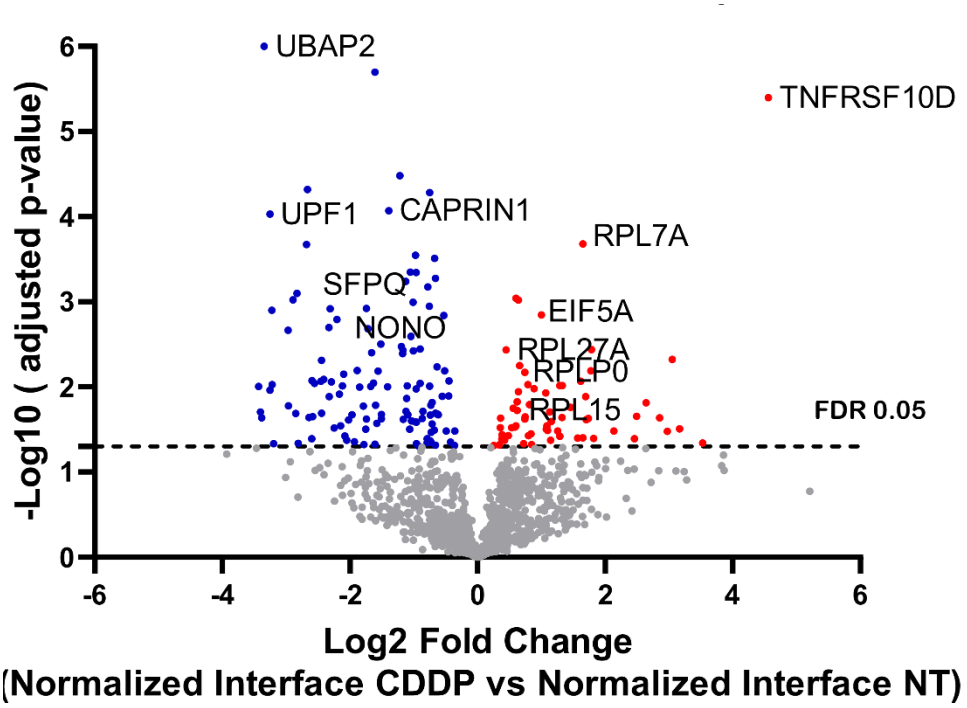

Figure 39: Quantitative analysis of the RBP-RNA interaction dynamicity upon CDDP-treatment

The volcano plot shows statistically significant (FDR-adjusted p-value < 0.05) changes, both enriched (in red) or depleted (in blue) in the interface upon CDDP treatment. The CDDP over NT fold change for each protein was normalized over the corresponding fold change in the WCE, to better highlight changes in RBP-RNA interaction and exclude indirect effects due to changes at the level of protein expression.

Among the most significantly down-regulated proteins, UBAP2, UPF1, and CAPRIN (Markmiller et al., 2018; Y. Sun et al., 2020)were annotated as SG components. SFPQ and NONO are considered core proteins of another type of MLO type, the paraspeckles (Bond & Fox, 2009). When we inspected the most up-regulated proteins, we noticed the presence of a tumor necrosis factor receptor superfamily member (TNFRSF10D).

Although this protein has never been described before as an RBP, it is a negative regulator of TRAIL-mediated apoptosis; therefore, its upregulation may represent one of the strategies adopted by the cells to overcome CDDP-induced death. In addition, among the most up-regulated proteins, we found a subset of ribosomal proteins (RPL7A, RPL27A, RPLP0, RPL15, RPL26, RPS10, RPS17, RPS12, MRPL42, MRLP2, MRPL12). This result was somewhat unexpected, given the fact that CDDP is described to cause a general block in translation, so we set to investigate this further. We then performed a functional analysis of the most enriched GO biological process of proteins significantly depleted or enriched in the interface (**Fig. 40**). Among the most depleted terms, “RNA processing” and “positive regulation of the translation” emerged, which are in line with the reported CDDP-mediated inhibition of mRNA translation (Becker et al., 2014). Surprisingly, the “stress granules assembly” term also belongs to this category. In line with this observation, we found published evidence that CDDP can induce the formation of SG-like cytoplasmic foci that - although positive for the G3BP1 marker, present substantially different protein composition than “canonical” SGs, are less dynamic, and with a kinetic of assembly that is dose-dependent with the drug (Pietras et al., 2022). This suggests that a subset of RBPs could establish RNA interactions leading to the aggregation of MLOs slightly different from the conventional SGs.

When we focused on the most enriched terms, we were particularly intrigued by the presence of the term “cytokine-mediated signaling pathway”, which is in line with our previous observation that CDDP induces the SASP secretory phenotype in EOC cell lines. Along this line, the enrichment of terms related to “regulation of exocytosis” and “regulation of cellular response to stress” are also particularly interesting in our opinion.

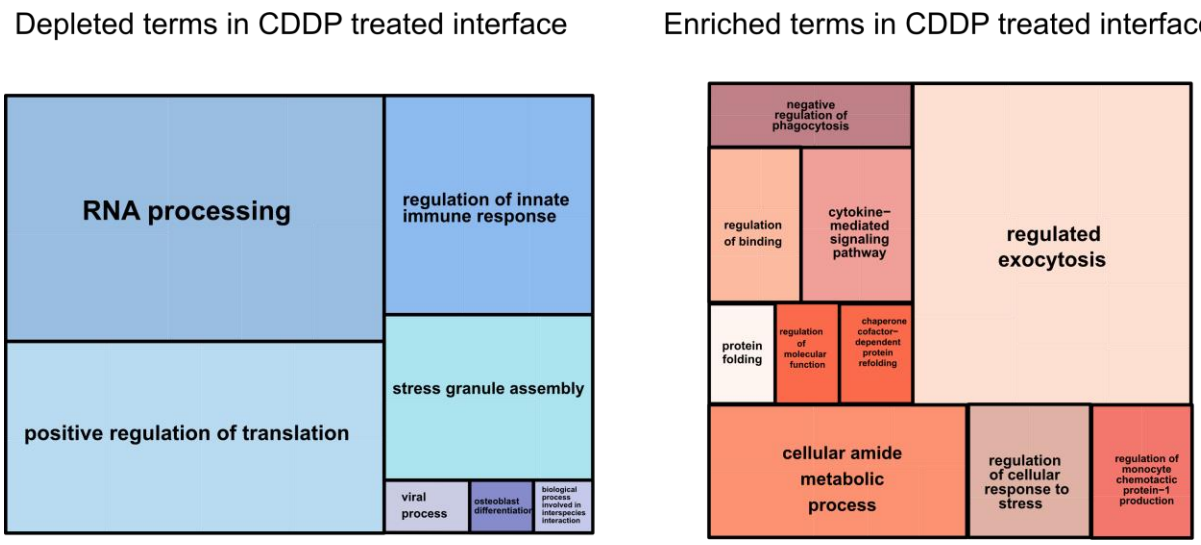

Figure 40: GO analysis of the dynamically regulated proteins in the interface from OOPS

Treemap representation of the GO-enriched biological processes enriched in proteins dynamically modulated in the interface fraction. GO analysis was performed by GOrilla and REVIGO on the set of up-regulated and down-regulated proteins in the interface, using WCE proteins as background.

These results set the basis for investigating a novel level of CDDP-resistance regulation mediated by RBPs. We performed a more in-depth GO analysis of the subset of ribosomal proteins that were up-regulated in the normalized interface. The use of the EuRBP database (Liao et al., 2020b) as background allowed the removal of the most generic terms related to their intrinsic RNA-binding feature, while the use of an FDR-adjusted p-value (q-score) gave statistical significance to the observed enrichment. This analysis showed that all the above-mentioned ribosomal proteins are enriched for GO terms related to “SRP-dependent co-translational targeting to membrane”, “protein targeting ER”, “regulation of stress response”, or “protein localization to ER” (**Fig. 41**). Since the Signal Recognition Particle (SRP)-dependent co-translational protein targeting to the Endoplasmic Reticulum (ER) represents an evolutionary-conserved mechanism to target proteins into the secretory pathway (Nyathi et al., 2013), our result is particularly intriguing and suggests that the ribosomal proteins enriched at the

interface may be linked to the increased translation of selected mRNAs involved in secretory phenotypes (such as SASP).

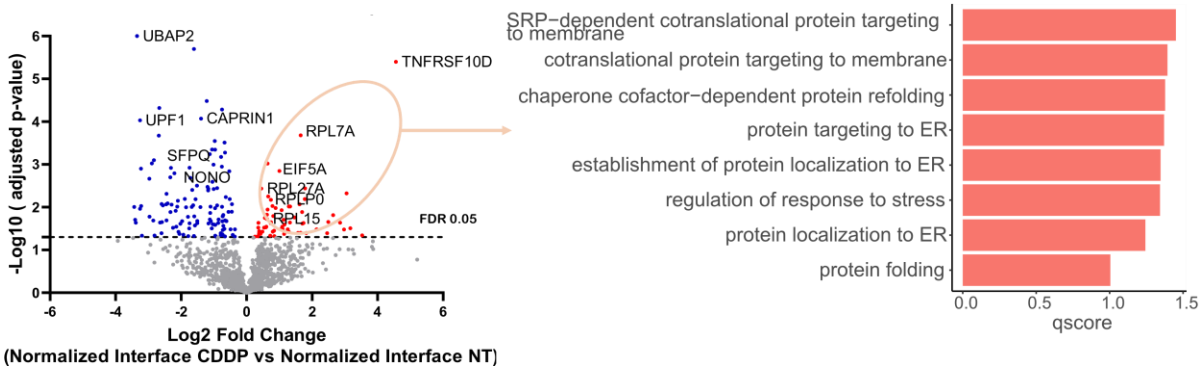

Figure 41: In-depth GO analysis of the ribosomal proteins up-regulated in the CDDP-treated interface

In-depth GO analysis was performed starting from the ribosomal proteins up-regulated in the volcano plot in Fig. 21. The bar-blot indicates the q-score value of the most enriched biological processes.

We then assessed whether the observed CDDP-triggered RBP-RNA interaction modulation occurs also in other CDDP-resistant EOC cell lines by performing the OOPS experiment followed by WB profiling of targeted RBPs in OV90 and COV362.4 cell lines. HuR, whose LFQ intensity value was unchanging among conditions, was used as loading control for the interface fraction. The presence of Vinculin was used to monitor the cross-contamination from non-RBP proteins. RPL7A and NONO were selected as representative of enriched and depleted proteins in the interface, respectively. In both OV90 and COV362.4 cells, WB profiling confirmed the data obtained in S-KO-V3. In particular, RPL7A and NONO were up- and down-regulated only in the interface upon CDDP, respectively (**Fig.42**). This validation is still preliminary and must be extended to other proteins; never the less these results suggest a common mechanism by which EOC cells resist to the platinum treatment through the alteration of RBP-RNA dynamics.

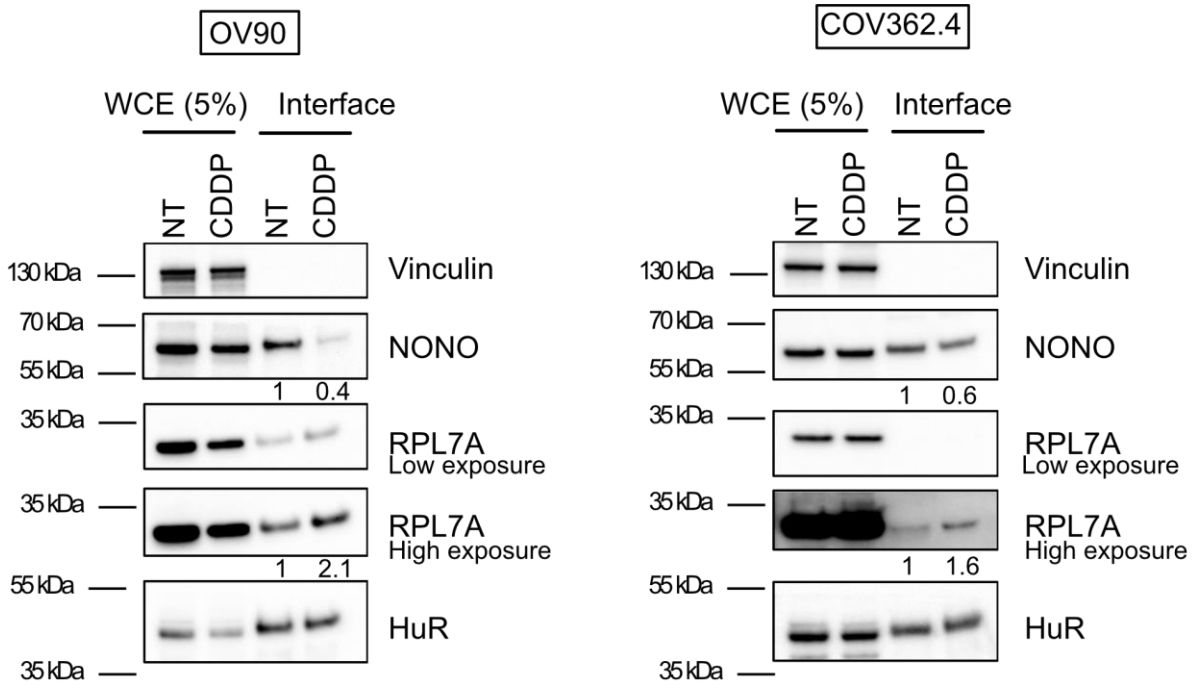

Figure 42: Validation of RBP-RNA dynamic interaction in other CDDP-resistant EOC cell lines

WB validation of the CDDP-triggered RBP-RNA dynamic interaction in OV90 and COV362.4 EOC cell lines. Vinculin was used as negative control, HuR as loading control for the interface, RPL7A and NONO as examples of proteins enriched and depleted in the CDDP-treated interface, respectively. Protein abundance in the interface upon different treatments was evaluated upon multiple normalizations of band intensities as described in the M&M section paragraph 4.7. (Replicate n=1).

5.8.4 Evaluation of the CDDP-induced RBP-RNA interaction remodeling as a consequence of R-methylation state changes

The OOPS-MS experiment revealed a substantial remodeling of RBP-RNA interactions induced by CDDP. To assess to what extent this effect could be ascribed to the modulation of the RBP R-methylation state, we first intersected the list of proteins dynamically modulated in the interface upon CDDP treatment with a list of proteins annotated as R-methylated with high-confidence in the in-house PrometheusDB (Massignani et al., 2022b)and in the open access repository for protein PTMs PhosphositePlus (Hornbeck et al., 2012). This intersection showed that the majority of proteins whose abundance in the interface changes upon CDDP treatment are already annotated as R-methylated (114 out

of 155) (**Fig. 43A**). Then, we intersected the same list of proteins with that containing the proteins enriched in the interface upon MS023 treatment: only 11 proteins (HSP90AB1, CCT4, EEF2, EEF1G, RANBP1, PPIA, EIF5A, EEF1A1, TAGLN2, PTGES3, S100A6) were modulated in the same direction by the two perturbations (**Fig. 43B**). This limited overlap could be explained by the fact that MS023 treatment reduces the levels of ADMA, but leads to a parallel increase of MMA (**Fig. 29**), while CDDP seems to impair both ADMA and MMA (Musiani et al., 2020). Hence, identifying the exact R-methylation sites regulated by CDDP and distinguishing the grades of R-methylation (MMA, ADMA, or SDMA) and how they are dynamically changed is crucial to better understand the mechanism affecting RNA-RBP interaction and, possibly, phase-separation.

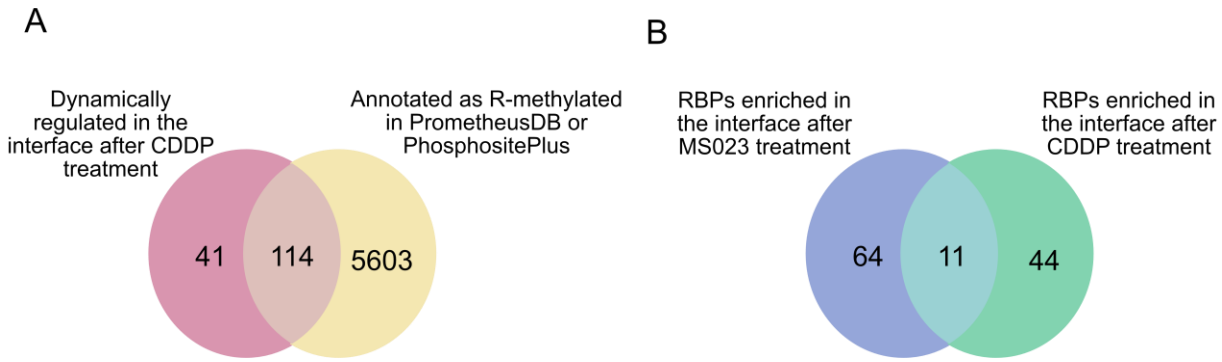

Figure 43: Assessment of the impact of R-methylation on CDDP-mediated RBP dynamicity

A) Intersection between the list of proteins dynamically regulated by CDDP in the interface and the PrometheusDB or the PhosphositePlus databases for R-methylated proteins. **B)** Venn diagram illustrating the intersection of the proteins enriched in the interface by MS023 and those enriched by CDDP.

To this aim, we set to perform an affinity purification experiment coupled with MS analysis (AP-MS) for a restricted set of candidates that were recruited at the interface in the OOPS-MS experiment upon CDDP. We started with RPL27A since it is one of the most up-regulated proteins, it is a structural constituent of the ribosome and, in

addition, good quality antibodies for affinity-purification are commercially available. Moreover, quite interestingly, this protein is already annotated in PhospshositePlus as mono-methylated at R12 and R65 in basal conditions, but no dynamic information is available. We performed the AP-MS experiment starting from both untreated (NT) and CDDP-treated S-KO-V3 whole-cell extracts (see M&M, paragraph 4.9.2). The affinity-purified material was split into a smaller part (1/10), used for WB analysis to control AP efficiency, and a remaining larger part (9/10) which was separated by SDS-PAGE. The gel slice corresponding to RPL27A molecular weight was “in-gel” trypsin digested and subjected to LC-MS/MS analysis for protein and PTM analysis (see M&M, paragraph 4.10) (**Fig. 44**).

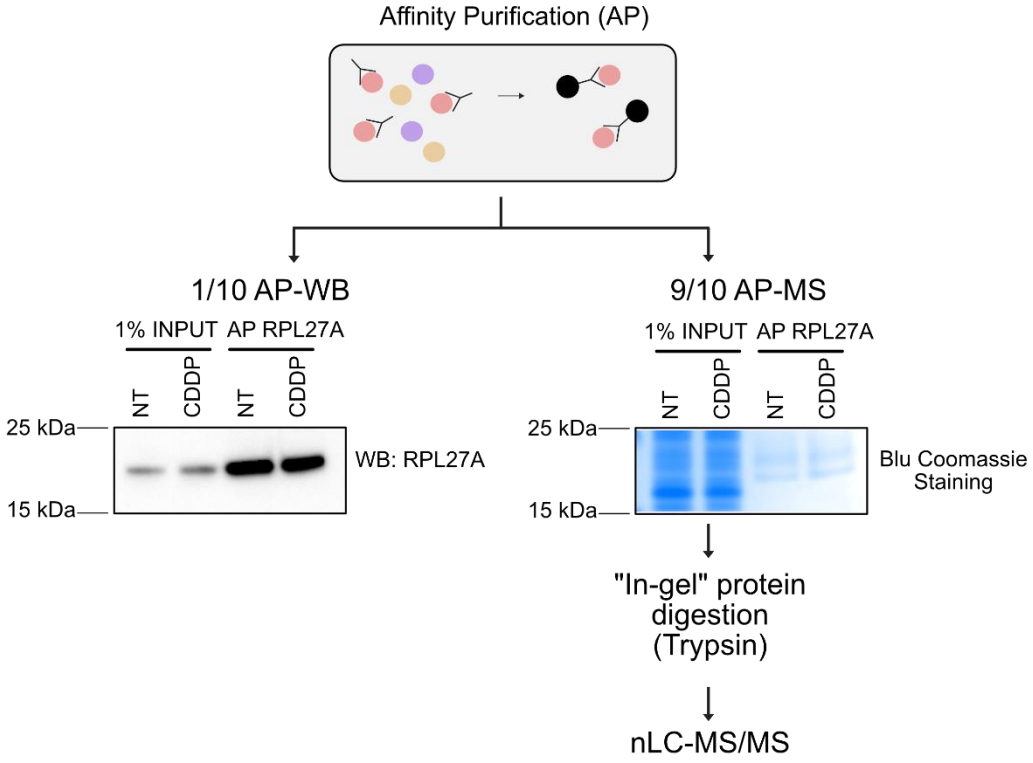

Figure 44: AP-MS RPL27A workflow

Schematic workflow of AP-MS experiment for RPL27A: 1/10 of the affinity-purified protein extract was used for WB profiling of RPL27A, to assess its enrichment in AP compared to input, while the remaining 9/10 was loaded on an SDS-PAGE. The protein content was stained by Instant Blue Coomassie, the gel slice around RPL27A molecular weight was excised, processed by “in-gel” digestion, and proteolytic peptide was subjected to LC-MS/MS analysis.

Acquired MS raw data were analyzed by MaxQuant. The information about the identified proteins and R-methyl sites was obtained from the “proteinGroup.txt”, “evidence.txt”, and “Methyl(KR)Sites.txt” MaxQuant output files, respectively. The RPL27A protein was identified with an andromeda score of 323 and 15 unique peptides, leading to an overall sequence coverage of 60%. This analysis led to the identification of a novel R-methyl site: the mono-methylated R105 (MS/MS spectrum of the peptide bearing the PTM in **Fig. 45**), which displayed a localization probability equal to 1, Posterior Error Probability (PEP) equal to 0.017, a score of 54.98, and a delta score of 25.23. These parameters suggest high-confidence identification of this PTM. Although a quantitative analysis was not possible from this experiment, quite interestingly, this R-methyl-site was identified only in the untreated condition but not in the CDDP-treated sample, which could indicate loss of MMA upon CDDP, in line with the observed global hypomethylation of RBP in response to this drug observed through the methyl-proteomics experiment.

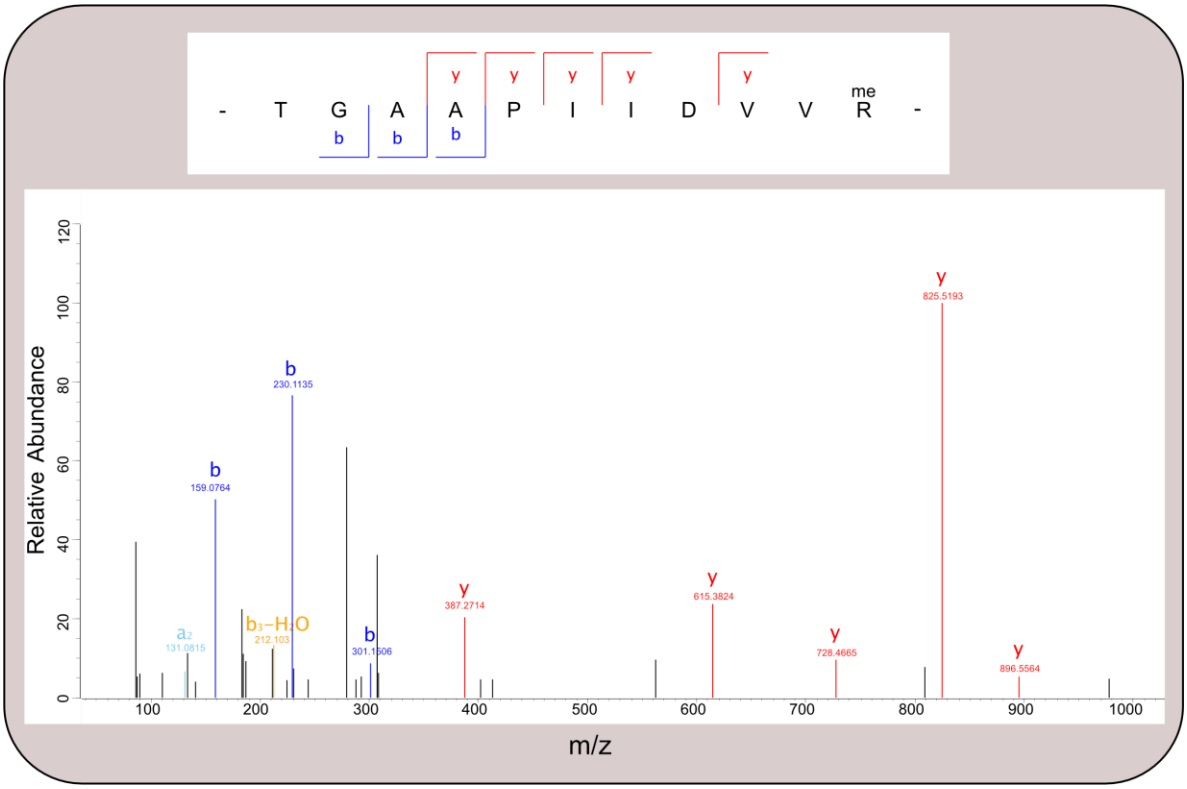

Figure 45: RPL27A MS/MS spectrum

MS/MS spectrum and corresponding annotated peptide sequence, with single-site identification of mono-methylation at R105 (C-terminal to the peptide), obtained by MaxQuant.

5.9 Analysis of the CDDP-induced changes at the transcriptomic level in the interface

Focusing on RBP-RNA interaction dynamics in the context of cancer cell response to genotoxic stress, we decided to investigate also the RNA changes in the OOPS experiments, in order to identify RNAs that are selectively recruited, or depleted, at the interface in response to CDDP. We reasoned that this piece of information could be crucial to test our hypothesis that the mRNAs of genes related to secretory phenotypes are selectively recruited to be actively translated. We then carried out OOPS experiments in basal and CDDP-treated conditions, followed by RNA-seq analysis of the pool of RNAs purified from the interface. Three biological replicates from untreated and CDDP conditions, for both total RNA extracts and interface-enriched RNA extracts, were prepared with the

rationale of using the whole RNA extracts to normalize the level of RNAs in the interface thus distinguishing RBP-interacting RNAs from merely transcriptional changes. (**Fig. 46**).

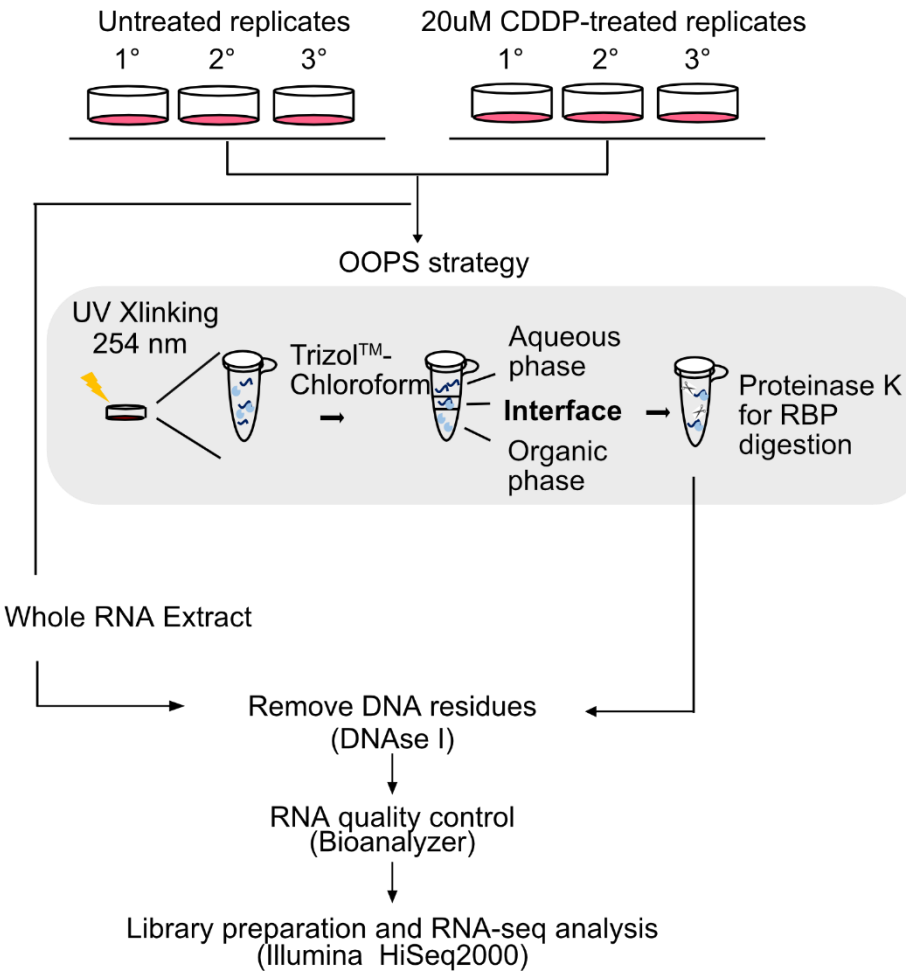

Figure 46: OOPS-RNAseq workflow

Workflow of the OOPS-RNAseq approach. S-KO-V3 cells were grown both in normal medium (NT) or treated with 20µM CDDP. Three biological replicates (n=3) for each condition (Whole RNA extract NT, Whole RNA extract CDDP, Interface-enriched RNA NT, and Interface-enriched RNA CDDP) were prepared. To obtain the interface-enriched RNAs, after UV-crosslinking and phase-partitioned through the Trizol™-chloroform mixture, the RBP-RNA complexes were treated with Proteinase K to remove the proteins. Both whole RNA extracts and Interface-enriched RNA extracts were purified from DNA through DNAseI treatment. Finally, sequencing libraries were prepared by TruSeq Stranded Total RNA Library Prep Gold, and RNA was sequenced by Illumina HiSeq2000 instrument.

While the analysis of RNA-seq data is still ongoing, in parallel, we inspected published evidence to identify candidate RNAs that could functionally link CDDP treatment and ER stress. Some

studies suggest a link between ER stress and CDDP resistance in EOC (Tian et al., 2017a), and a recent article describes that, upon ER stress, a particular type of MLO slightly different from canonical SGs is induced in the proximity of ER and that the mRNA of GRP94 (coding for HSP90B1 protein), but not of GRP78 (coding for HSPA5 protein), is enriched within this novel type of MLOs (Child et al., 2021). To test if CDDP-induced ER stress could lead to the enrichment of this mRNA in the interface from OOPS, we profiled by RT-qPCR the level of both the GRP94 and the GRP78 mRNAs in both whole RNA extract and interface, normalizing them over the 18S expression level in each corresponding fraction. The observation that only GRP94 is enriched in the interface upon CDDP treatment (**Fig. 47**) is, in our opinion, a promising preliminary result supporting our hypothesis. However, the broader view that we will achieve by RNA-seq analysis will provide an unbiased confirmation of this initial evidence, and possibly, novel candidates to follow up functionally.

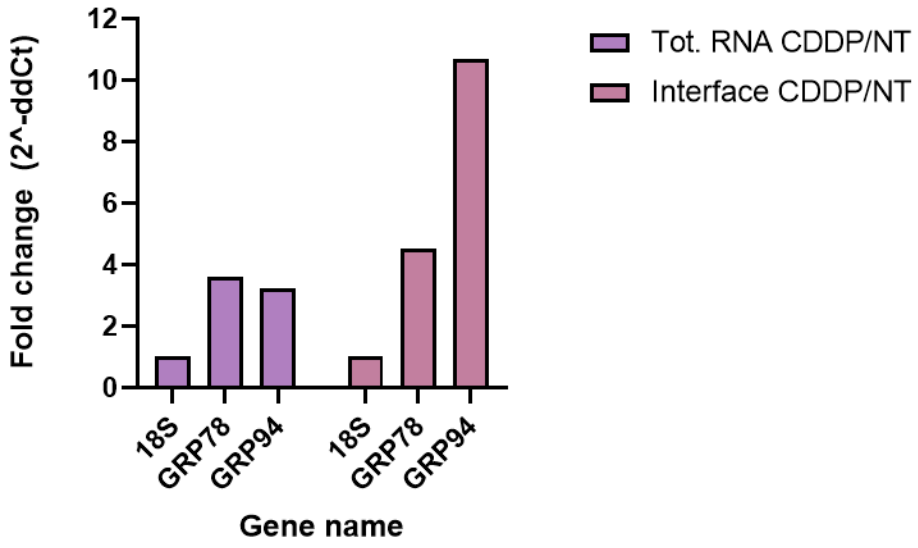

Figure 47: RT-qPCR analysis of ER chaperone gene GRP94 and GRP78

Quantitative real-time PCR analysis of GRP78 and GRP94, both from total RNA extracts and interface-enriched RNA extracts. The relative gene expression fold change was calculated through the 2^-ddCt method. The fold changes thus obtained were then normalized over the corresponding ones for the housekeeping 18S gene, as a control.

6. DISCUSSION

In this study, we employed MS-based proteomics to investigate the role of R-methylation in regulating RBP-RNA interaction, both directly, through PRMT pharmacological inhibition, and indirectly, through CDDP-induced R-methylation remodeling.

In the first part, we inhibited PRMT1 and PRMT5, the two major representatives of PRMT type I and type II families, respectively, with the drugs MS023 and GSK591. While GSK591 is a PRMT5 selective inhibitor (Duncan et al., 2016), MS023 can inhibit other PTMTs type I (Eram et al., 2016). Even if 85% of R-methylation was ascribed to PRMT1 activity and we previously experimentally evaluated that at the selected dose and time window MS023 meanly act on PRMT1, we cannot exclude that the observed effects could represent the sum of the modulation of other PRMTs type I too. Indeed, PRMTs often share the same substrate and it has been shown that the absence of PRMT1 can induce a substrate-scavenging effect (Dhar et al., 2013). A PRMT1 selective inhibitor named TC-E 5003 (Kim et al., 2020) has been marketed; however, we could not appreciate a significant reduction of ADMA or H4R3me2a. We further validated the unequivocal involvement of PRMT1 the observed RBP-RNA interaction dynamics by depleting the enzyme by two distinct shRNAs selectively targeting PRMT1. Nevertheless, the possible involvement -maybe to a minor extent- of other PRMTs cannot completely ruled out and could be object of future investigations.

The OOPS was chosen as strategy to achieved an unbiased and comprehensive enrichment of RBP-RNA complexes, reasoning on the fact that it exploits the physicochemical properties of RBP-RNA complexes to enrich them from a whole cell extract at the interface of the Trizol^{TM}-chloroform phase partition. The RIC experiment -used as orthogonal validation to profile the role of R-methylation on global protein-mRNA interaction- partially validated the OOPS data but also revealed a significant difference in the size of the protein datasets obtained. This difference is probably to be ascribed mainly

to the distinctive enrichment principle on which two techniques rely: enrichment of RBPs associated with all the RNA types for OOPS and pull-down of RBPs associated with poly-(A)-mRNA only for RIC, as it was also observed and discussed in a recent publication on Nature Communications (Hoefig et al., 2021).

To link the observed MS023-mediated modulation of RBP-RNA interaction to the R-methylation remodeling of candidate RBPs, we profiled the R-methylation state of some representative RBPs which resulted up-regulated in the MS023-treated interface upon IP from total protein extract. Immunoprecipitation of proteins from the interface followed by WB readout might allow linking more directly changes in the R-methylation state with differential RNA-binding capability. Unfortunately, since proteins are denatured during Trizol™-chloroform extraction, immunoprecipitation from the interface resulted not feasible. A possible solution could be to apply our well-established strategy for immuno-affinity enrichment of R-methyl-peptides with pan-methyl-R antibodies upon protein digestion and HpH peptide fractionation from the interface fraction. This very appealing strategy was not feasible until now due to the technical restrained linked to the very large starting amount of proteins required for the peptide-affinity enrichment. Noteworthy, last month CST-signaling has released a new kit of anti-MMA antibodies with much higher affinity that should require only 1 mg of digested proteins as starting input material: this could represent a real breakthrough for our studies, and we are planning to test this immuno-affinity enrichment down-stream of OOPS and prior to MS as soon as possible to address this crucial point.

For what concern the possible phase-separation properties of these RBPs, it has been reported that for single protein the loss of R-methylation can induce LLPS and MLOs formation (C. Huang et al., 2020; Kawahara et al., 2021; Mersaoui et al., 2019; Qamar et al., 2018). Since most of the RBPs in the interface are enriched for RGG/RG regions, that are both PRMT preferred targets and disordered regions conferring LLP properties (Chong et al., 2018), the link between R-methylation regulation and LLPS could be possible. Here

we experimentally evaluated *in-vivo* that two MS023-upregulated proteins in the interface are also capable to form MLOs in the same condition.

Overall, the data acquired in Musiani at al. 2020 and the results obtained in the first part of this work, led us to formulate a more complex model, which includes several layers of regulation of the R-methylation remodeling in response to CDDP (**Fig. 48**).

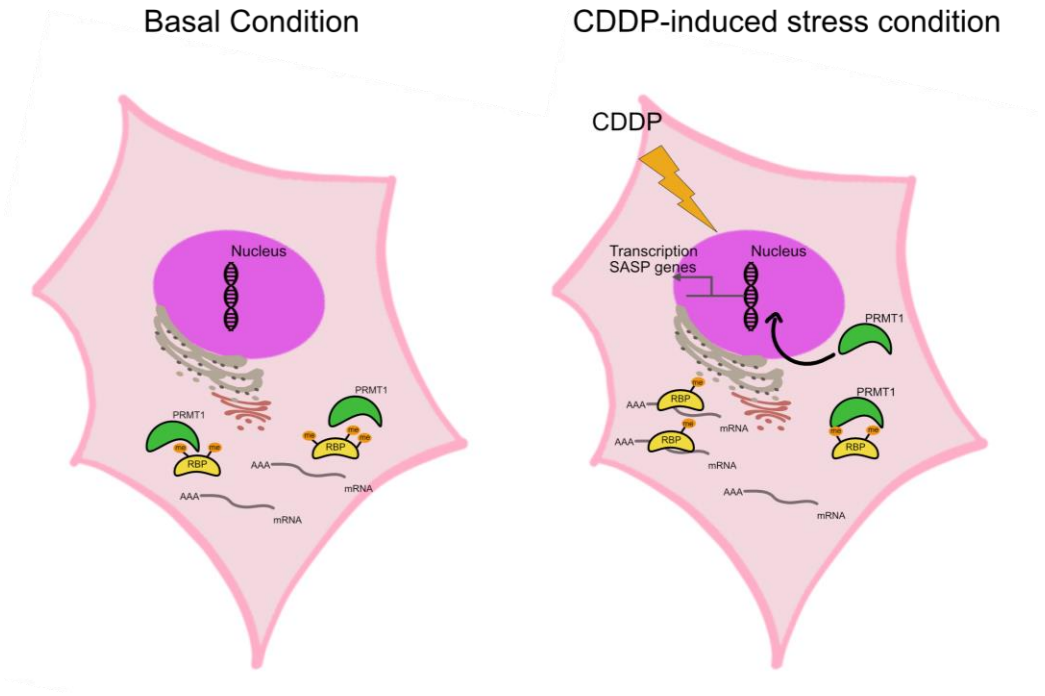

Figure 48: New proposed cell model

Graphic representation of the more complex hypothesized model. In CDDP-induced stress condition, R-hypomethylated RBP targets of PRMT1 increase the affinity for cognate RNAs. Most of them belong to the class of ribosomal protein and seem to be involved in the co-translation of specific mRNA targeting to ER

The first level of regulation is related to the chromatin-associated activity of PRMT1, triggered by CDDP, which was shown to cause the increase of H4R3me2a and the transcriptional activation of the SASP genes upon CDDP.

The second layer of regulation could be represented by the observed global R-hypomethylation of soluble and mainly cytosolic proteins, which we hypothesized to

result from PRMT1 accumulation on the chromatin triggered by CDDP. This class of hypomethylated proteins is mainly represented by RPBs and we demonstrated that the R-methylation reduction could impact their interaction with cognate RNAs as a consequence of ADMA/MMA balance modulation.

These observations encouraged us to evaluate the impact of remodeling R methylation in a more interesting context, such as platinum-based resistance in ovarian cancer. Here, OOPS revealed some interesting candidates, especially considering that modulation of RNA binding capability by lack of methylation may have positive (increased mRNA binding in some case) or negative (decreased RNA binding and increased SG accumulation) effects on RBP function. These observations could be particularly interesting in line of the fact that the RBP RBM3 was described as favorable prognostic marker that correlate with CDDP sensitivity (Åsa Ehlén et al. 2010), but also that other RBP, such as in the case of CSDE1, can act as tumor suppressor or promote oncogene-induced senescence in a context dependent manner (Avolio et al. 2022).

We are well aware that not all the observed dynamic behaviors in OOPS can be attributed solely to protein R-methylation changes: for instance, protein-phosphorylation has already been shown to mediate both the signaling cascade in response to CDDP-induced stress and SGs formation (Pietras et al. 2022). Moreover, it is well-documented that a crosstalk between R-methylation and ST phosphorylation on same protein targeted is underpinning different biological processes, such as apoptosis (M. Chen et al., 2016). The identification of the 14-3-3 proteins (readers of S/T phosphorylation) among the most MS023-enriched proteins at the interface of OOPS, seems to support the existence of this crosstalk. In the lab we are currently carrying out experiment to dig more in phospho-proteomic dynamics upon CDDP in total extract and OOPS to investigate how the two modification-proteomes cross-talk.

Obviously, we are conscious that the mechanisms adopted by the cell to cope with stressors so strong as CDDP may intersect the fine-tuning of multiple pathways and

signals and that the risk of over-simplification is high. For instance, that data we have at hand on RBP-RNA dynamics upon PRMT inhibition were collected in HeLa cells while the response to CDDP was carried out in S-KO-V3 cells. Hence, the use of different cell models could explain the limited overlap between the two proteomic datasets. Also, the different number of biological replicates in HeLa versus S-KO-V3 cells, together with my increased experience and technical skills, might explain why the number of identified proteins is significantly higher in the second OOPS-MS experiment (1106 upon CDDP versus 433 proteins upon PRMT inhibitors) compared with the first. Last, we also know (from the literature and from our experimental validation) that MS023 reduces the level of ADMA with a concomitant increase of the MMA level, while CDDP impairs both ADMA and MMA levels, but not to the same extent at global level. (**Fig. 49**).

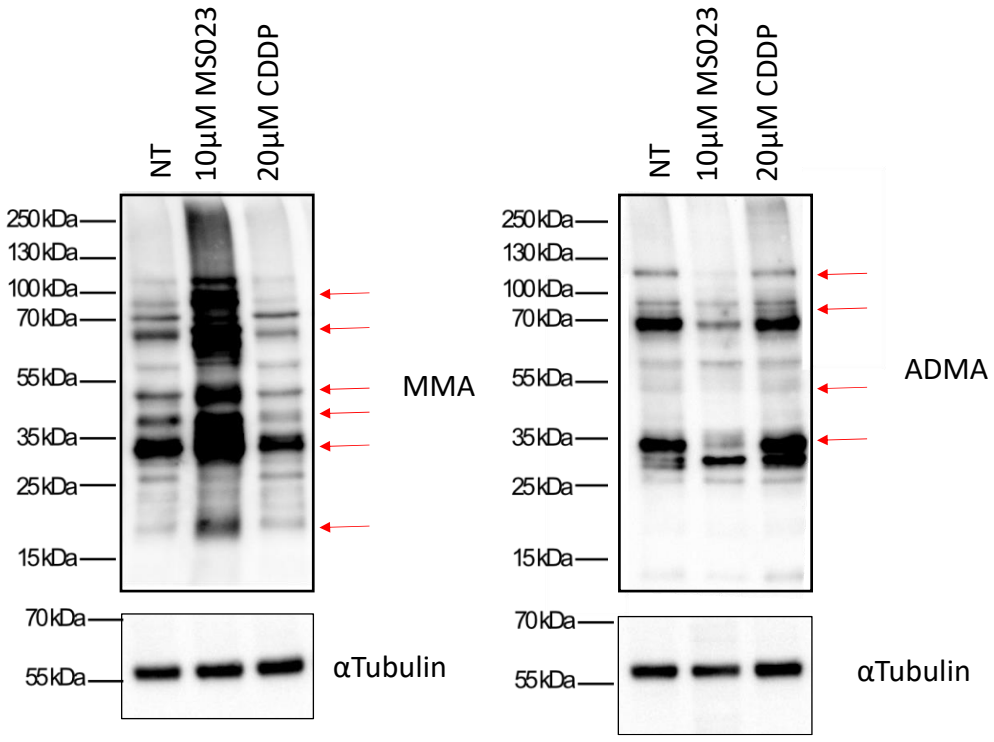

Figure 49: Evaluation of CDDP- and MS023-mediate impact on R-methylation remodeling

WB profiling of dynamic regulation of protein R-mono-methylation (MMA) and asymmetric R-di-methylation (ADMA). WB analysis was carried out in untreated (NT) samples and upon MS023 and CDDP treatment. αTubulin was used as loading control.

To investigate the impact of CDDP-induced R-methylation remodeling at individual protein level, we have recently set up an AP-MS experiment of RBPs that resulted up-regulated in the OOPS-MS experiment upon CDDP treatment. AP-MS analysis of RPL27A constitutes a preliminary result, which may be reinforced by orthogonal validations, such as the use of hmSILAC for the high-confidence identification of the *in-vivo* R-methylation and double enzymatic digestion with the trypsin and LysargiNase. Once we will have identified the R-methyl sites of RPL27A, RPL7A, and RPLP0 dynamically regulated by CDDP, we could perform specific amino acid site mutation through the CRISPR-Cas9 system (Ma et al., 2017). This experiment will be able to link the observed behavior with specific R-methylated site remodeling. In particular, we plan to investigate: a) the role in modulating the binding with cognate RNAs; b) the impact on protein subcellular localization and possible MLOs formation; c) if it is crucial to translate SASP-related mRNAs and mediate CDDP resistance (**Fig. 50**).

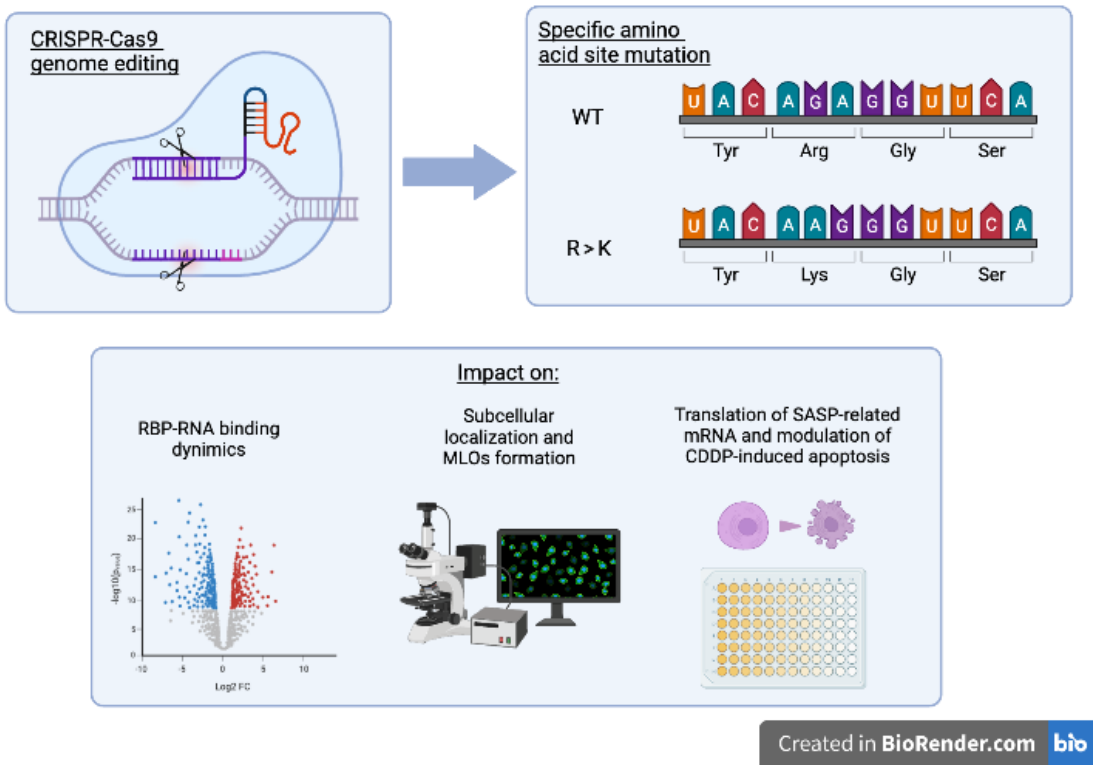

Figure 50: Impact of specific R site mutation on different biological aspects

Genome editing achieved through CRISPR-Cas9 system will allow to selectively mutate specific amino acid coding sequence, for instance from arginine (R) to lysine (K). This will result in a still “methylable” residues but different from R, so that we can compare the impact of R-methylation remodeling versus the not arginine-dependent model. If the selected R-methyl-site was the driver of the different behavior, it mutation could impact on RBP-RNA interaction, subcellular localization and selective mRNA translation. This figure has been created in BioRender.com

Since we hypothesized that the loss of R-methylation on candidate RBPs was responsible for the increased binding to specific RNAs, we are preparing an *ad hoc* S-KO-V3 cell model in which PRMT1 is over-expressed. According to our hypothesis, hyper-R-methylated RBPs could not anymore bind cognate RNAs; hence PRMT1 overexpression could represent an internal control of our model.

Queiroz and colleagues made the important observation that glycosylated proteins share the physicochemical properties of RNA–protein complexes, thus they can be enriched in the OOPS interface leading to the miss-identification of new putative RBPs

(Queiroz et al., 2019). When we intersected our list of putative RBPs in the CDDP-treated interface with the list of glycosylated proteins annotate in the N-GlycositeAtlas (a database of human glycosite-containing peptides) (S. Sun et al., 2019), almost half of them turn out to be annotated as glycoproteins (**Fig. 51**).

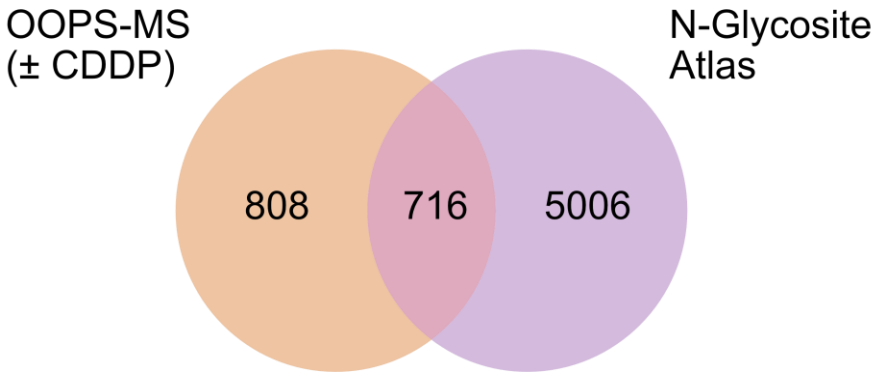

Figure 51: Evaluation of the percentage of glycosylated proteins enriched in the OOPS-MS experiment

Intersection between the list of quantifiable proteins in the interface (with or without CDDP) and the dataset of glycosylated proteins from N-Glycosite Atlas.

However, by inspecting the proteins in common, we noticed that most of them are well-known RBPs, such as RNA helicases, ribosomal proteins, or splicing factors. Since glycosylated proteins are enriched in the interface because of their physicochemical properties, their presence in the interface should be independent of the UV-crosslinking. For this reason, we will re-evaluate the interface enrichment of the most promising candidates with and without UV-crosslinking, to experimentally prove that they are enriched because they form RBP-RNA complexes. More importantly, we will perform further experiments, such as radioactive labelling with PNK, specifically designed to proof if new putative RBPs -like TNFRSF10D- really possess RNA-binding properties.

However, the observation that a subset of ribosomal proteins targeting the ER are upregulated in the CDDP-treated interface is particularly intriguing and it was not observed in previous analyses from a total proteome. Indeed, the CDDP treatment induces a general shot down of translation, so we may hypothesize that these ribosomal proteins translate mRNAs that are important to mediate drug resistance. To evaluate if the enrichment of co-translational pathways targeting to ER is only mediated by the subset of ribosomal proteins, we repeated the GO analysis of the most enriched biological process upon the removal of the 11 ribosomal proteins (**Fig. 52**). The GO terms related to co-translation targeting to ER are not anymore the most enriched, while terms related to neutrophil degranulation and activation and chaperon cofactor-dependent protein refolding (all driven by HSP90AB1 and HSPA8 proteins) emerges. Of course, we have to also take into account the fact that this type of analysis needs a large number of terms, so it is not entirely suitable for such small dataset.

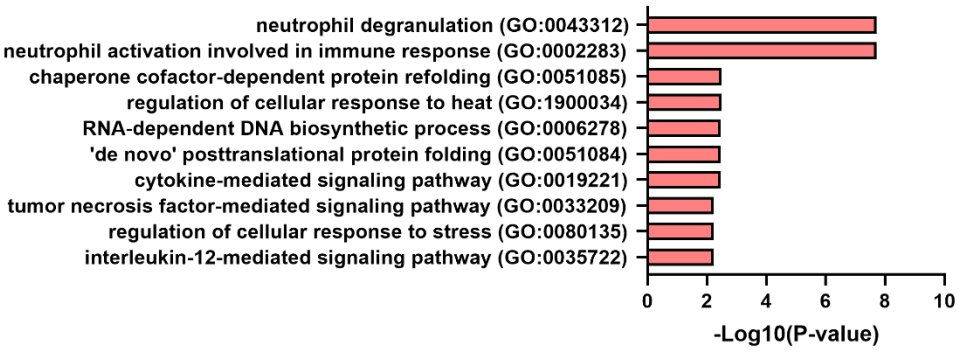

Figure 52: Evaluation of the impact of the significantly enriched ribosomal proteins

GO analysis of the most enriched biological processes was performed starting from the RBP significantly regulated in the OOPS-MS experiment upon removal of the significantly enriched ribosomal proteins. The bar-blot indicates the -LOG_{10}(p-value) of the most enriched biological processes

We are also currently set up an imaging screening, similar to the previous one performed upon PRMT inhibitor, to evaluate the subcellular localization of the most dynamically regulated RBPs in the CDDP-treated interface, the possible co-localization with RNA and formation of SG-like granules e their possible co-localization with ER

marker. For this purpose, we will select G3BP1 as SG marked and Calnexin as ER marker (Ellgaard & Helenius, 2001): this analysis should allow us to confirm whether CDDP-upregulated proteins in the interface are involved in the translation of selected mRNAs across the ER and whether CDDP treatment can lead to the formation of specific SGs, different from the canonical, located in the proximity of the ER. This hypothesis is particularly intriguing in light of the shown evidence that SG formation can confer survival advantage and chemotherapeutic resistance to cancer cells. Among the different chemotherapeutic drugs, CDDP prevents translation by increasing 4E-BP1 dephosphorylation and eIF2α phosphorylation and it can inhibit the canonical SG formation in a concentration- and time-dependent manner (Asadi et al., 2021; Pietras et al., 2022). Hence, targeting CDDP-driven SG formation may represent a potential strategy to overcome drug resistance (Zhan et al., 2020) or at least mediate chemo-resistance in cancer (El-Naggar & Sorensen, 2018; Loll-Krippleber & Brown, 2017). This will allow us to suggested a possible mechanism of CDDP-resistance with greater confidence among CDDP-resistant EOC cells that could be further reinforce through validation on CDDP-sensitive EOC cells.

The in-depth analysis of the CDDP-modulated transcripts from the interface will give us an important piece of information about the identification of specific mRNAs selectively enriched. We will evaluate whether, in a general context of CDDP-induced block of translation, they are selected to be translated and immediately released from the ER to mediate resistance to CDDP-induced death. As an additional experiment, we will perform the eCLIP experiment to evaluate which RNAs are specifically bound to the RBPs of interest.

Overall, the data collected during my Ph.D. lay the background for the global and unbiased analysis of the impact of R-methylation remodeling on RBP-RNA interaction. In particular, our data suggest that the modulation of ADMA/MMA balance in a set of

RBPs may be the major player in this dynamics. By analyzing R-methylation remodeling into CDDP-resistance EOC cells, we found some interesting candidates, both well-known RBPs and new putative RBPs, whose activity can be strongly modulated in the CDDP-induced stress context. They could represent promising biomarkers that could be then evaluated by tissue microarray (in collaboration with the Unit of Gynecological Oncology Research in IEO) as potential biomarker in a large numbers of patient with different degree of sensitivity to platinum treatment.

7. REFERENCES

Aebersold, R., & Mann, M. (2003). Mass spectrometry-based proteomics. *Nature*, *422*(6928), 198–207. https://doi.org/10.1038/nature01511

Albakova, Z., Mangasarova, Y., Albakov, A., & Gorenkova, L. (2022). HSP70 and HSP90 in Cancer: Cytosolic, Endoplasmic Reticulum and Mitochondrial Chaperones of Tumorigenesis. *Frontiers in Oncology*, *12*. https://doi.org/10.3389/fonc.2022.829520

Antonysamy, S., Bonday, Z., Campbell, R. M., Doyle, B., Druzina, Z., Gheyi, T., Han, B., Jungheim, L. N., Qian, Y., Rauch, C., Russell, M., Sauder, J. M., Wasserman, S. R., Weichert, K., Willard, F. S., Zhang, A., & Emtage, S. (2012). Crystal structure of the human PRMT5:MEP50 complex. *Proceedings of the National Academy of Sciences*, *109*(44), 17960–17965. https://doi.org/10.1073/pnas.1209814109

Aravind, L., & Koonin, E. v. (2000). SAP – a putative DNA-binding motif involved in chromosomal organization. *Trends in Biochemical Sciences*, *25*(3), 112–114. https://doi.org/10.1016/S0968-0004(99)01537-6

Argon, Y., & Simen, B. B. (1999). GRP94, an ER chaperone with protein and peptide binding properties. *Seminars in Cell & Developmental Biology*, *10*(5), 495–505. https://doi.org/10.1006/scdb.1999.0320

Asadi, M. R., Moslehian, M. S., Sabaie, H., Poornabi, M., Ghasemi, E., Hassani, M., Hussen, B. M., Taheri, M., & Rezazadeh, M. (2021). Stress Granules in the Anti-Cancer Medications Mechanism of Action: A Systematic Scoping Review. *Frontiers in Oncology*, *11*. https://doi.org/10.3389/fonc.2021.797549

Avolio R, Inglés-Ferrándiz M, Ciocia A, Coll O, Bonnin S, Guitart T, Ribó A, Gebauer F. Coordinated post-transcriptional control of oncogene-induced senescence by UNR/CSDE1. Cell Rep. 2022 Jan 11;38(2):110211. doi: 10.1016/j.celrep.2021.110211. PMID: 35021076.

Bachand, F., & Silver, P. A. (2004). PRMT3 is a ribosomal protein methyltransferase that affects the cellular levels of ribosomal subunits. *The EMBO Journal*, *23*(13), 2641–2650. https://doi.org/10.1038/sj.emboj.7600265

Bai, X., Sui, C., Liu, F., Chen, T., Zhang, L., Zheng, Y., Liu, B., & Gao, C. (2022). The protein arginine methyltransferase PRMT9 attenuates MAVS activation through arginine methylation. *Nature Communications*, *13*(1), 5016. https://doi.org/10.1038/s41467-022-32628-y

Batth, T. S., Francavilla, C., & Olsen, J. v. (2014). Off-Line High-pH Reversed-Phase Fractionation for In-Depth Phosphoproteomics. *Journal of Proteome Research*, *13*(12), 6176–6186. https://doi.org/10.1021/pr500893m

Becker, J. P., Weiss, J., & Theile, D. (2014). Cisplatin, oxaliplatin, and carboplatin unequally inhibit in vitro mRNA translation. *Toxicology Letters*, *225*(1), 43–47. https://doi.org/10.1016/j.toxlet.2013.11.015

Bedford, M. T., & Clarke, S. G. (2009). Protein Arginine Methylation in Mammals: Who, What, and Why. *Molecular Cell*, *33*(1), 1–13. https://doi.org/10.1016/j.molcel.2008.12.013

Bedford, M. T., & Richard, S. (2005). Arginine Methylation. *Molecular Cell*, *18*(3), 263–272. https://doi.org/10.1016/j.molcel.2005.04.003

Bikkavilli, R. K., Avasarala, S., van Scoyk, M., Karuppusamy Rathinam, M. K., Tauler, J., Borowicz, S., & Winn, R. A. (2014). In vitro Methylation Assay to Study Protein Arginine Methylation. *Journal of Visualized Experiments*, *92*. https://doi.org/10.3791/51997

Biswas, S., & Rao, C. M. (2018). Epigenetic tools (The Writers, The Readers and The Erasers) and their implications in cancer therapy. *European Journal of Pharmacology*, *837*, 8–24. https://doi.org/10.1016/j.ejphar.2018.08.021

Blackwell, E., & Ceman, S. (2012). Arginine methylation of RNA-binding proteins regulates cell function and differentiation. *Molecular Reproduction and Development*, *79*(3), 163–175. https://doi.org/10.1002/mrd.22024

Blanc, R. S., & Richard, S. (2017). Arginine Methylation: The Coming of Age. *Molecular Cell*, *65*(1), 8–24. https://doi.org/10.1016/j.molcel.2016.11.003

BOLTE, S., & CORDELIÈRES, F. P. (2006). A guided tour into subcellular colocalization analysis in light microscopy. *Journal of Microscopy*, *224*(3), 213–232. https://doi.org/10.1111/j.1365-2818.2006.01706.x

Bond, C. S., & Fox, A. H. (2009). Paraspeckles: nuclear bodies built on long noncoding RNA. *Journal of Cell Biology*, *186*(5), 637–644. https://doi.org/10.1083/jcb.200906113

Bounedjah, O., Desforges, B., Wu, T.-D., Pioche-Durieu, C., Marco, S., Hamon, L., Curmi, P. A., Guerquin-Kern, J.-L., Piétrement, O., & Pastré, D. (2014). Free mRNA in excess upon polysome dissociation is a scaffold for protein multimerization to form stress granules. *Nucleic Acids Research*, *42*(13), 8678–8691. https://doi.org/10.1093/nar/gku582

Bremang, M., Cuomo, A., Agresta, A. M., Stugiewicz, M., Spadotto, V., & Bonaldi, T. (2013). Mass spectrometry-based identification and characterisation of lysine and arginine methylation in the human proteome. *Molecular BioSystems*, *9*(9), 2231. https://doi.org/10.1039/c3mb00009e

Calabretta, S., & Richard, S. (2015). Emerging Roles of Disordered Sequences in RNA-Binding Proteins. *Trends in Biochemical Sciences*, *40*(11), 662–672. https://doi.org/10.1016/j.tibs.2015.08.012

Castello, A., Fischer, B., Eichelbaum, K., Horos, R., Beckmann, B. M., Strein, C., Davey, N. E., Humphreys, D. T., Preiss, T., Steinmetz, L. M., Krijgsveld, J., & Hentze, M. W. (2012). Insights into RNA Biology from an Atlas of Mammalian mRNA-Binding Proteins. *Cell*, *149*(6), 1393–1406. https://doi.org/10.1016/j.cell.2012.04.031

Castello, A., Fischer, B., Frese, C. K., Horos, R., Alleaume, A.-M., Foehr, S., Curk, T., Krijgsveld, J., & Hentze, M. W. (2016). Comprehensive Identification of RNA-Binding Domains in Human Cells. *Molecular Cell*, *63*(4), 696–710. https://doi.org/10.1016/j.molcel.2016.06.029

Castello, A., Frese, C. K., Fischer, B., Järvelin, A. I., Horos, R., Alleaume, A.-M., Foehr, S., Curk, T., Krijgsveld, J., & Hentze, M. W. (2017). Identification of RNA-binding domains of RNA-binding proteins in cultured cells on a system-wide scale with RBDmap. *Nature Protocols*, *12*(12), 2447–2464. https://doi.org/10.1038/nprot.2017.106

Castello, A., Horos, R., Strein, C., Fischer, B., Eichelbaum, K., Steinmetz, L. M., Krijgsveld, J., & Hentze, M. W. (2013). System-wide identification of RNA-binding proteins by interactome capture. *Nature Protocols*, *8*(3), 491–500. https://doi.org/10.1038/nprot.2013.020

Chen, C.-Y., Kawasumi, M., Lan, T.-Y., Poon, C.-L., Lin, Y.-S., Wu, P.-J., Chen, Y.-C., Chen, B.-H., Wu, C.-H., Lo, J.-F., Weng, R. R., Sun, Y.-C., & Hung, K.-F. (2020). Adaptation to Endoplasmic Reticulum Stress Enhances Resistance of Oral Cancer Cells to Cisplatin by Up-Regulating Polymerase η and Increasing DNA Repair Efficiency. *International Journal of Molecular Sciences*, *22*(1), 355. https://doi.org/10.3390/ijms22010355

Chen, E. I., Cociorva, D., Norris, J. L., & Yates, J. R. (2007). Optimization of Mass Spectrometry-Compatible Surfactants for Shotgun Proteomics. *Journal of Proteome Research*, *6*(7), 2529–2538. https://doi.org/10.1021/pr060682a

Chen, M., Qu, X., Zhang, Z., Wu, H., Qin, X., Li, F., Liu, Z., Tian, L., Miao, J., & Shu, W. (2016). Cross-talk between Arg methylation and Ser phosphorylation modulates apoptosis signal–regulating kinase 1 activation in endothelial cells. *Molecular Biology of the Cell*, *27*(8), 1358–1366. https://doi.org/10.1091/mbc.E15-10-0738

Child, J. R., Chen, Q., Reid, D. W., Jagannathan, S., & Nicchitta, C. v. (2021). Recruitment of endoplasmic reticulum-targeted and cytosolic mRNAs into membrane-associated stress granules. *RNA*, *27*(10), 1241–1256. https://doi.org/10.1261/rna.078858.121

Chong, P. A., Vernon, R. M., & Forman-Kay, J. D. (2018). RGG/RG Motif Regions in RNA Binding and Phase Separation. *Journal of Molecular Biology*, *430*(23), 4650–4665. https://doi.org/10.1016/j.jmb.2018.06.014

Chuang, C.-Y., Chang, C.-P., Lee, Y.-J., Lin, W.-L., Chang, W.-W., Wu, J.-S., Cheng, Y.-W., Lee, H., & Li, C. (2017). PRMT1 expression is elevated in head and neck cancer and inhibition of protein arginine methylation by adenosine dialdehyde or PRMT1 knockdown downregulates proliferation and migration of oral cancer cells. *Oncology Reports*, *38*(2), 1115–1123. https://doi.org/10.3892/or.2017.5737

Cook KB, Kazan H, Zuberi K, Morris Q, Hughes TR. RBPDB: a database of RNA-binding specificities. Nucleic Acids Res. 2011 Jan;39(Database issue):D301-8. doi: 10.1093/nar/gkq1069. Epub 2010 Oct 29. PMID: 21036867; PMCID: PMC3013675.

Corazzari, M., Gagliardi, M., Fimia, G. M., & Piacentini, M. (2017). Endoplasmic Reticulum Stress, Unfolded Protein Response, and Cancer Cell Fate. *Frontiers in Oncology*, *7*. https://doi.org/10.3389/fonc.2017.00078

Corley, M., Burns, M. C., & Yeo, G. W. (2020). How RNA-Binding Proteins Interact with RNA: Molecules and Mechanisms. *Molecular Cell*, *78*(1), 9–29. https://doi.org/10.1016/j.molcel.2020.03.011

Cox, J., Hein, M. Y., Luber, C. A., Paron, I., Nagaraj, N., & Mann, M. (2014). Accurate Proteome-wide Label-free Quantification by Delayed Normalization and Maximal Peptide Ratio Extraction, Termed MaxLFQ. *Molecular & Cellular Proteomics*, *13*(9), 2513–2526. https://doi.org/10.1074/mcp.M113.031591

Cox, J., & Mann, M. (2008). MaxQuant enables high peptide identification rates, individualized p.p.b.-range mass accuracies and proteome-wide protein quantification. *Nature Biotechnology*, *26*(12), 1367–1372. https://doi.org/10.1038/nbt.1511

Cura, V., & Cavarelli, J. (2021). Structure, Activity and Function of the PRMT2 Protein Arginine Methyltransferase. *Life*, *11*(11), 1263. https://doi.org/10.3390/life11111263

Dhar, S., Vemulapalli, V., Patananan, A. N., Huang, G. L., di Lorenzo, A., Richard, S., Comb, M. J., Guo, A., Clarke, S. G., & Bedford, M. T. (2013). Loss of the major Type I arginine methyltransferase PRMT1 causes substrate scavenging by other PRMTs. *Scientific Reports*, *3*(1), 1311. https://doi.org/10.1038/srep01311

Dong, F., Li, Q., Yang, C., Huo, D., Wang, X., Ai, C., Kong, Y., Sun, X., Wang, W., Zhou, Y., Liu, X., Li, W., Gao, W., Liu, W., Kang, C., & Wu, X. (2018). PRMT2 links histone H3R8 asymmetric dimethylation to oncogenic activation and tumorigenesis of glioblastoma. *Nature Communications*, *9*(1), 4552. https://doi.org/10.1038/s41467-018-06968-7

Dong, R., Li, X., & Lai, K.-O. (2021). Activity and Function of the PRMT8 Protein Arginine Methyltransferase in Neurons. *Life*, *11*(11), 1132. https://doi.org/10.3390/life11111132

Duncan, K. W., Rioux, N., Boriack-Sjodin, P. A., Munchhof, M. J., Reiter, L. A., Majer, C. R., Jin, L., Johnston, L. D., Chan-Penebre, E., Kuplast, K. G., Porter Scott, M., Pollock, R. M., Waters, N. J., Smith, J. J., Moyer, M. P., Copeland, R. A., & Chesworth, R. (2016). Structure and Property Guided Design in the Identification of PRMT5 Tool Compound EPZ015666. *ACS Medicinal Chemistry Letters*, *7*(2), 162–166. https://doi.org/10.1021/acsmedchemlett.5b00380

Düster, R., Kaltheuner, I. H., Schmitz, M., & Geyer, M. (2021). 1,6-Hexanediol, commonly used to dissolve liquid–liquid phase separated condensates, directly impairs kinase and phosphatase activities. *Journal of Biological Chemistry*, *296*, 100260. https://doi.org/10.1016/j.jbc.2021.100260

Edelmann, M. J. (2011). Strong Cation Exchange Chromatography in Analysis of Posttranslational Modifications: Innovations and Perspectives. *Journal of Biomedicine and Biotechnology*, *2011*, 1–7. https://doi.org/10.1155/2011/936508

Eden, E., Navon, R., Steinfeld, I., Lipson, D., & Yakhini, Z. (2009). GOrilla: a tool for discovery and visualization of enriched GO terms in ranked gene lists. *BMC Bioinformatics*, *10*(1), 48. https://doi.org/10.1186/1471-2105-10-48

Ehlén, Å., Brennan, D.J., Nodin, B. et al. Expression of the RNA-binding protein RBM3 is associated with a favourable prognosis and cisplatin sensitivity in epithelial ovarian cancer. J Transl Med 8, 78 (2010). https://doi.org/10.1186/1479-5876-8-78

Elias, J. E., & Gygi, S. P. (2010). *Target-Decoy Search Strategy for Mass Spectrometry-Based Proteomics* (pp. 55–71). https://doi.org/10.1007/978-1-60761-444-9_5

Ellgaard, L., & Helenius, A. (2001). ER quality control: towards an understanding at the molecular level. *Current Opinion in Cell Biology*, *13*(4), 431–437. https://doi.org/10.1016/S0955-0674(00)00233-7

El-Naggar, A. M., & Sorensen, P. H. (2018). Translational control of aberrant stress responses as a hallmark of cancer. *The Journal of Pathology*, *244*(5), 650–666. https://doi.org/10.1002/path.5030

Eram, M. S., Shen, Y., Szewczyk, M. M., Wu, H., Senisterra, G., Li, F., Butler, K. v., Kaniskan, H. Ü., Speed, B. A., dela Seña, C., Dong, A., Zeng, H., Schapira, M., Brown, P. J., Arrowsmith, C. H., Barsyte-Lovejoy, D., Liu, J., Vedadi, M., & Jin, J. (2016). A Potent, Selective, and Cell-Active Inhibitor of Human Type I Protein Arginine Methyltransferases. *ACS Chemical Biology*, *11*(3), 772–781. https://doi.org/10.1021/acschembio.5b00839

Fedoriw, A., Rajapurkar, S. R., O'Brien, S., Gerhart, S. v., Mitchell, L. H., Adams, N. D., Rioux, N., Lingaraj, T., Ribich, S. A., Pappalardi, M. B., Shah, N., Laraio, J., Liu, Y., Butticello, M., Carpenter, C. L., Creasy, C., Korenchuk, S., McCabe, M. T., McHugh, C. F., … Mohammad, H. P. (2019). Anti-tumor Activity of the Type I PRMT Inhibitor, GSK3368715, Synergizes with PRMT5 Inhibition through MTAP Loss. *Cancer Cell*, *36*(1), 100-114.e25. https://doi.org/10.1016/j.ccell.2019.05.014

Ficarro, S. B., McCleland, M. L., Stukenberg, P. T., Burke, D. J., Ross, M. M., Shabanowitz, J., Hunt, D. F., & White, F. M. (2002). Phosphoproteome analysis by mass spectrometry and its application to Saccharomyces cerevisiae. *Nature Biotechnology*, *20*(3), 301–305. https://doi.org/10.1038/nbt0302-301

Finehout, E. J., & Lee, K. H. (2004). An introduction to mass spectrometry applications in biological research. *Biochemistry and Molecular Biology Education*, *32*(2), 93–100. https://doi.org/10.1002/bmb.2004.494032020331

Fong, J. Y., Pignata, L., Goy, P.-A., Kawabata, K. C., Lee, S. C.-W., Koh, C. M., Musiani, D., Massignani, E., Kotini, A. G., Penson, A., Wun, C. M., Shen, Y., Schwarz, M., Low, D. HP., Rialdi, A., Ki, M., Wollmann, H., Mzoughi, S., Gay, F., … Guccione, E. (2019). Therapeutic Targeting of RNA Splicing Catalysis through Inhibition of Protein Arginine Methylation. *Cancer Cell*, *36*(2), 194-209.e9. https://doi.org/10.1016/j.ccell.2019.07.003

Forgrave, L. M., Wang, M., Yang, D., & DeMarco, M. L. (2022). Proteoforms and their expanding role in laboratory medicine. *Practical Laboratory Medicine*, *28*, e00260. https://doi.org/10.1016/j.plabm.2021.e00260

Frankel, A., Yadav, N., Lee, J., Branscombe, T. L., Clarke, S., & Bedford, M. T. (2002). The Novel Human Protein Arginine N-Methyltransferase PRMT6 Is a Nuclear Enzyme Displaying Unique Substrate Specificity. *Journal of Biological Chemistry*, *277*(5), 3537–3543. https://doi.org/10.1074/jbc.M108786200

Fulton, M. D., Brown, T., & Zheng, Y. G. (2019). The Biological Axis of Protein Arginine Methylation and Asymmetric Dimethylarginine. *International Journal of Molecular Sciences*, *20*(13), 3322. https://doi.org/10.3390/ijms20133322

Gagliardi, M., & Matarazzo, M. R. (2016). *RIP: RNA Immunoprecipitation* (pp. 73–86). https://doi.org/10.1007/978-1-4939-6380-5_7

Gilman, B., Tijerina, P., & Russell, R. (2017). Distinct RNA-unwinding mechanisms of DEAD-box and DEAH-box RNA helicase proteins in remodeling structured RNAs and RNPs. *Biochemical Society Transactions*, *45*(6), 1313–1321. https://doi.org/10.1042/BST20170095

Giuliani, V., Miller, M. A., Liu, C.-Y., Hartono, S. R., Class, C. A., Bristow, C. A., Suzuki, E., Sanz, L. A., Gao, G., Gay, J. P., Feng, N., Rose, J. L., Tomihara, H., Daniele, J. R., Peoples, M. D., Bardenhagen, J. P., Geck Do, M. K., Chang, Q. E., Vangamudi, B., … Heffernan, T. P. (2021). PRMT1-dependent regulation of RNA metabolism and DNA damage response sustains pancreatic ductal adenocarcinoma. *Nature Communications*, *12*(1), 4626. https://doi.org/10.1038/s41467-021-24798-y

Gomes, E., & Shorter, J. (2019). The molecular language of membraneless organelles. *Journal of Biological Chemistry*, *294*(18), 7115–7127. https://doi.org/10.1074/jbc.TM118.001192

Guccione, E., & Richard, S. (2019). The regulation, functions and clinical relevance of arginine methylation. *Nature Reviews Molecular Cell Biology*, *20*(10), 642–657. https://doi.org/10.1038/s41580-019-0155-x

Hadjikyriacou, A., Yang, Y., Espejo, A., Bedford, M. T., & Clarke, S. G. (2015). Unique Features of Human Protein Arginine Methyltransferase 9 (PRMT9) and Its Substrate RNA Splicing Factor SF3B2. *Journal of Biological Chemistry*, *290*(27), 16723–16743. https://doi.org/10.1074/jbc.M115.659433

Hafner, M., Katsantoni, M., Köster, T., Marks, J., Mukherjee, J., Staiger, D., Ule, J., & Zavolan, M. (2021). CLIP and complementary methods. *Nature Reviews Methods Primers*, *1*(1), 20. https://doi.org/10.1038/s43586-021-00018-1

Haghandish, N., Baldwin, R. M., Morettin, A., Dawit, H. T., Adhikary, H., Masson, J.-Y., Mazroui, R., Trinkle-Mulcahy, L., & Côté, J. (2019). PRMT7 methylates eukaryotic translation initiation factor 2α and regulates its role in stress granule formation. *Molecular Biology of the Cell*, *30*(6), 778–793. https://doi.org/10.1091/mbc.E18-05-0330

Hart-Smith, G., Yagoub, D., Tay, A. P., Pickford, R., & Wilkins, M. R. (2016). Large Scale Mass Spectrometry-based Identifications of Enzyme-mediated Protein Methylation Are Subject to High False Discovery Rates. *Molecular & Cellular Proteomics*, *15*(3), 989–1006. https://doi.org/10.1074/mcp.M115.055384

Hoefig, K. P., Reim, A., Gallus, C., Wong, E. H., Behrens, G., Conrad, C., Xu, M., Kifinger, L., Ito-Kureha, T., Defourny, K. A. Y., Geerlof, A., Mautner, J., Hauck, S. M., Baumjohann, D., Feederle, R., Mann, M., Wierer, M., Glasmacher, E., & Heissmeyer, V. (2021). Defining the RBPome of primary T helper cells to elucidate higher-order Roquin-mediated mRNA regulation. *Nature Communications*, *12*(1), 5208. https://doi.org/10.1038/s41467-021-25345-5

Hornbeck, P. v., Kornhauser, J. M., Tkachev, S., Zhang, B., Skrzypek, E., Murray, B., Latham, V., & Sullivan, M. (2012). PhosphoSitePlus: a comprehensive resource for investigating the structure and function of experimentally determined post-translational modifications in man and mouse. *Nucleic Acids Research*, *40*(D1), D261–D270. https://doi.org/10.1093/nar/gkr1122

Huang, C., Chen, Y., Dai, H., Zhang, H., Xie, M., Zhang, H., Chen, F., Kang, X., Bai, X., & Chen, Z. (2020). UBAP2L arginine methylation by PRMT1 modulates stress granule assembly. *Cell Death & Differentiation*, *27*(1), 227–241. https://doi.org/10.1038/s41418-019-0350-5

Huang, R., Han, M., Meng, L., & Chen, X. (2018). Capture and Identification of RNA-binding Proteins by Using Click Chemistry-assisted RNA-interactome Capture (CARIC) Strategy. *Journal of Visualized Experiments*, *140*. https://doi.org/10.3791/58580

Hwang, J. W., Cho, Y., Bae, G.-U., Kim, S.-N., & Kim, Y. K. (2021). Protein arginine methyltransferases: promising targets for cancer therapy. *Experimental & Molecular Medicine*, *53*(5), 788–808. https://doi.org/10.1038/s12276-021-00613-y

Hwang, J. W., Kim, S.-N., Myung, N., Song, D., Han, G., Bae, G.-U., Bedford, M. T., & Kim, Y. K. (2020). PRMT5 promotes DNA repair through methylation of 53BP1 and is regulated by Src-mediated phosphorylation. *Communications Biology*, *3*(1), 428. https://doi.org/10.1038/s42003-020-01157-z

Jain, K., & Clarke, S. G. (2019). PRMT7 as a unique member of the protein arginine methyltransferase family: A review. *Archives of Biochemistry and Biophysics*, *665*, 36–45. https://doi.org/10.1016/j.abb.2019.02.014

Jao, C. Y., & Salic, A. (2008). Exploring RNA transcription and turnover *in vivo* by using click chemistry. *Proceedings of the National Academy of Sciences*, *105*(41), 15779–15784. https://doi.org/10.1073/pnas.0808480105

Jarrold, J., & Davies, C. C. (2019). PRMTs and Arginine Methylation: Cancer's Best-Kept Secret? *Trends in Molecular Medicine*, *25*(11), 993–1009. https://doi.org/10.1016/j.molmed.2019.05.007

Jensen, O. N. (2006). Interpreting the protein language using proteomics. *Nature Reviews Molecular Cell Biology*, *7*(6), 391–403. https://doi.org/10.1038/nrm1939

Jenuwein, T., & Allis, C. D. (2001). Translating the Histone Code. *Science*, *293*(5532), 1074–1080. https://doi.org/10.1126/science.1063127

Jing, P., Zhao, N., Ye, M., Zhang, Y., Zhang, Z., Sun, J., Wang, Z., Zhang, J., & Gu, Z. (2018). Protein arginine methyltransferase 5 promotes lung cancer metastasis via the epigenetic regulation of miR-99 family/FGFR3 signaling. *Cancer Letters*, *427*, 38–48. https://doi.org/10.1016/j.canlet.2018.04.019

Jongjitwimol, J., Baldock, R. A., Morley, S. J., & Watts, F. Z. (2016). Sumoylation of eIF4A2 affects stress granule formation. *Journal of Cell Science*. https://doi.org/10.1242/jcs.184614

Kaufmann, R. (1995). Matrix-assisted laser desorption ionization (MALDI) mass spectrometry: a novel analytical tool in molecular biology and biotechnology. *Journal of Biotechnology*, *41*(2–3), 155–175. https://doi.org/10.1016/0168-1656(95)00009-F

Kawahara, D., Suzuki, T., & Nakaya, T. (2021). Cytoplasmic granule formation by FUS-R495X is attributable to arginine methylation in all Gly-rich, RGG1 and RGG2 domains. *Genes to Cells*, *26*(3), 190–197. https://doi.org/10.1111/gtc.12827

Khong, A., Matheny, T., Jain, S., Mitchell, S. F., Wheeler, J. R., & Parker, R. (2017). The Stress Granule Transcriptome Reveals Principles of mRNA Accumulation in Stress Granules. *Molecular Cell*, *68*(4), 808-820.e5. https://doi.org/10.1016/j.molcel.2017.10.015

Kiledjian, M., & Dreyfuss, G. (1992). Primary structure and binding activity of the hnRNP U protein: binding RNA through RGG box. *The EMBO Journal*, *11*(7), 2655–2664. https://doi.org/10.1002/j.1460-2075.1992.tb05331.x

Kim, E., Jang, J., Park, J. G., Kim, K.-H., Yoon, K., Yoo, B. C., & Cho, J. Y. (2020). Protein Arginine Methyltransferase 1 (PRMT1) Selective Inhibitor, TC-E 5003, Has Anti-Inflammatory Properties in TLR4 Signaling. *International Journal of Molecular Sciences*, *21*(9), 3058. https://doi.org/10.3390/ijms21093058

Kolb, J., Anders-Maurer, M., Müller, T., Hau, A.-C., Grebbin, B. M., Kallenborn-Gerhardt, W., Behrends, C., & Schulte, D. (2018). Arginine Methylation Regulates MEIS2 Nuclear Localization to Promote Neuronal Differentiation of Adult SVZ Progenitors. *Stem Cell Reports*, *10*(4), 1184–1192. https://doi.org/10.1016/j.stemcr.2018.03.010

Konermann, L., Ahadi, E., Rodriguez, A. D., & Vahidi, S. (2013). Unraveling the Mechanism of Electrospray Ionization. *Analytical Chemistry*, *85*(1), 2–9. https://doi.org/10.1021/ac302789c

Krasny, L., & Huang, P. H. (2021). Data-independent acquisition mass spectrometry (DIA-MS) for proteomic applications in oncology. *Molecular Omics*, *17*(1), 29–42. https://doi.org/10.1039/D0MO00072H

Lattouf, H., Poulard, C., & le Romancer, M. (2019). PRMT5 prognostic value in cancer. *Oncotarget*, *10*(34), 3151–3153. https://doi.org/10.18632/oncotarget.26883

Liao, J.-Y., Yang, B., Zhang, Y.-C., Wang, X.-J., Ye, Y., Peng, J.-W., Yang, Z.-Z., He, J.-H., Zhang, Y., Hu, K., Lin, D.-C., & Yin, D. (2020). EuRBPDB: a comprehensive resource for annotation, functional and oncological investigation of eukaryotic RNA binding proteins (RBPs). *Nucleic Acids Research*, *48*(D1), D307–D313. https://doi.org/10.1093/nar/gkz823

Loll-Krippleber, R., & Brown, G. W. (2017). P-body proteins regulate transcriptional rewiring to promote DNA replication stress resistance. *Nature Communications*, *8*(1), 558. https://doi.org/10.1038/s41467-017-00632-2

Ma, X., Chen, C., Veevers, J., Zhou, X., Ross, R. S., Feng, W., & Chen, J. (2017). CRISPR/Cas9-mediated gene manipulation to create single-amino-acid-substituted and floxed mice with a cloning-free method. *Scientific Reports*, *7*(1), 42244. https://doi.org/10.1038/srep42244

Maiwen Caudron-Herger, Ralf E Jansen, Elsa Wassmer, Sven Diederichs, RBP2GO: a comprehensive pan-species database on RNA-binding proteins, their interactions and functions, Nucleic Acids Research, Volume 49, Issue D1, 8 January 2021, Pages D425–D436, https://doi.org/10.1093/nar/gkaa1040

Maniaci, M., Boffo, F. L., Massignani, E., & Bonaldi, T. (2021). Systematic Analysis of the Impact of R-Methylation on RBPs-RNA Interactions: A Proteomic Approach. *Frontiers in Molecular Biosciences*, *8*. https://doi.org/10.3389/fmolb.2021.688973

Maniaci, M., Marini, F., Massignani, E., & Bonaldi, T. (2022). A Mass Spectrometry-Based Proteomics Approach for Global and High-Confidence Protein R-Methylation Analysis. *Journal of Visualized Experiments*, *182*. https://doi.org/10.3791/62409

Marcelo, A., Koppenol, R., de Almeida, L. P., Matos, C. A., & Nóbrega, C. (2021). Stress granules, RNA-binding proteins and polyglutamine diseases: too much aggregation? *Cell Death & Disease*, *12*(6), 592. https://doi.org/10.1038/s41419-021-03873-8

Markmiller, S., Soltanieh, S., Server, K. L., Mak, R., Jin, W., Fang, M. Y., Luo, E.-C., Krach, F., Yang, D., Sen, A., Fulzele, A., Wozniak, J. M., Gonzalez, D. J., Kankel, M. W., Gao, F.-B., Bennett, E. J., Lécuyer, E., & Yeo, G. W. (2018). Context-Dependent and Disease-Specific Diversity in Protein Interactions within Stress Granules. *Cell*, *172*(3), 590-604.e13. https://doi.org/10.1016/j.cell.2017.12.032

Massignani, E., Cuomo, A., Musiani, D., Jammula, S., Pavesi, G., & Bonaldi, T. (2019). hmSEEKER: Identification of hmSILAC Doublets in MaxQuant Output Data. *PROTEOMICS*, *19*(5), 1800300. https://doi.org/10.1002/pmic.201800300

Massignani, E., Giambruno, R., Maniaci, M., Nicosia, L., Yadav, A., Cuomo, A., Raimondi, F., & Bonaldi, T. (2022). ProMetheusDB: An In-Depth Analysis of the High-Quality Human Methyl-proteome. *Molecular & Cellular Proteomics*, *21*(7), 100243. https://doi.org/10.1016/j.mcpro.2022.100243

Mazroui, R., Sukarieh, R., Bordeleau, M.-E., Kaufman, R. J., Northcote, P., Tanaka, J., Gallouzi, I., & Pelletier, J. (2006). Inhibition of Ribosome Recruitment Induces Stress Granule Formation Independently of Eukaryotic Initiation Factor 2α Phosphorylation. *Molecular Biology of the Cell*, *17*(10), 4212–4219. https://doi.org/10.1091/mbc.e06-04-0318

McNulty, D. E., & Annan, R. S. (2008). Hydrophilic Interaction Chromatography Reduces the Complexity of the Phosphoproteome and Improves Global Phosphopeptide Isolation and Detection. *Molecular & Cellular Proteomics*, *7*(5), 971–980. https://doi.org/10.1074/mcp.M700543-MCP200

Mersaoui, S. Y., Yu, Z., Coulombe, Y., Karam, M., Busatto, F. F., Masson, J., & Richard, S. (2019). Arginine methylation of the <scp>DDX</scp> 5 helicase <scp>RGG</scp> / <scp>RG</scp> motif by <scp>PRMT</scp> 5 regulates resolution of RNA:DNA hybrids. *The EMBO Journal*, *38*(15). https://doi.org/10.15252/embj.2018100986

Michalski, A., Damoc, E., Hauschild, J.-P., Lange, O., Wieghaus, A., Makarov, A., Nagaraj, N., Cox, J., Mann, M., & Horning, S. (2011). Mass Spectrometry-based Proteomics Using Q Exactive, a High-performance Benchtop Quadrupole Orbitrap Mass Spectrometer. *Molecular & Cellular Proteomics*, *10*(9), M111.011015. https://doi.org/10.1074/mcp.M111.011015

Min, Z., Xiaomeng, L., Zheng, L., Yangge, D., Xuejiao, L., Longwei, L., Xiao, Z., Yunsong, L., Ping, Z., & Yongsheng, Z. (2019). Asymmetrical methyltransferase PRMT3 regulates human mesenchymal stem cell osteogenesis via miR-3648. *Cell Death & Disease*, *10*(8), 581. https://doi.org/10.1038/s41419-019-1815-7

Musiani, D., Bok, J., Massignani, E., Wu, L., Tabaglio, T., Ippolito, M. R., Cuomo, A., Ozbek, U., Zorgati, H., Ghoshdastider, U., Robinson, R. C., Guccione, E., & Bonaldi, T. (2019). Proteomics profiling of arginine methylation defines PRMT5 substrate specificity. *Science Signaling*, *12*(575). https://doi.org/10.1126/scisignal.aat8388

Musiani, D., Giambruno, R., Massignani, E., Ippolito, M. R., Maniaci, M., Jammula, S., Manganaro, D., Cuomo, A., Nicosia, L., Pasini, D., & Bonaldi, T. (2020). PRMT1 Is Recruited via DNA-PK to Chromatin Where It Sustains the Senescence-Associated Secretory Phenotype in Response to Cisplatin. *Cell Reports*, *30*(4). https://doi.org/10.1016/j.celrep.2019.12.061

Nielsen, M. L., Savitski, M. M., & Zubarev, R. A. (2006). Extent of Modifications in Human Proteome Samples and Their Effect on Dynamic Range of Analysis in Shotgun Proteomics. *Molecular & Cellular Proteomics*, *5*(12), 2384–2391. https://doi.org/10.1074/mcp.M600248-MCP200

Nyathi, Y., Wilkinson, B. M., & Pool, M. R. (2013). Co-translational targeting and translocation of proteins to the endoplasmic reticulum. *Biochimica et Biophysica Acta (BBA) - Molecular Cell Research*, *1833*(11), 2392–2402. https://doi.org/10.1016/j.bbamcr.2013.02.021

Ohn, T., & Anderson, P. (2010). The role of posttranslational modifications in the assembly of stress granules. *Wiley Interdisciplinary Reviews: RNA*, *1*(3), 486–493. https://doi.org/10.1002/wrna.23

Olsen, J. v, Macek, B., Lange, O., Makarov, A., Horning, S., & Mann, M. (2007). Higher-energy C-trap dissociation for peptide modification analysis. *Nature Methods*, *4*(9), 709–712. https://doi.org/10.1038/nmeth1060

Olsen, J. v., & Mann, M. (2013). Status of Large-scale Analysis of Post-translational Modifications by Mass Spectrometry. *Molecular & Cellular Proteomics*, *12*(12), 3444–3452. https://doi.org/10.1074/mcp.O113.034181

Ong, S.-E., Blagoev, B., Kratchmarova, I., Kristensen, D. B., Steen, H., Pandey, A., & Mann, M. (2002). Stable Isotope Labeling by Amino Acids in Cell Culture, SILAC, as a Simple and

Accurate Approach to Expression Proteomics. *Molecular & Cellular Proteomics*, *1*(5), 376–386. https://doi.org/10.1074/mcp.M200025-MCP200
Ong, S.-E., Mittler, G., & Mann, M. (2004). Identifying and quantifying in vivo methylation sites by heavy methyl SILAC. *Nature Methods*, *1*(2), 119–126. https://doi.org/10.1038/nmeth715
O'Shea, J. P., Chou, M. F., Quader, S. A., Ryan, J. K., Church, G. M., & Schwartz, D. (2013). pLogo: a probabilistic approach to visualizing sequence motifs. *Nature Methods*, *10*(12), 1211–1212. https://doi.org/10.1038/nmeth.2646
Perez-Perri, J. I., Rogell, B., Schwarzl, T., Stein, F., Zhou, Y., Rettel, M., Brosig, A., & Hentze, M. W. (2018). Discovery of RNA-binding proteins and characterization of their dynamic responses by enhanced RNA interactome capture. *Nature Communications*, *9*(1), 4408. https://doi.org/10.1038/s41467-018-06557-8
Perkins, D. N., Pappin, D. J. C., Creasy, D. M., & Cottrell, J. S. (1999). Probability-based protein identification by searching sequence databases using mass spectrometry data. *Electrophoresis*, *20*(18), 3551–3567. https://doi.org/10.1002/(SICI)1522-2683(19991201)20:18<3551::AID-ELPS3551>3.0.CO;2-2
Pietras, P., Aulas, A., Fay, M. M., Leśniczak-Staszak, M., Sowiński, M., Lyons, S. M., Szaflarski, W., & Ivanov, P. (2022). Translation inhibition and suppression of stress granules formation by cisplatin. *Biomedicine & Pharmacotherapy*, *145*, 112382. https://doi.org/10.1016/j.biopha.2021.112382
Qamar, S., Wang, G., Randle, S. J., Ruggeri, F. S., Varela, J. A., Lin, J. Q., Phillips, E. C., Miyashita, A., Williams, D., Ströhl, F., Meadows, W., Ferry, R., Dardov, V. J., Tartaglia, G. G., Farrer, L. A., Kaminski Schierle, G. S., Kaminski, C. F., Holt, C. E., Fraser, P. E., … St George-Hyslop, P. (2018). FUS Phase Separation Is Modulated by a Molecular Chaperone and Methylation of Arginine Cation-π Interactions. *Cell*, *173*(3), 720-734.e15. https://doi.org/10.1016/j.cell.2018.03.056
Quattrone, A., & Dassi, E. (2019). The Architecture of the Human RNA-Binding Protein Regulatory Network. *IScience*, *21*, 706–719. https://doi.org/10.1016/j.isci.2019.10.058
Queiroz, R. M. L., Smith, T., Villanueva, E., Marti-Solano, M., Monti, M., Pizzinga, M., Mirea, D.-M., Ramakrishna, M., Harvey, R. F., Dezi, V., Thomas, G. H., Willis, A. E., & Lilley, K. S. (2019). Comprehensive identification of RNA–protein interactions in any organism using orthogonal organic phase separation (OOPS). *Nature Biotechnology*, *37*(2), 169–178. https://doi.org/10.1038/s41587-018-0001-2
Raposo, A. E., & Piller, S. C. (2018). Protein arginine methylation: an emerging regulator of the cell cycle. *Cell Division*, *13*(1), 3. https://doi.org/10.1186/s13008-018-0036-2
Rappsilber, J., Mann, M., & Ishihama, Y. (2007). Protocol for micro-purification, enrichment, pre-fractionation and storage of peptides for proteomics using StageTips. *Nature Protocols*, *2*(8), 1896–1906. https://doi.org/10.1038/nprot.2007.261
Ries, R. J., Zaccara, S., Klein, P., Olarerin-George, A., Namkoong, S., Pickering, B. F., Patil, D. P., Kwak, H., Lee, J. H., & Jaffrey, S. R. (2019). m6A enhances the phase separation potential of mRNA. *Nature*, *571*(7765), 424–428. https://doi.org/10.1038/s41586-019-1374-1
Rogoyski, O., & Gerber, A. P. (2021). RNA-binding proteins modulate drug sensitivity of cancer cells. *Emerging Topics in Life Sciences*, *5*(5), 681–685. https://doi.org/10.1042/ETLS20210193
Roje, S. (2006). S-Adenosyl-l-methionine: Beyond the universal methyl group donor. *Phytochemistry*, *67*(15), 1686–1698. https://doi.org/10.1016/j.phytochem.2006.04.019
Ryu, J.-W., Kim, S.-K., Son, M.-Y., Jeon, S.-J., Oh, J.-H., Lim, J. H., Cho, S., Jung, C.-R., Hamamoto, R., Kim, D.-S., & Cho, H.-S. (2017). Novel prognostic marker PRMT1 regulates cell growth via downregulation of CDKN1A in HCC. *Oncotarget*, *8*(70), 115444–115455. https://doi.org/10.18632/oncotarget.23296
Schindelin, J., Arganda-Carreras, I., Frise, E., Kaynig, V., Longair, M., Pietzsch, T., Preibisch, S., Rueden, C., Saalfeld, S., Schmid, B., Tinevez, J.-Y., White, D. J., Hartenstein, V., Eliceiri, K., Tomancak, P., & Cardona, A. (2012). Fiji: an open-source platform for biological-image analysis. *Nature Methods*, *9*(7), 676–682. https://doi.org/10.1038/nmeth.2019
Schneider, L., Herkt, S., Wang, L., Feld, C., Wesely, J., Kuvardina, O. N., Meyer, A., Oellerich, T., Häupl, B., Seifried, E., Bonig, H., & Lausen, J. (2021). PRMT6 activates cyclin D1 expression

in conjunction with the transcription factor LEF1. *Oncogenesis*, *10*(5), 42. https://doi.org/10.1038/s41389-021-00332-z
Schwanhäusser, B., Gossen, M., Dittmar, G., & Selbach, M. (2009). Global analysis of cellular protein translation by pulsed SILAC. *PROTEOMICS*, *9*(1), 205–209. https://doi.org/10.1002/pmic.200800275
Shannon, P., Markiel, A., Ozier, O., Baliga, N. S., Wang, J. T., Ramage, D., Amin, N., Schwikowski, B., & Ideker, T. (2003). Cytoscape: A Software Environment for Integrated Models of Biomolecular Interaction Networks. *Genome Research*, *13*(11), 2498–2504. https://doi.org/10.1101/gr.1239303
Shevchenko, A., Tomas, H., Havli, J., Olsen, J. v, & Mann, M. (2006). In-gel digestion for mass spectrometric characterization of proteins and proteomes. *Nature Protocols*, *1*(6), 2856–2860. https://doi.org/10.1038/nprot.2006.468
Shishkova, E., Zeng, H., Liu, F., Kwiecien, N. W., Hebert, A. S., Coon, J. J., & Xu, W. (2017). Global mapping of CARM1 substrates defines enzyme specificity and substrate recognition. *Nature Communications*, *8*(1), 15571. https://doi.org/10.1038/ncomms15571
Shteynberg, D. D., Deutsch, E. W., Campbell, D. S., Hoopmann, M. R., Kusebauch, U., Lee, D., Mendoza, L., Midha, M. K., Sun, Z., Whetton, A. D., & Moritz, R. L. (2019). PTMProphet: Fast and Accurate Mass Modification Localization for the Trans-Proteomic Pipeline. *Journal of Proteome Research*, *18*(12), 4262–4272. https://doi.org/10.1021/acs.jproteome.9b00205
Singhroy, D. N., Mesplède, T., Sabbah, A., Quashie, P. K., Falgueyret, J.-P., & Wainberg, M. A. (2013). Automethylation of protein arginine methyltransferase 6 (PRMT6) regulates its stability and its anti-HIV-1 activity. *Retrovirology*, *10*(1), 73. https://doi.org/10.1186/1742-4690-10-73
Sinha, R., Allemand, E., Zhang, Z., Karni, R., Myers, M. P., & Krainer, A. R. (2010). Arginine Methylation Controls the Subcellular Localization and Functions of the Oncoprotein Splicing Factor SF2/ASF. *Molecular and Cellular Biology*, *30*(11), 2762–2774. https://doi.org/10.1128/MCB.01270-09
Song, C., Chen, T., He, L., Ma, N., Li, J., Rong, Y.-F., Fang, Y., Liu, M., Xie, D., & Lou, W. (2020). PRMT1 promotes pancreatic cancer growth and predicts poor prognosis. *Cellular Oncology*, *43*(1), 51–62. https://doi.org/10.1007/s13402-019-00435-1
Spadotto, V., Giambruno, R., Massignani, E., Mihailovich, M., Maniaci, M., Patuzzo, F., Ghini, F., Nicassio, F., & Bonaldi, T. (2020a). PRMT1-mediated methylation of the microprocessor-associated proteins regulates microRNA biogenesis. *Nucleic Acids Research*, *48*(1), 96–115. https://doi.org/10.1093/nar/gkz1051
Srour, N., Khan, S., & Richard, S. (2022). The Influence of Arginine Methylation in Immunity and Inflammation. *Journal of Inflammation Research*, *Volume 15*, 2939–2958. https://doi.org/10.2147/JIR.S364190
Sun, S., Hu, Y., Ao, M., Shah, P., Chen, J., Yang, W., Jia, X., Tian, Y., Thomas, S., & Zhang, H. (2019). N-GlycositeAtlas: a database resource for mass spectrometry-based human N-linked glycoprotein and glycosylation site mapping. *Clinical Proteomics*, *16*(1), 35. https://doi.org/10.1186/s12014-019-9254-0
Sun, Y., Eshov, A., Zhou, J., Isiktas, A. U., & Guo, J. U. (2020). C9orf72 arginine-rich dipeptide repeats inhibit UPF1-mediated RNA decay via translational repression. *Nature Communications*, *11*(1), 3354. https://doi.org/10.1038/s41467-020-17129-0
Supek, F., Bošnjak, M., Škunca, N., & Šmuc, T. (2011). REVIGO Summarizes and Visualizes Long Lists of Gene Ontology Terms. *PLoS ONE*, *6*(7), e21800. https://doi.org/10.1371/journal.pone.0021800
Suresh, S., Huard, S., & Dubois, T. (2021). CARM1/PRMT4: Making Its Mark beyond Its Function as a Transcriptional Coactivator. *Trends in Cell Biology*, *31*(5), 402–417. https://doi.org/10.1016/j.tcb.2020.12.010
SWIERCZ, R., PERSON, M. D., & BEDFORD, M. T. (2005). Ribosomal protein S2 is a substrate for mammalian PRMT3 (protein arginine methyltransferase 3). *Biochemical Journal*, *386*(1), 85–91. https://doi.org/10.1042/BJ20041466
Szewczyk, M. M., Ishikawa, Y., Organ, S., Sakai, N., Li, F., Halabelian, L., Ackloo, S., Couzens, A. L., Eram, M., Dilworth, D., Fukushi, H., Harding, R., dela Seña, C. C., Sugo, T., Hayashi, K.,

McLeod, D., Zepeda, C., Aman, A., Sánchez-Osuna, M., … Barsyte-Lovejoy, D. (2020). Pharmacological inhibition of PRMT7 links arginine monomethylation to the cellular stress response. *Nature Communications*, *11*(1), 2396. https://doi.org/10.1038/s41467-020-16271-z

Szklarczyk, D., Gable, A. L., Lyon, D., Junge, A., Wyder, S., Huerta-Cepas, J., Simonovic, M., Doncheva, N. T., Morris, J. H., Bork, P., Jensen, L. J., & Mering, C. von. (2019). STRING v11: protein–protein association networks with increased coverage, supporting functional discovery in genome-wide experimental datasets. *Nucleic Acids Research*, *47*(D1), D607–D613. https://doi.org/10.1093/nar/gky1131

Tang, J., Frankel, A., Cook, R. J., Kim, S., Paik, W. K., Williams, K. R., Clarke, S., & Herschman, H. R. (2000). PRMT1 Is the Predominant Type I Protein Arginine Methyltransferase in Mammalian Cells. *Journal of Biological Chemistry*, *275*(11), 7723–7730. https://doi.org/10.1074/jbc.275.11.7723

Taxman, D. J., Moore, C. B., Guthrie, E. H., & Huang, M. T.-H. (2010). *Short Hairpin RNA (shRNA): Design, Delivery, and Assessment of Gene Knockdown* (pp. 139–156). https://doi.org/10.1007/978-1-60761-657-3_10

Tewary, S. K., Zheng, Y. G., & Ho, M.-C. (2019). Protein arginine methyltransferases: insights into the enzyme structure and mechanism at the atomic level. *Cellular and Molecular Life Sciences*, *76*(15), 2917–2932. https://doi.org/10.1007/s00018-019-03145-x

Thandapani, P., O'Connor, T. R., Bailey, T. L., & Richard, S. (2013). Defining the RGG/RG Motif. *Molecular Cell*, *50*(5), 613–623. https://doi.org/10.1016/j.molcel.2013.05.021

Thiebaut, C., Eve, L., Poulard, C., & le Romancer, M. (2021). Structure, Activity, and Function of PRMT1. *Life*, *11*(11), 1147. https://doi.org/10.3390/life11111147

Thompson, A., Schäfer, J., Kuhn, K., Kienle, S., Schwarz, J., Schmidt, G., Neumann, T., & Hamon, C. (2003). Tandem Mass Tags: A Novel Quantification Strategy for Comparative Analysis of Complex Protein Mixtures by MS/MS. *Analytical Chemistry*, *75*(8), 1895–1904. https://doi.org/10.1021/ac0262560

Thompson, P. R., & Fast, W. (2006). Histone Citrullination by Protein Arginine Deiminase: Is Arginine Methylation a Green Light or a Roadblock? *ACS Chemical Biology*, *1*(7), 433–441. https://doi.org/10.1021/cb6002306

Tian, J., Liu, R., & Qu, Q. (2017). Role of endoplasmic reticulum stress on cisplatin resistance in ovarian carcinoma. *Oncology Letters*, *13*(3), 1437–1443. https://doi.org/10.3892/ol.2017.5580

Trendel, J., Schwarzl, T., Horos, R., Prakash, A., Bateman, A., Hentze, M. W., & Krijgsveld, J. (2019). The Human RNA-Binding Proteome and Its Dynamics during Translational Arrest. *Cell*, *176*(1–2), 391-403.e19. https://doi.org/10.1016/j.cell.2018.11.004

Tsai, W.-C., Gayatri, S., Reineke, L. C., Sbardella, G., Bedford, M. T., & Lloyd, R. E. (2016). Arginine Demethylation of G3BP1 Promotes Stress Granule Assembly. *Journal of Biological Chemistry*, *291*(43), 22671–22685. https://doi.org/10.1074/jbc.M116.739573

Tyanova, S., & Cox, J. (2018). *Perseus: A Bioinformatics Platform for Integrative Analysis of Proteomics Data in Cancer Research* (pp. 133–148). https://doi.org/10.1007/978-1-4939-7493-1_7

Tyanova, S., Temu, T., & Cox, J. (2016). The MaxQuant computational platform for mass spectrometry-based shotgun proteomics. *Nature Protocols*, *11*(12), 2301–2319. https://doi.org/10.1038/nprot.2016.136

Urdaneta, E. C., Vieira-Vieira, C. H., Hick, T., Wessels, H.-H., Figini, D., Moschall, R., Medenbach, J., Ohler, U., Granneman, S., Selbach, M., & Beckmann, B. M. (2019). Purification of cross-linked RNA-protein complexes by phenol-toluol extraction. *Nature Communications*, *10*(1), 990. https://doi.org/10.1038/s41467-019-08942-3

Valverde, R., Edwards, L., & Regan, L. (2008). Structure and function of KH domains. *FEBS Journal*, *275*(11), 2712–2726. https://doi.org/10.1111/j.1742-4658.2008.06411.x

Vieira-Vieira, C. H., Dauksaite, V., Sporbert, A., Gotthardt, M., & Selbach, M. (2022). Proteome-wide quantitative RNA-interactome capture identifies phosphorylation sites with regulatory potential in RBM20. *Molecular Cell*, *82*(11), 2069-2083.e8. https://doi.org/10.1016/j.molcel.2022.03.024

Walport, L. J., Hopkinson, R. J., Chowdhury, R., Schiller, R., Ge, W., Kawamura, A., & Schofield, C. J. (2016). Arginine demethylation is catalysed by a subset of JmjC histone lysine demethylases. *Nature Communications*, *7*(1), 11974. https://doi.org/10.1038/ncomms11974

Wang, X., He, Y., Ye, Y., Zhao, X., Deng, S., He, G., Zhu, H., Xu, N., & Liang, S. (2018). SILAC–based quantitative MS approach for real-time recording protein-mediated cell-cell interactions. *Scientific Reports*, *8*(1), 8441. https://doi.org/10.1038/s41598-018-26262-2

Ward, J. H. (1963). Hierarchical Grouping to Optimize an Objective Function. *Journal of the American Statistical Association*, *58*(301), 236–244. https://doi.org/10.1080/01621459.1963.10500845

Wheeler, J. R., Matheny, T., Jain, S., Abrisch, R., & Parker, R. (2016). Distinct stages in stress granule assembly and disassembly. *ELife*, *5*. https://doi.org/10.7554/eLife.18413

Wiese, S., Reidegeld, K. A., Meyer, H. E., & Warscheid, B. (2007). Protein labeling by iTRAQ: A new tool for quantitative mass spectrometry in proteome research. *PROTEOMICS*, *7*(3), 340–350. https://doi.org/10.1002/pmic.200600422

Xu, D., Liang, S.-Q., Yang, H., Lüthi, U., Riether, C., Berezowska, S., Marti, T. M., Hall, S. R. R., Bruggmann, R., Kocher, G. J., Schmid, R. A., & Peng, R.-W. (2018). Increased sensitivity to apoptosis upon endoplasmic reticulum stress-induced activation of the unfolded protein response in chemotherapy-resistant malignant pleural mesothelioma. *British Journal of Cancer*, *119*(1), 65–75. https://doi.org/10.1038/s41416-018-0145-3

XU, Y., WANG, C., SU, J., XIE, Q., MA, L., ZENG, L., YU, Y., LIU, S., LI, S., LI, Z., & SUN, L. (2015). Tolerance to endoplasmic reticulum stress mediates cisplatin resistance in human ovarian cancer cells by maintaining endoplasmic reticulum and mitochondrial homeostasis. *Oncology Reports*, *34*(6), 3051–3060. https://doi.org/10.3892/or.2015.4283

Yamaguchi, A., & Kitajo, K. (2012). The Effect of PRMT1-Mediated Arginine Methylation on the Subcellular Localization, Stress Granules, and Detergent-Insoluble Aggregates of FUS/TLS. *PLoS ONE*, *7*(11), e49267. https://doi.org/10.1371/journal.pone.0049267

Yang, F., Shen, Y., Camp, D. G., & Smith, R. D. (2012). High-pH reversed-phase chromatography with fraction concatenation for 2D proteomic analysis. *Expert Review of Proteomics*, *9*(2), 129–134. https://doi.org/10.1586/epr.12.15

Yang, P., Mathieu, C., Kolaitis, R.-M., Zhang, P., Messing, J., Yurtsever, U., Yang, Z., Wu, J., Li, Y., Pan, Q., Yu, J., Martin, E. W., Mittag, T., Kim, H. J., & Taylor, J. P. (2020). G3BP1 Is a Tunable Switch that Triggers Phase Separation to Assemble Stress Granules. *Cell*, *181*(2), 325-345.e28. https://doi.org/10.1016/j.cell.2020.03.046

Yang, Y., Hadjikyriacou, A., Xia, Z., Gayatri, S., Kim, D., Zurita-Lopez, C., Kelly, R., Guo, A., Li, W., Clarke, S. G., & Bedford, M. T. (2015). PRMT9 is a Type II methyltransferase that methylates the splicing factor SAP145. *Nature Communications*, *6*(1), 6428. https://doi.org/10.1038/ncomms7428

Yates, J. R., Eng, J. K., McCormack, A. L., & Schieltz, David. (1995). Method to Correlate Tandem Mass Spectra of Modified Peptides to Amino Acid Sequences in the Protein Database. *Analytical Chemistry*, *67*(8), 1426–1436. https://doi.org/10.1021/ac00104a020

You, K., Huang, Q., Yu, C., Shen, B., Sevilla, C., Shi, M., Hermjakob, H., Chen, Y., & Li, T. (2020). PhaSepDB: a database of liquid–liquid phase separation related proteins. *Nucleic Acids Research*, *48*(D1), D354–D359. https://doi.org/10.1093/nar/gkz847

Zhan, Y., Wang, H., Ning, Y., Zheng, H., Liu, S., Yang, Y., Zhou, M., & Fan, S. (2020). Understanding the roles of stress granule during chemotherapy for patients with malignant tumors. *American Journal of Cancer Research*, *10*(8), 2226–2241.

Zhang, F., Kerbl-Knapp, J., Rodriguez Colman, M. J., Meinitzer, A., Macher, T., Vujić, N., Fasching, S., Jany-Luig, E., Korbelius, M., Kuentzel, K. B., Mack, M., Akhmetshina, A., Pirchheim, A., Paar, M., Rinner, B., Hörl, G., Steyrer, E., Stelzl, U., Burgering, B., … Madl, T. (2021). Global analysis of protein arginine methylation. *Cell Reports Methods*, *1*(2), 100016. https://doi.org/10.1016/j.crmeth.2021.100016

Zhang, Y., Fonslow, B. R., Shan, B., Baek, M.-C., & Yates, J. R. (2013). Protein Analysis by Shotgun/Bottom-up Proteomics. *Chemical Reviews*, *113*(4), 2343–2394. https://doi.org/10.1021/cr3003533

Zubarev, R. A., Horn, D. M., Fridriksson, E. K., Kelleher, N. L., Kruger, N. A., Lewis, M. A., Carpenter, B. K., & McLafferty, F. W. (2000). Electron Capture Dissociation for Structural Characterization of Multiply Charged Protein Cations. *Analytical Chemistry*, *72*(3), 563–573. https://doi.org/10.1021/ac990811p

8. LIST OF PUBLICATION ACHIEVED DURING THE Ph.D.

- Massignani E, **Maniaci M**, Bonaldi T, Heavy methyl SILAC metabolic labelling of human cell lines for high-confidence identification of R/K-methylated peptides by high-resolution Mass Spectrometry, Book: SILAC. Methods in Molecular Biology - Springer Nature, *in press*

- **Maniaci M**, Marini F, Massignani E, Bonaldi T. A Mass Spectrometry-Based Proteomics Approach for Global and High-Confidence Protein R-Methylation Analysis. J Vis Exp. 2022 Apr 28;(182). doi:10.3791/62409. PMID: 35575502.

- Massignani E, Giambruno R, **Maniaci M**, Nicosia L, Yadav A, Cuomo A, Raimondi F, Bonaldi T. ProMetheusDB: an in-depth analysis of the high-quality human methyl-proteome. Mol Cell Proteomics. 2022 May 13:100243. doi: 10.1016/j.mcpro.2022.100243. Epub ahead of print. PMID: 35577067.

- **Maniaci M**, Boffo FL, Massignani E, Bonaldi T. Systematic Analysis of the Impact of R-Methylation on RBPs-RNA Interactions: A Proteomic Approach. Front Mol Biosci. 2021 Sep 7;8:688973. doi:10.3389/fmolb.2021.688973. PMID: 34557518; PMCID: PMC8454774.

- Musiani D, Giambruno R, Massignani E, Ippolito MR, **Maniaci M**, Jammula S, Manganaro D, Cuomo A, Nicosia L, Pasini D, Bonaldi T. PRMT1 Is Recruited via DNA-PK to Chromatin Where It Sustains the Senescence-Associated Secretory Phenotype in Response to Cisplatin. Cell Rep. 2020 Jan 28;30(4):1208- 1222.e9. doi: 10.1016/j.celrep.2019.12.061. PMID: 31995759.

- Spadotto V, Giambruno R, Massignani E, Mihailovich M, **Maniaci M**, Patuzzo F, Ghini F, Nicassio F, Bonaldi T. PRMT1-mediated methylation of the microprocessor-associated proteins regulates microRNA biogenesis. Nucleic Acids Res. 2020 Jan 10;48(1):96-115. doi: 10.1093/nar/gkz1051. PMID: 31777917; PMCID: PMC6943135.

9. Acknowledgments

I would like to thank my PhD supervisor Tiziana Bonaldi for giving me the opportunity to work in her laboratory.

I would also like to thank all the current and former members of the Bonaldi group, you have been irreplaceable traveling companions.

I would like to thank my internal advisor Francesco Nicassio and my external advisor Kathryn S. Lilley for their precious advices.

I would like to thank my family, nothing of this would have been possible without you.

I would like to thank all my friends, you have made me the scientist - but more importantly- the person I am today.

Last but not least, I would like to thank Gabriele for supporting and putting up with me over these years.